NASA Technical Memorandum 88326

Conservative Zonal Schemes for Patched Grids in Two and Three Dimensions

Kristin A. Hessenius

April 1987

National Aeronautics and
Space Administration

NASA Technical Memorandum 88326

Conservative Zonal Schemes for Patched Grids in Two and Three Dimensions

Kristin A. Hessenius, Ames Research Center, Moffett Field, California

April 1987

National Aeronautics and
Space Administration

Ames Research Center
Moffett Field, California 94035

CHAPTER 1

INTRODUCTION

There is a current emphasis in computational fluid dynamics (CFD) to develop techniques for solving flow fields about geometrically complex bodies in two and three dimensions. A major difficulty in the computation of such flows is the specification of a proper discretization of the flow field about the geometry of interest. A numerical solution of the governing partial differential equations for the flow about a given body requires the generation of an appropriate grid (a set of points or volumes) spanning the region of interest. The differential equations are then approximated by a set of coupled, algebraic, difference equations, and the system is solved for functional values at each point or volume. Traditionally, a single curvilinear grid is generated for the entire flow-field region, and is often "body-oriented" (body surface corresponds to a constant grid-coordinate surface) to aid in the application of boundary conditions and/or to permit a simplification of the governing equations. Problems with complex geometries, however, pose difficult challenges for grid generators; the creation of a single grid of acceptable quality about the entire configuration may even be impossible. In fact, Chapman (1980) and Kutler (1985) have identified this problem of three-dimensional grid generation as a primary pacing item for the field of CFD.

The discretization of a flow field directly affects both the smoothness and the accuracy of a numerical solution; hence, attention must be given to the quality of the chosen grid. Unfortunately, there are few quantitative measures of the "goodness" of a mesh and most assessment, in practice, is done by eye. Nevertheless, there are some important, qualitative considerations.

To best represent the flow-field solution, the grid should be clustered in expected high solution-gradient regions. However, the efficient use of computer resources precludes the employment of a fine mesh throughout the field but suggests the use of nonuniform

grids with gradual stretching from coarse areas to the desired fine areas. Thompson et al. (1982) show that the truncation error in difference expressions is a function of local grid spacing and rate of change of the spacing, as well as the departure of the grid from orthogonality. To obtain a numerical solution, derivatives along the mesh coordinate lines must be evaluated. Therefore, abrupt changes in either grid-line orientation or spacing will lead to inaccuracies in the estimation of these derivatives. Often these inaccuracies are manifest as local "kinks" in the solution contours. Smoothly varying grid coordinate lines and spacings are highly desirable, as are nearly orthogonal coordinate-line intersections. Furthermore, Steger (1982) warns that grid properties such as smoothness, skewness, and mesh cell aspect ratio may not only affect the accuracy of the solution but also the convergence rate of the numerical algorithm. Some algorithms appear to be very sensitive to undesirable mesh properties (e.g., successive line overrelaxation iterative methods and cell aspect ratio variations; the Beam-Warming algorithm and highly skewed grids).

The foregoing considerations impose stringent constraints on the task of grid generation; consequently, the development of sophisticated algebraic and differential techniques for grid generation is an active area of research. But multiple-body and geometrically complex problems, especially in three dimensions, are difficult with even the most advanced methods. Often the resulting grid about the configuration (after significant investment in research time) is of compromising quality.

A perhaps obvious alternative to the specification of a single grid in a complex region is the use of some sort of blocked or zonal approach to grid generation. The zonal concept is intended to simplify mesh generation by a subdividing the flow field and generating grids within each subregion. Researchers are exploring block approaches for three primary reasons: (1) to permit the solution of problems which are intractable with a single-grid approach because of their geometric complexity; (2) to increase solution accuracy by selectively refining subregions of a previously specified, global, single grid; (3) to facilitate a block-processing computational approach wherein information for only one zone needs

to reside in the computer core at any given time, thereby relaxing memory limitations, or where computers operate in parallel to compute the flow fields in various zones. The use of such a zonal approach requires the development of a technique for treating the grid interface boundaries. Ideally, the procedure used to transmit information from subregion to subregion will maintain a stable, accurate, and conservative computation.

There are two general classes of blocked approaches to grid generation and solution methodology: overlapping grid systems and patched grid systems (point-continuous and point-discontinuous). Figure 1 illustrates these concepts for a simple, two-dimensional, single-body problem. The salient features of each class are discussed in the following paragraphs.

The overlapping approach (fig. 1a) provides the most flexibility in grid generation of the blocked schemes. A mesh is generated about each body or component of a complex configuration with the sole constraint that there be some degree of overlap between neighboring grids. This method is especially attractive for time-dependent applications in which one body is in unspecified motion with respect to another (such as in a store-separation computation). Atta (1981) and Atta and Vadyak (1982) test this approach with the full potential equations in two and three dimensions for steady-state problems. They employ either Dirichlet or Neumann boundary conditions at mesh interfaces using interpolated values from neighboring grids. Similarly, Thompson (1981) uses an overlapping grid system in computing transonic wing/body/store flow fields by solving the small disturbance potential equation. More recently, Steger et al. (1983), Benek et al. (1983), Benek et al. (1985), and Dougherty (1985) carefully outline the data structure details for an overset grid scheme they refer to as "chimera." It is clear from their work that the overlapping approach greatly simplifies the task of grid generation but does complicate data management. Also, Benek et al. (1983) document problems with the scheme as a shock wave passes through the grid boundaries and speculate that the cause is the lack of conservation in these regions because of the nonconservative interpolations at the interfaces. There is

further evidence that this may indeed be the case based on the work of Hessenius and Pulliam (1982) and Rai et al. (1984). Both references cite examples of computations in which the introduction of a degree of nonconservation in the vicinity of a shock wave produces a converged but incorrect solution (the shock does not assume the proper strength, shape, and/or position). Berger (1984) outlines a conservative treatment of arbitrarily oriented overlap boundaries for two-dimensional computations by performing a flux balance at the interface. Unfortunately, the generality and flexibility of the overlapping scheme geometrically complicate the procedure of balancing fluxes. To date, Berger's method has not been implemented.

Overlapping grid systems, while providing a simplified treatment of complex geometries, are used for other reasons as well. Berger (1982) develops a technique for hyperbolic problems for automatically inserting or deleting overlapping grids based on local truncation error, thereby increasing the accuracy of the computations in an efficient manner. Caruso (1985) modifies Berger's approach for use in solving elliptic flow problems. Similarly, Lombard and Venkatapathy (1985) examine the use of overset grids for improved resolution of flow field features. Chang et al. (1985) overcome limitations in computer core memory by zoning the internal flow field in the Space Shuttle main engine using point-continuous but overlapping meshes.

There are two main variations of the patched grid approach to numerical computations: point-continuous and point-discontinuous (see figs. 1b and 1c). Both types of patched grid systems permit a segmentation of the flow field into zones, but require that neighboring zones meet along a common boundary (curve in two dimensions or surface in three dimensions). The point-continuous system, however, also requires continuity of grid lines across the patch boundaries. Two-dimensional examples of the point-continuous solution approach are found in the work of Lasinski et al. (1982) in computing the flow about a tri-element airfoil and in the work of Norton et al. (1983) in calculation of the flow through turbine cascades. Rubbert and Lee (1982) use a point-continuous patching

approach for the generation of three-dimensional grids about aircraft configurations, as do Weatherill and Forsey (1984) for wing-canard computations.

The point-continuous patched schemes referenced above, while permitting component adaptive grids for each body or component part, still necessitate the development of fairly sophisticated generation techniques because of the enforcement of pointwise continuity at the interfaces. (The grids within each block cannot be generated completely independently.) Furthermore, the pointwise-continuous constraint invariably forces the introduction of one or more mesh singularities which require special treatment in the flow solver. However, the "interpolation-free" zonal interface conditions make the computation naturally conservative (an attractive feature), unlike other methods discussed thus far.

The point-discontinuous approach has been used in a grid refinement mode by Berger and Jameson (1984), Baker et al. (1985), Holst et al. (1985), and Eriksson (1985) wherein a global coarse mesh is selectively refined in "high action" regions (usually by the subdivision of a single coarse grid cell into several fine grid cells). However, it may still be a difficult and time-consuming task to generate the initial coarse grid. Nevertheless, localized patching provides the desired resolution in important areas of the flow.

A more general point-discontinuous, patched grid scheme (fig. 1c) allows for independent discretization of each subregion or zone; often undesirable mesh singularities may be completely avoided. If the zones are judiciously chosen to be rather simple regions, existing grid generation techniques (often algebraic) can be used. As with overlapping grid systems, special boundary procedures must be developed to handle the mismatch of grid lines at the zonal interfaces. Cambier et al. (1984) and Veuillot and Cambier (1984) introduce a characteristic boundary method for patching two-dimensional, point-discontinuous grids. Because their procedure is nonconservative in nature, they have fit the shock waves in transonic flow computations. The resulting solutions are smooth and continuous across the patch boundaries. Bush (1985) also uses a characteristic (and therefore nonconservative) patching method in two dimensions to compute the flow about an external compression

inlet.

Rai (1986) outlines a fully conservative treatment of zonal boundaries for two dimensional Euler equation computations on discontinuous, patched grid systems. Success with this method has been clearly demonstrated in the solution of both steady-state and time-dependent problems (two-dimensional rotor-stator interactions) in subsonic and supersonic flows (Hessenius and Rai, 1986; Rai, 1985a; Rai, 1985b; Rai, 1985c). Discontinuities move freely through the grid interfaces to assume their proper locations, a consequence of the conservative nature of the scheme, and the solution is continuous across these boundaries.

Rai's approach to patched grid computations has the desired qualities of a zonal scheme. By subdividing the flow field into well-shaped regions or zones, grid generation for complex geometries is greatly simplified and may be accomplished with existing techniques. The zones permit a block-processing approach to computation. The interfacing procedure is shown to be stable and accurate and is fully conservative in the discrete sense.

The purposes of this work are (1) to establish the usefulness of Rai's (1986) technique in the solution of geometrically complex problems in two dimensions, and (2) to extend the zonal scheme for use in three dimensions and demonstrate the procedure with a multiple-body application. To this end, Chapter 2 contains a review of the two-dimensional method as outlined by Rai (1986), while Chapter 3 presents computational results for flow about a double-airfoil configuration using two different patched grid systems. The development of the three-dimensional technique comprises Chapter 4. Demonstration computations of flow about a wing-canard combination are contained in Chapter 5. Concluding remarks and recommendations for further study are given in Chapter 6.

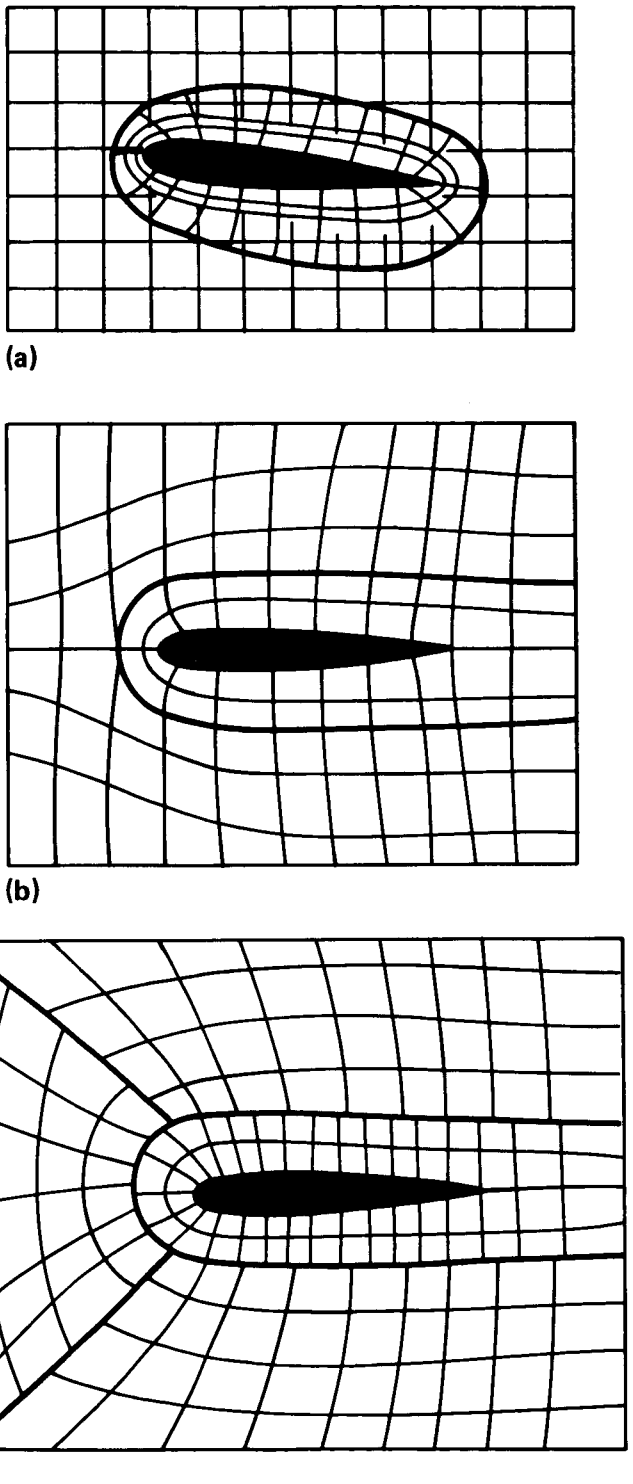

Fig. 1 Block approaches to grid generation (a) overlapping
(b) patched: point-continuous (c) patched: point-discontinuous

CHAPTER 2

REVIEW OF RAI'S TWO-DIMENSIONAL PATCHED GRID SCHEME

Rai's (1986) technique permits the patching together of subgrids to form a global, two-dimensional grid (see fig. 1c). Neighboring subgrids share a common "zonal" boundary (a coordinate line), but along this boundary the grids may be point discontinuous. The proper treatment of the zonal-boundary points is crucial to the maintenance of a conservative, accurate, and stable computation. Rai's method ensures global conservation of mass, momentum, and energy in a discrete sense at the zonal interface. (A scheme is globally conservative if a summation of the fluxes throughout the flow field results in a sum of only the boundary fluxes (i.e., all interior fluxes cancel) with no residual fluxes at a zonal interface.)

This technique (Rai, 1986) is developed within an explicit, first-order accurate (in time and space), finite-difference framework for the Euler equations and will be outlined as such in this chapter. However, the method has been extended for use with second-order accurate, implicit integration schemes (Rai, 1985).

Consider the patched grid of figure 2. This two-zone grid, sketched for a supersonic blunt-body application, contains a single zonal boundary along a constant η-coordinate line. Note that across this line (line AB) the grids are discontinuous and created independently.

The method of solution on this patched grid may be considered a three-step process:

1) The interior grid points in zones 1 and 2 are updated by integration of the governing equations in any conventional manner.
2) The zonal-boundary points in one of the two zones are updated using a procedure that guarantees conservation across the boundary. (The choice of the zone to update first does not affect the conservation properties of this method.) For example, if one

chooses to update the zone-2 points on the zonal boundary, the procedure to update point (j,1) (see fig. 2) involves an integration of the governing equations using the flux cell RSTU. Fluxes at sides UR, RS, and ST are available from zone 2. The flux at side UT is determined by an integration of the zone-1 flux distribution along the line CD between points U and T.

3) The solution at points on the zonal boundary in the neighboring zone (in this case, zone 1) is found by interpolating the solution from step 2 along this boundary.

2.1 Solution at Interior Points

The unsteady Euler equations in two dimensions may be written as

$$Q_t + E_x + F_y = 0 \tag{2.1}$$

where

$$Q = \begin{pmatrix} \rho \\ \rho u \\ \rho v \\ e \end{pmatrix} \quad E = \begin{pmatrix} \rho u \\ p + \rho u^2 \\ \rho uv \\ (e+p)u \end{pmatrix} \quad F = \begin{pmatrix} \rho v \\ \rho uv \\ p + \rho v^2 \\ (e+p)v \end{pmatrix}$$

and

$$p = (\gamma - 1)[e - \frac{1}{2}\rho(u^2 + v^2)]$$

(Note that ρ is the density; p the pressure; u and v are the velocity components in the x and y directions, respectively; and e is the total energy per unit volume.) Applying the independent-variable transformation

$$\tau^{(i)} = t$$

$$\xi^{(i)} = \xi^{(i)}(x, y, t) \qquad i = \begin{cases} 1 & \text{for zone 1} \\ 2 & \text{for zone 2} \end{cases}$$

$$\eta^{(i)} = \eta^{(i)}(x, y, t)$$

to equation (2.1) for each zone of figure 2, one obtains the Euler equations in generalized coordinates

$$\tilde{Q}^{(i)}_{\tau^{(i)}} + \tilde{E}^{(i)}_{\xi^{(i)}} + \tilde{F}^{(i)}_{\eta^{(i)}} = 0 \tag{2.2}$$

where

$$\tilde{Q}^{(i)} = Q/J^{(i)}$$

$$\tilde{E}^{(i)}(Q,\xi) = (\xi_t^{(i)}Q + \xi_x^{(i)}E + \xi_y^{(i)}F)/J^{(i)}$$

$$\tilde{F}^{(i)}(Q,\eta) = (\eta_t^{(i)}Q + \eta_x^{(i)}E + \eta_y^{(i)}F)/J^{(i)}$$

$$J^{(i)} = \xi_x^{(i)}\eta_y^{(i)} - \eta_x^{(i)}\xi_y^{(i)}$$

with the following metric identities

$$\xi_x^{(i)} = J^{(i)}y_\eta^{(i)} \qquad \eta_x^{(i)} = -J^{(i)}y_\xi^{(i)}$$

$$\xi_y^{(i)} = -J^{(i)}x_\eta^{(i)} \qquad \eta_y^{(i)} = J^{(i)}x_\xi^{(i)}$$

$$\xi_t^{(i)} = -x_\tau^{(i)}\xi_x^{(i)} - y_\tau^{(i)}\xi_y^{(i)} \qquad \eta_t^{(i)} = -x_\tau^{(i)}\eta_x^{(i)} - y_\tau^{(i)}\eta_y^{(i)}$$

A conservative finite-difference scheme for integrating equation (2.2) is given by

$$\frac{\tilde{Q}^{(i)^{n+1}} - \tilde{Q}^{(i)^n}}{\Delta\tau^{(i)}} + \frac{\hat{E}^{(i)}_{j+1/2,k} - \hat{E}^{(i)}_{j-1/2,k}}{\Delta\xi^{(i)}} + \frac{\hat{F}^{(i)}_{j,k+1/2} - \hat{F}^{(i)}_{j,k-1/2}}{\Delta\eta^{(i)}} = 0 \qquad (2.3)$$

where $\hat{E}_{j+1/2,k}$ and $\hat{F}_{j,k+1/2}$ are numerical fluxes consistent with the transformed fluxes $\tilde{E}$ and $\tilde{F}$. An evaluation of the numerical fluxes $\hat{E}$ and $\hat{F}$ at time-level n in updating $\tilde{Q}^n$ to $\tilde{Q}^{n+1}$ would characterize an explicit finite-difference scheme. The following discussion assumes the use of such a scheme.

The interior points of both zones 1 and 2 (fig. 2) are explicitly updated using equation (2.3) with centrally differenced metric terms. Points along the zonal boundary are updated as outlined in the following section.

2.2 Solution at the Zonal Boundary

Consider the point (j,1) of zone 2 on the zonal interface and its associated cell area, RSTU (fig. 2). (Note that the fluxes in eq. (2.3) are defined at half points and are, therefore, evaluated at cell sides SR, ST, TU, and RU.) This cell area is found by an extrapolation of the coordinate lines of region 2 to a previously determined flux-balance line (labeled CD) in the neighboring zone 1. The flux balance line is chosen halfway between the last two constant η-coordinate lines in zone 1. The metrics at the point (j,1)

are then defined

$$
\begin{aligned}
(x_\xi)_{j,1} &= \frac{1}{2\Delta\xi}(x_{j+1,1} - x_{j-1,1}) \\
(y_\xi)_{j,1} &= \frac{1}{2\Delta\xi}(y_{j+1,1} - y_{j-1,1}) \\
(x_\eta)_{j,1} &= \frac{1}{\Delta\eta}(x_{j,3/2} - x_{j,1/2}) \\
(y_\eta)_{j,1} &= \frac{1}{\Delta\eta}(y_{j,3/2} - y_{j,1/2})
\end{aligned}
\tag{2.4}
$$

Metrics at cell sides (half points) are obtained by averaging the above expressions between neighboring grid points.

Three of the required four fluxes necessary to update the point (j,1) of zone 2 using equation (2.3) are constructed using only zone-2 information. The ξ-direction fluxes ($\hat{E}_{j-1/2,1}$ and $\hat{E}_{j+1/2,1}$ through cell sides RU and ST, respectively) are formed using the metrics x_η and y_η at the half points and values of the dependent variables at points (j-1,1), (j,1), and (j+1,1). The η-direction flux $\hat{F}_{j,3/2}$ through cell side SR is computed using the ξ-difference metrics (at half points) and values of the dependent variables at points (j,1) and (j,2). Thus far, this is the standard procedure for updating interior points as well. However, the flux into the region 2 cell at point (j,1) from region 1 (the $\hat{F}_{j,1/2}$ term) must be conservatively interpolated from known zone-1 information in the following manner.

First, one constructs the numerical flux in zone 1 at all points along the flux balance line using values of the dependent variables in zone 1 along the last two constant η-coordinate lines and zone-1 metrics. These fluxes are then divided by an appropriate unit of length, the metric corresponding to a zone-1 cell side along the balance line, to create flux per unit length. The unit of length for zone-1 point l is best thought of and computed as the arc length along the balance line between $l + 1/2$ and $l - 1/2$. Then assuming a piecewise-constant variation of the zone-1 numerical flux along the flux balance line (see fig. 3; l points (•) are from zone 1 and j points (x) are from zone 2), one obtains the flux into the zone-2 zonal-boundary cell by an integration of the zone-1 flux distribution along the appropriate portion of the flux-balance line. (Consider s a running parameter

along this line: increasing s with increasing ξ.) Therefore, the flux from zone 1 into the cell RSTU (fig. 2) is computed by integration along the balance line of the zone-1 flux per unit length from s = U to s = T. This flux may be expressed as

$$\begin{aligned}\hat{F}^{(2)}_{j,1/2} &= \int_U^T \frac{\hat{F}^{(1)}_l}{[s^{(1)}_{l+1/2} - s^{(1)}_{l-1/2}]} ds \\ &= [s^{(2)}_{j+1/2} - s^{(2)}_{j-1/2}] \sum_{l=p}^{q} N_{j,l} \frac{\hat{F}^{(1)}_l}{[s^{(1)}_{l+1/2} - s^{(1)}_{l-1/2}]}\end{aligned} \tag{2.5}$$

where the $N_{j,l}$ values are interpolation coefficients that note the dependence of the flux at the jth point (zone 2) on the lth point flux (zone 1) and

$$\sum_{l=p}^{q} N_{j,l} = 1$$

Once the necessary flux from the adjacent zone is determined, the zonal-boundary points of zone 2 may then be updated by solution of equation (2.3). Values of the dependent variables in zone 1 at the zonal boundary are obtained by linearly interpolating the newly obtained zone-2 solution along the boundary, thus ensuring a continuity of the solution across the zonal interface.

Global conservation is maintained identically in the discrete sense with the above procedure. Flux conservation across the flux-balance line CD (see fig. 2) requires the satisfaction of the following equation (from Rai, 1986)

$$\begin{aligned}&\frac{1}{2}(\hat{F}^{(2)}_1 + \hat{F}^{(2)}_{JMAX}) + \sum_{j=2}^{JMAX-1} \hat{F}^{(2)}_j \\ =&\frac{1}{2}(\hat{F}^{(1)}_1 + \hat{F}^{(1)}_{LMAX}) + \sum_{l=2}^{LMAX-1} \hat{F}^{(1)}_l\end{aligned} \tag{2.6}$$

(As before, j points are zone-2 points extrapolated to the balance line and l points are zone-1 points along this line.) As noted by Rai (1986), the left and right sides of equation (2.6) are but discrete forms of the line integral of the numerical flux $\hat{F}$ along the flux-balance line with zone-2 and zone-1 points, respectively. The equating of the two discrete integrals

represents conservation of flux across the balance line and hence the zonal boundary. Equation (2.6) does not uniquely define the unknown $\hat{F}_j^{(2)}$, however. Equation (2.5) may be shown to satisfy the above statement of global conservation while uniquely specifying these fluxes.

The zonal scheme is not restricted to problems with simple, two-zone interfaces as in figure 2, but instead may be used on patched grids with an arbitrary number and placement of zonal boundaries. Consider, for example, the six-zone grid for the computation of flow about a double-airfoil configuration (fig. 4). This grid is complicated by the intersection of zonal boundaries (e.g., point A). Zonal-interface points near these intersections require careful attention to strictly maintain conservation; often the flux cells associated with these points have six or more sides.

Treatment of these unusual cells may be explained with reference to figure 5. The flux cells depicted here (denoted by dashed lines and bounded on at least one edge by a flux-balance line) are typical of those found near the zonal-boundary intersections in the grid of figure 4, where zones 1, 2, and 3 or zones 4, 5, and 6 meet. Note that for the given choice of flux-balance lines, one zonal-boundary cell is constrained to be six-sided. (Points along zonal boundary AA in zone 3 and zonal boundary BB in zone 1 are updated by the integration of eq. (2.3) using the flux cells as shown, whereas points along these boundaries in zone 2 are interpolated from this solution.) To update point K of zone 3, the $\hat{E}_{j+1/2,k}$, $\hat{E}_{j-1/2,k}$, and $\hat{F}_{j,k-1/2}$ fluxes are obtained as usual, using the cell sides EF, BA, and FA, respectively, with metrics such as

$$x_\eta = (x)_E - (x)_F \qquad for \qquad \hat{E}_{j+1/2,k}$$

$$x_\xi = (x)_F - (x)_A \qquad for \qquad \hat{F}_{j,k-1/2}$$

However, $\hat{E}_{j-1/2,k}$ must be modified to $\hat{E}^*_{j-1/2,k}$ to include the flux through side DC by adding an integration along the flux-balance line from C to D.

$$\hat{E}^*_{j-1/2,k} = \hat{E}_{j-1/2,k} + \int_C^D \frac{\hat{E}_l}{[s_{l+1/2} - s_{l-1/2}]} ds$$

Similarly, the flux $\hat{F}_{j,k+1/2}$ is the sum of two terms, each term an integration of fluxes along a different flux-balance line

$$\hat{F}_{j,k+1/2} = \int_B^C \frac{\hat{F}_m}{[s_{m+1/2} - s_{m-1/2}]} ds + \int_D^E \frac{\hat{F}_n}{[s_{n+1/2} - s_{n-1/2}]} ds$$

(The subscripts l,m, and n are running indices along the flux-balance lines.) Given these flux definitions, point K may now be explicitly updated using equation (2.3).

The patched grid approach allows independent grid generation in each zone. This flexibility may result in meshes with discontinuous grid lines or grid-line slopes or both at zonal boundaries. Slope or metric discontinuities require attention for accuracy reasons. Consider the points along the symmetry line in the grid of figure 4. One such flux cell is sketched in figure 6. Although there is grid-point continuity between the two zones (and therefore no need for special flux interpolations), the use of the standard central-differencing technique for evaluating the metrics in the η-direction leads to inaccuracies. (Depending on the chosen numerical method, numerical flux may be a nonlinear function of the slope of the grid lines.) A recommended treatment of these cells is to consider them as six-sided and to compute fluxes through each face, using metrics appropriate to each side (BA, CB, DC, DE, EF, and FA). This idea is also used in conjunction with point-discontinuous boundaries.

2.3 Summary of Scheme Properties

The results presented by Rai (1986) and in other publications (Hessenius and Rai, 1986; Rai, 1985a; Rai, 1985b; Rai, 1985c) illustrate the favorable properties of this patched grid scheme. Solution discontinuities, such as shock waves and contact surfaces, will move smoothly through grid interfaces with minimal distortion to assume their proper location and strength, a direct consequence of the conservative nature of the scheme. Solution contours are smooth and continuous across the zonal boundaries. The procedure is nu-

merically stable despite the transition of strong discontinuities from zone to zone. Also, vortices are shown to move freely through zonal interfaces without distortion (Rai, 1985).

As reported by Rai (1986), the zonal-boundary flux interpolation (eq. (2.5)) is not perfectly free-stream preserving. However, the drift in the dependent variables near the zonal boundary when integrating free-stream conditions (without boundary conditions) is due to a term that is second-order in magnitude and is proportional to the curvature of this boundary. Hence, the departure from free stream may be lessened by increasing the number of grid points along a curved zonal boundary. Rai reports free-stream drifts in density of only 0.1% after repeated integrations on a grid such as that of figure 2.

The references cited in the preceding paragraphs describe extensions of this two-dimensional method for use with second-order accurate, implicit integration schemes. The zonal boundary condition can also be made time-accurate, a necessity for predicting flow fields in which zones move with respect to one another such as in a zonal computation of flow about a helicopter rotor/fuselage.

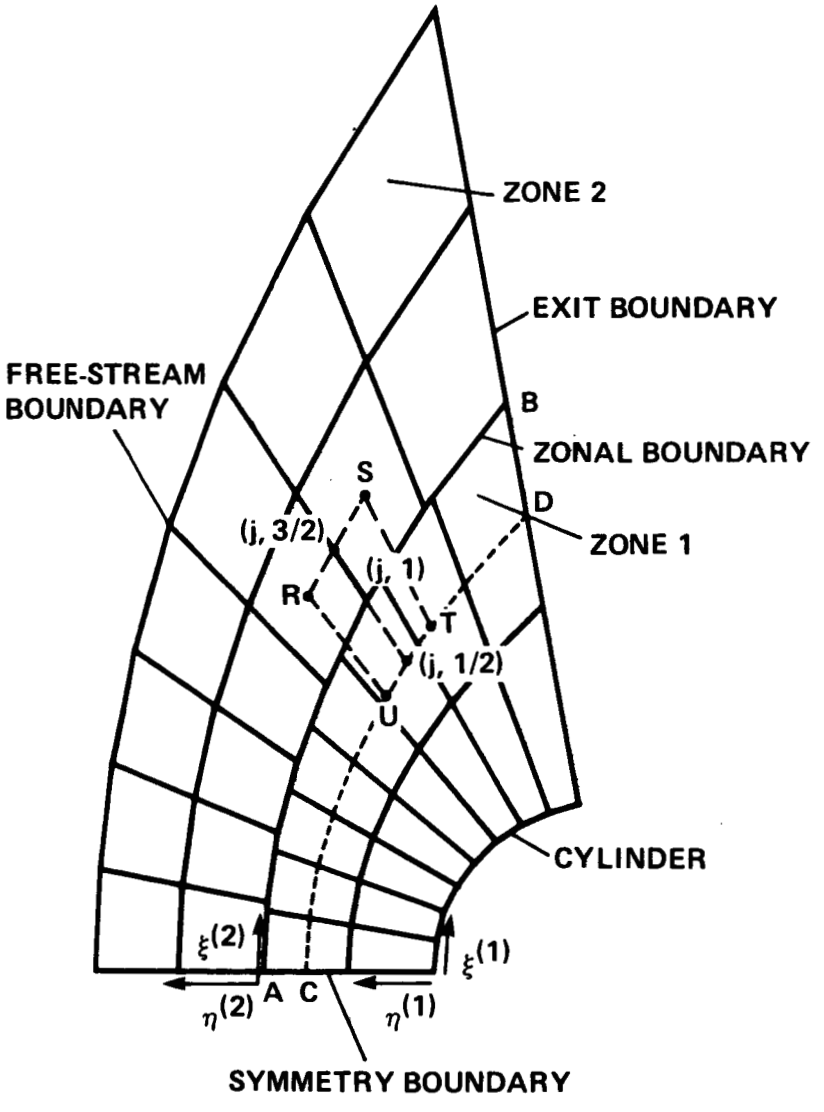

Fig. 2 Two-zone grid illustrating zonal scheme in curvilinear coordinates

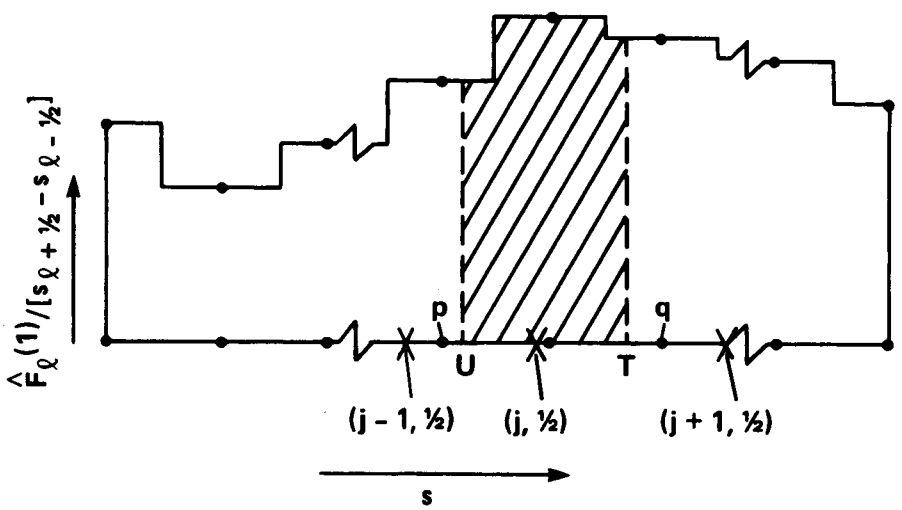

Fig. 3 Piecewise-constant variation of the numerical flux $\hat{F}$ as a function of s.

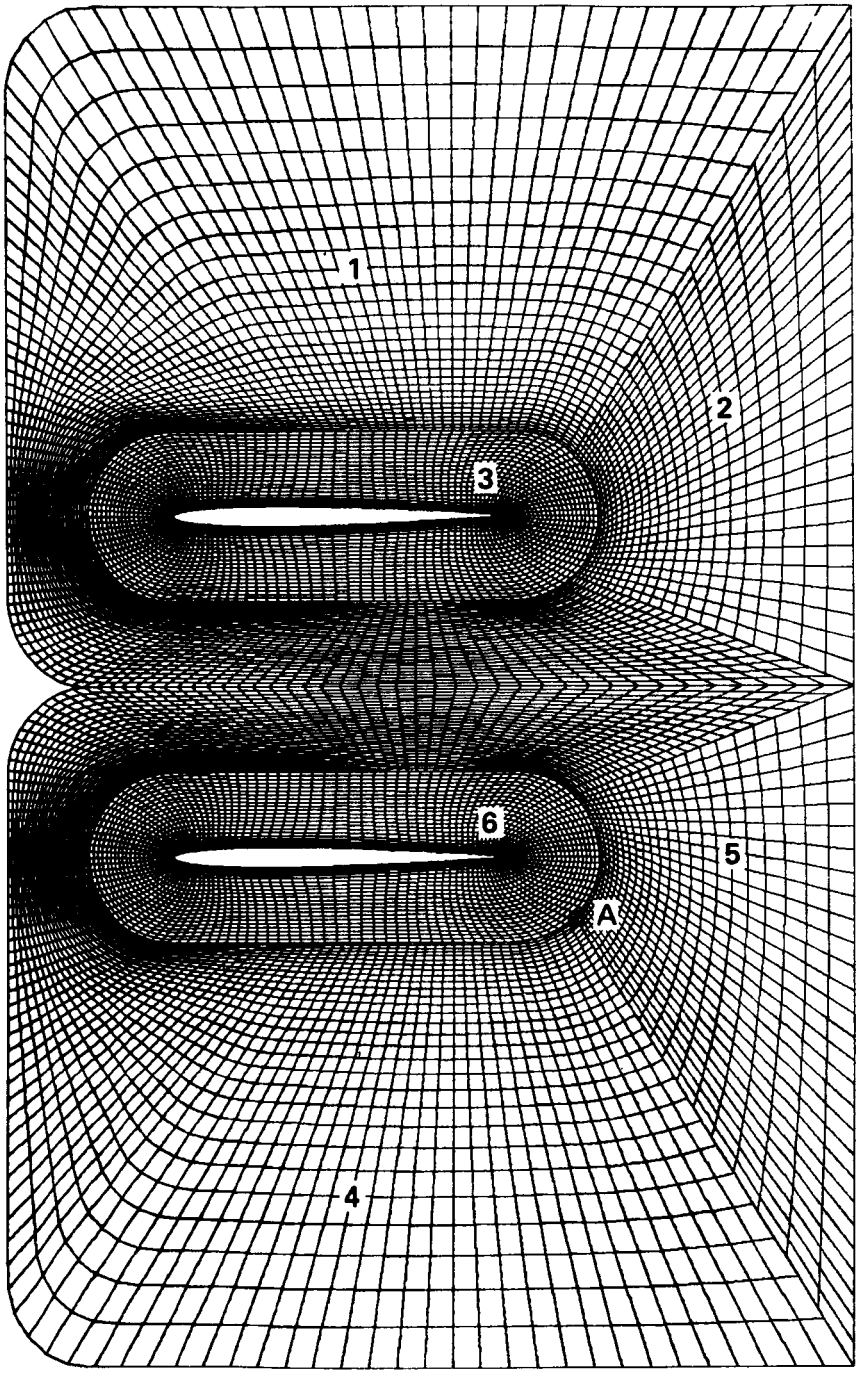

Fig. 4 Six-zone grid for a double airfoil configuration

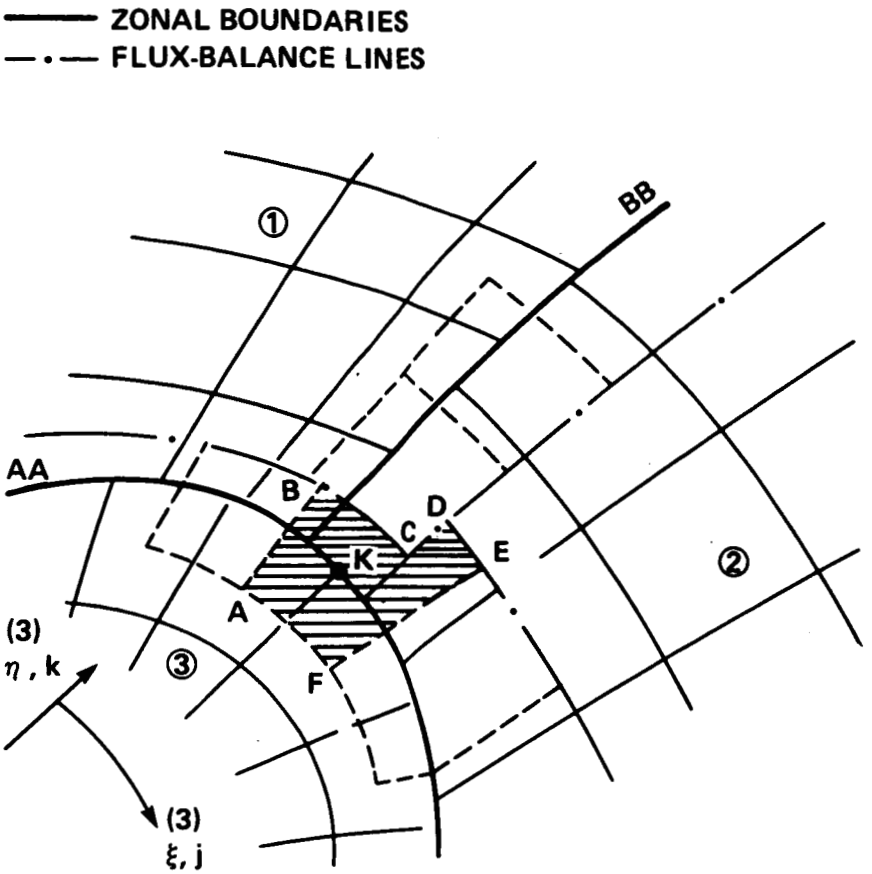

Fig. 5 Flux cells near the intersection of zonal boundaries.

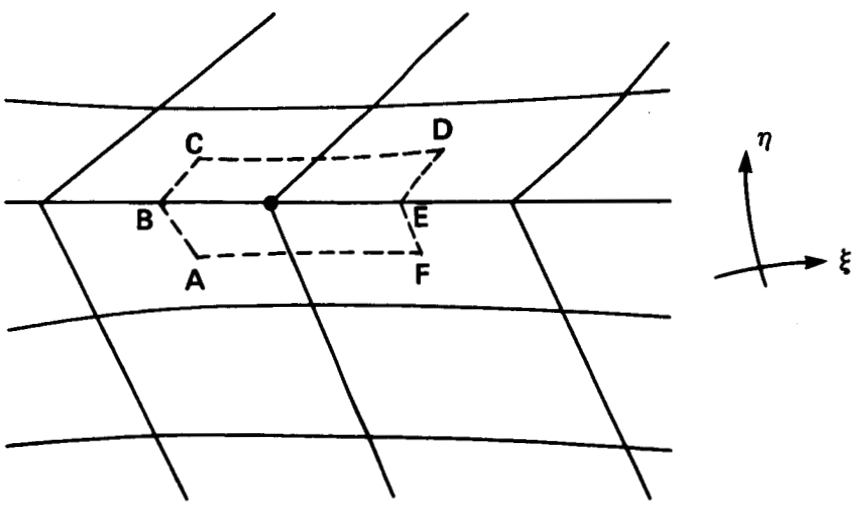

Fig. 6 Flux cell near a metric discontinuity

CHAPTER 3

APPLICATIONS OF RAI'S TWO-DIMENSIONAL PATCHED GRID SCHEME

Rai's results (1986) clearly indicate the feasibility of using a conservative grid-patching scheme in the numerical simulation of fluid flow. This chapter contains a validation of Rai's zonal blunt body computation and a first demonstration of the usefulness of this patched grid method in the solution of geometrically complex problems.

3.1 Zonal Blunt-Body Computation

To substantiate the results of Rai (1986) and to validate a newly developed two-dimensional Euler code, the supersonic flow about a blunt body (as depicted in fig. 2) was computed at a free-stream Mach number of 2.0. The numerical procedure used at interior points and at the zonal boundary was described in Chapter 2. Equation (2.3) was integrated to convergence using the first-order accurate, explicit, split-flux scheme of Steger and Warming (1981). The numerical fluxes $\hat{E}$ and $\hat{F}$ for the Steger and Warming scheme may be written as

$$\begin{aligned} \hat{E}_{j+1/2,k} &= \tilde{E}^{-}(Q_{j+1,k}) + \tilde{E}^{+}(Q_{j,k}) \\ \hat{F}_{j,k+1/2} &= \tilde{F}^{-}(Q_{j,k+1}) + \tilde{F}^{+}(Q_{j,k}) \end{aligned} \tag{3.1}$$

where

$$\tilde{E}^{+} = \left(\frac{\partial \tilde{E}}{\partial \tilde{Q}}\right)^{+} \tilde{Q}$$

$$\tilde{E}^{-} = \left(\frac{\partial \tilde{E}}{\partial \tilde{Q}}\right)^{-} \tilde{Q}$$

and $\tilde{Q}$, $\tilde{E}$, and $\tilde{F}$ are defined in equation (2.2). The flow field was initialized with free-stream conditions everywhere. Flow tangency was enforced at the cylinder boundary, and a reflection principle was used to enforce symmetry along the lower boundary (see fig. 2). The free-stream boundary was held fixed throughout the computation; the supersonic

exit boundary was naturally treated with purely backward ξ-differences by the split-flux formulation.

Computations were performed on the patched, two-zone grids of figures 7a and 8a. The zonal interface in the grid of figure 8a was designed to coincide with the converged shock location. In the transient solution, a bow shock forms at the body and moves leftward (through the zonal interface in fig. 7a) to its steady-state position. The converged results of figures 7b and 8b (pressure contours) are typical of first-order accurate computations of this flow. As in Rai's calculations for this same flow, the captured shock lies slightly to the left of the converged shock location of Lyubimov and Rusanov (1973) (shown as square symbols in these figures). Note the smoothness of the contours across the zonal boundary despite the discontinuity in grid lines. No convergence problems were found with either computation. These results are of identical quality to those of Rai (1986).

3.2 Applications to Geometrically Complex Problems

The ability of the patched grid method to simplify grid generation about complex topologies, and in doing so, to easily enable grid refinement in selected regions is demonstrated in the zonal solution of a multiple-body problem. A four-zone solution was computed about a double-airfoil configuration (both NACA 0006 airfoils); the grid is shown in figure 9. With the addition of appropriate source terms in the governing equations for axisymmetric flow, this calculation could represent flow about a hollow projectile or an axisymmetric cowl, as is the case studied by Nietubicz et al. (1979). (The results presented here are two dimensional, however.) Unlike that of Nietubicz et al., grid generation for the problem was a relatively simple task. An elliptic grid generator was used to obtain the meshes in zone 1 and zone 3 (zones 2 and 4 are merely reflections of 1 and 3, respectively). The use of a C mesh about the airfoils avoids the introduction of an H-grid singularity at the leading edge. The subregional meshes were then patched together to form a global grid. Note the discontinuity of grid lines along the zonal boundaries between regions 1 and 3 and regions 2 and 4 (fig. 9b).

The computational results for the flow about the two-airfoil configuration were obtained by integrating equation (2.3) to convergence using the first-order-accurate, explicit Osher scheme with numerical flux defined as (from Chakravarthy and Osher, 1982)

$$\hat{E}_{j+1/2,k} = \tilde{E}_{j+1,k} - \int_{Q_{j,k}}^{Q_{j+1,k}} \left(\frac{\partial \tilde{E}}{\partial Q} \right)^{+} dQ$$
$$\hat{F}_{j,k+1/2} = \tilde{F}_{j,k+1} - \int_{Q_{j,k}}^{Q_{j,k+1}} \left(\frac{\partial \tilde{F}}{\partial Q} \right)^{+} dQ \qquad (3.2)$$

As in the blunt-body computations, the dependent variables were initially set equal to free-stream values. The inflow and upper/lower boundaries were fixed at free-stream conditions. Tangency was enforced along the airfoil surfaces, and the supersonic flow at the downstream exit boundary was properly treated with backward differences of the governing equations.

Converged pressure contours are presented in figure 10 for the flow about the double-airfoil configuration at free-stream Mach number of 1.5 and zero angle of attack. The two bow shocks upstream of the airfoils are apparent in figure 10. These shocks intersect in the region between the airfoils and are very quickly dissipated thereafter by the expansion waves that are generated by the surface curvature of the airfoils. The flow then expands to a pressure minimum in this "nozzle" region and approaches free-stream conditions at the outflow boundary. Note that the contours are continuous across the zonal boundaries (shown as dashed lines), even in shock regions. The smoothness of the contour lines is a result of the conservative nature of the scheme and the enforcement of continuity in interpolating values at the zonal boundary.

The choice of the grid system shown in figure 9 is an arbitrary one. It is possible to zone a flow field in a number of different ways and obtain results, but as in any computation, there are usually advantages of one grid over another. The grid system of figure 9 is preferred for this computation. The C mesh provides the best treatment of the airfoil trailing-edge, the wake, and the nozzle region because of the orthogonality of the grid. This system has additional advantages in that it minimizes the number of zones and it provides

simple, two-zone interfaces. Nevertheless, one may wish to use a different patched-grid system for the same problem, such as that of figure 11. Again, the airfoils are contained within body-conforming meshes (this time O grids) which are easily generated with an elliptic grid generator (GRAPE, from Sorenson, 1980). The meshes in the remaining regions are simply generated algebraically. Pressure contours for this grid are shown in figure 12 (identical contour levels are plotted in figs. 10 and 12). The same flow-field features are apparent in figure 12, with a pressure maximum behind the bow-shock intersection and an overexpansion in the nozzle region before returning to free-stream conditions. Again, the contour lines pass smoothly through the zonal boundaries. (An occasional mismatch of contour lines may be observed at zonal boundaries. The interpolation technique in the contour-plotting routine is different from the interpolation procedure used at the zonal boundary; hence, small errors may arise in plotting.)

As expected, only qualitative comparisons may be made between the first-order results of the two zonal grid systems. Close quantitative agreement would require second-order-accurate computations which are less grid dependent. The six-zone results (fig. 12), although believed to be inferior to those shown in figure 10 because of the metric discontinuities and cell skewness in the grid of figure 11, are included to demonstrate the capability of the zonal scheme to produce stable and smooth solutions given an arbitrary zoning of the flow field.

3.3 Other Possible Two-Dimensional Applications

The difficulty in generating a single grid for regions about complicated configurations is alleviated with the patched grid technique. The use of this technique is now described in the case of two other complex, two-dimensional problems of current interest.

The flow about a tri-element airfoil, or "augmentor wing" airfoil, has been computed by several researchers (Lasinski et al., 1982; Flores et al., 1984). Although a type of zoning was employed by Lasinski et al. (1982), the coordinate lines of the grid were still required to be continuous across zonal interfaces. This restriction resulted in the introduction of

grid singularities in the flow field (also the case in Flores et al., 1984), as well as a reduction in clustering and spacing control. The ability of the patched grid method to interface grids that are discontinuous across zonal boundaries permits the use of a grid system such as that of figure 13. The grids in each zone can be individually generated using algebraic or elliptic grid generators. Zones may also be refined at will, with no continuity restrictions at zonal boundaries.

Another candidate for the zonal approach using discontinuous grids is shown in figure 14. The dual-throat nozzle problem (further described by Chakravarthy, 1981) requires a fine mesh in zone 2 to adequately resolve a normal shock. The zoning technique allows for an abrupt refinement in this region. Note that the zonal grid for this problem may be obtained using a simple algebraic procedure.

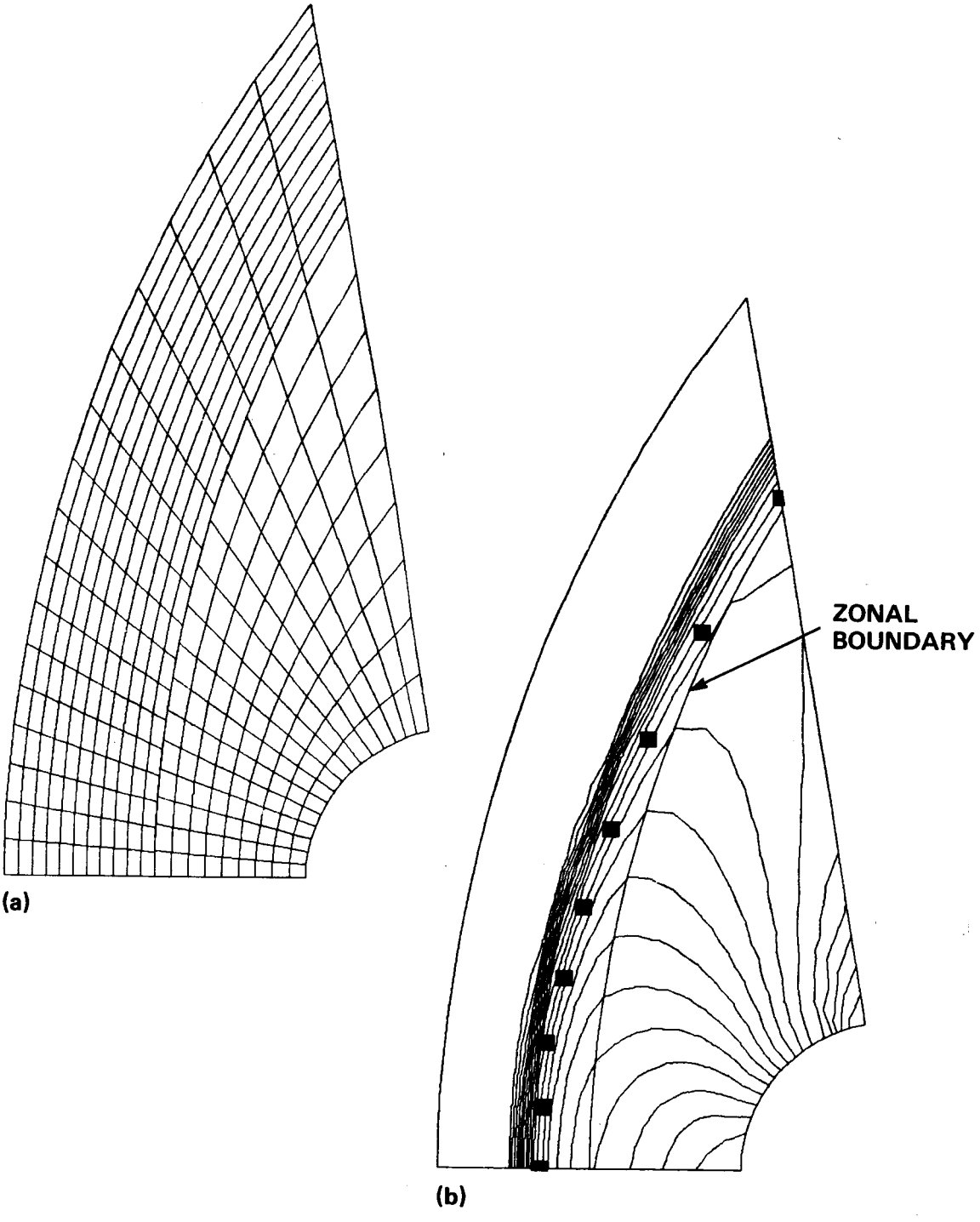

Fig. 7 Results of a two-zone, blunt-body computation
(a) two-zone grid (b) pressure contours at $M_\infty = 2.0$

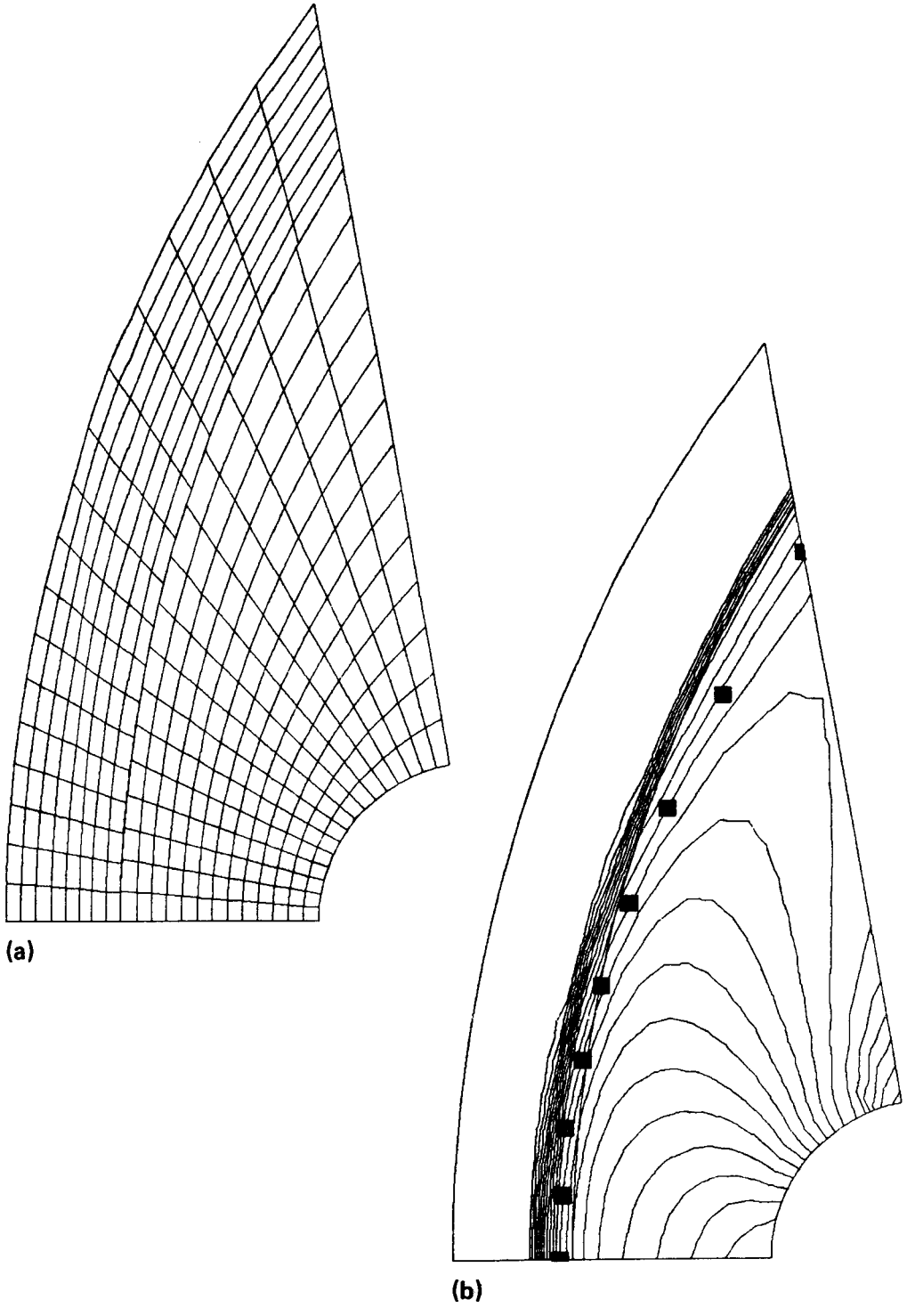

Fig. 8 Results of a two-zone blunt body computation
(a) two-zone grid (b) pressure contours: $M_\infty = 2.0$

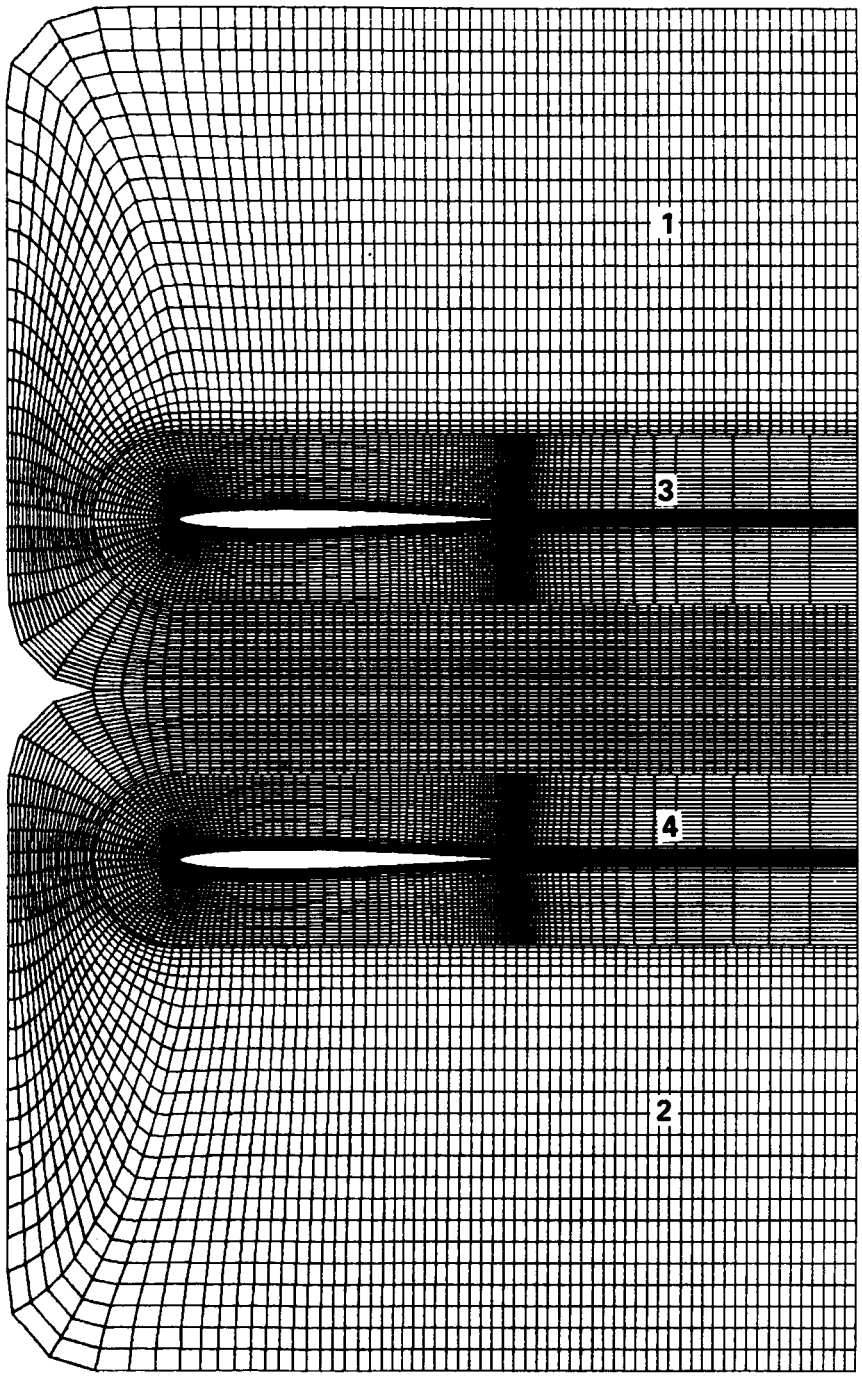

Fig. 9 Four-zone grid for the two-airfoil configuration (a) zones 1-4.

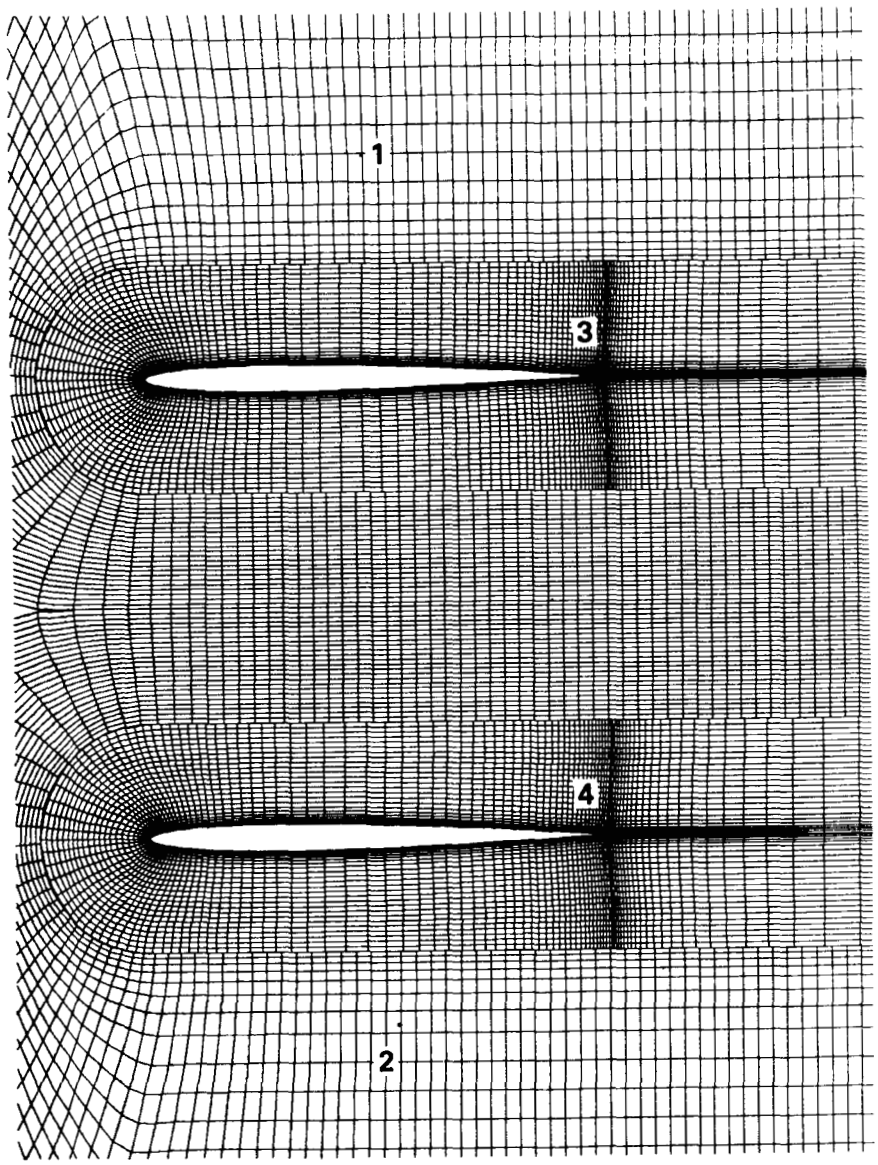

Fig. 9 Four-zone grid for the two-airfoil configuration
(b) enlarged view of zones 3 and 4

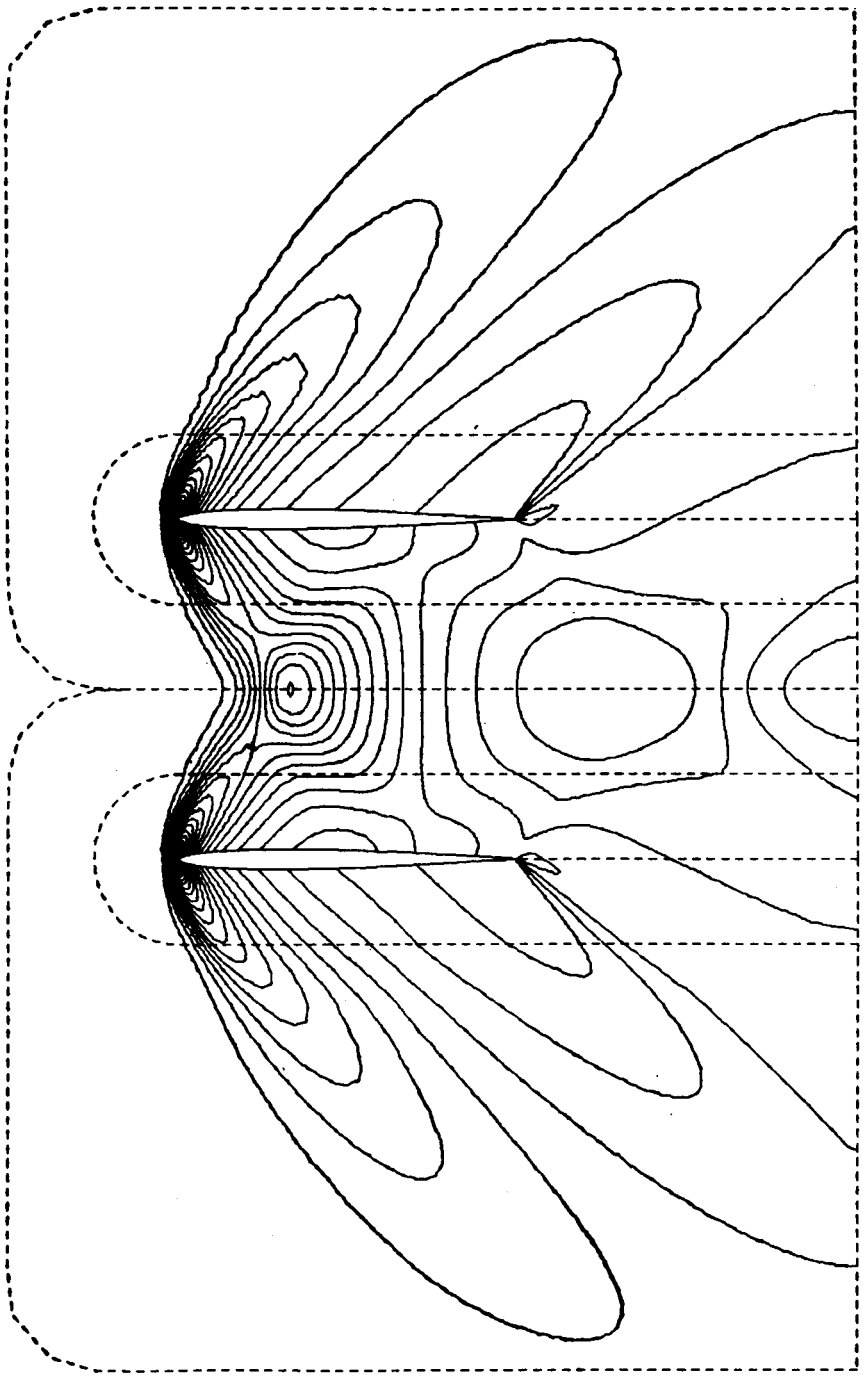

Fig. 10 Pressure contours for supersonic flow about the double-airfoil configuration, computed on the four-zone grid $M_\infty = 1.5$, $\alpha = 0°$

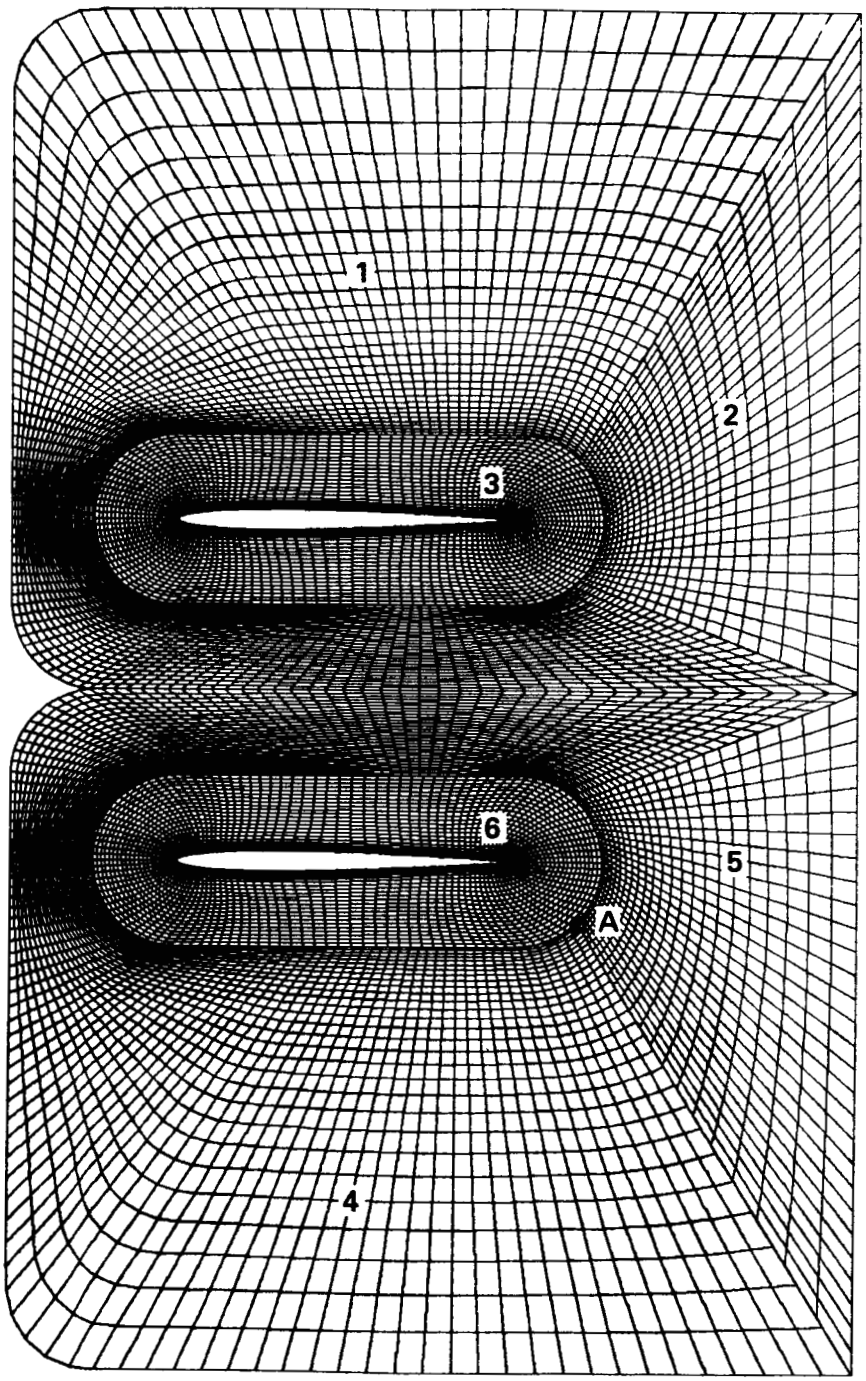

Fig. 11 Six-zone grid for the two-airfoil configuration (a) zones 1-6

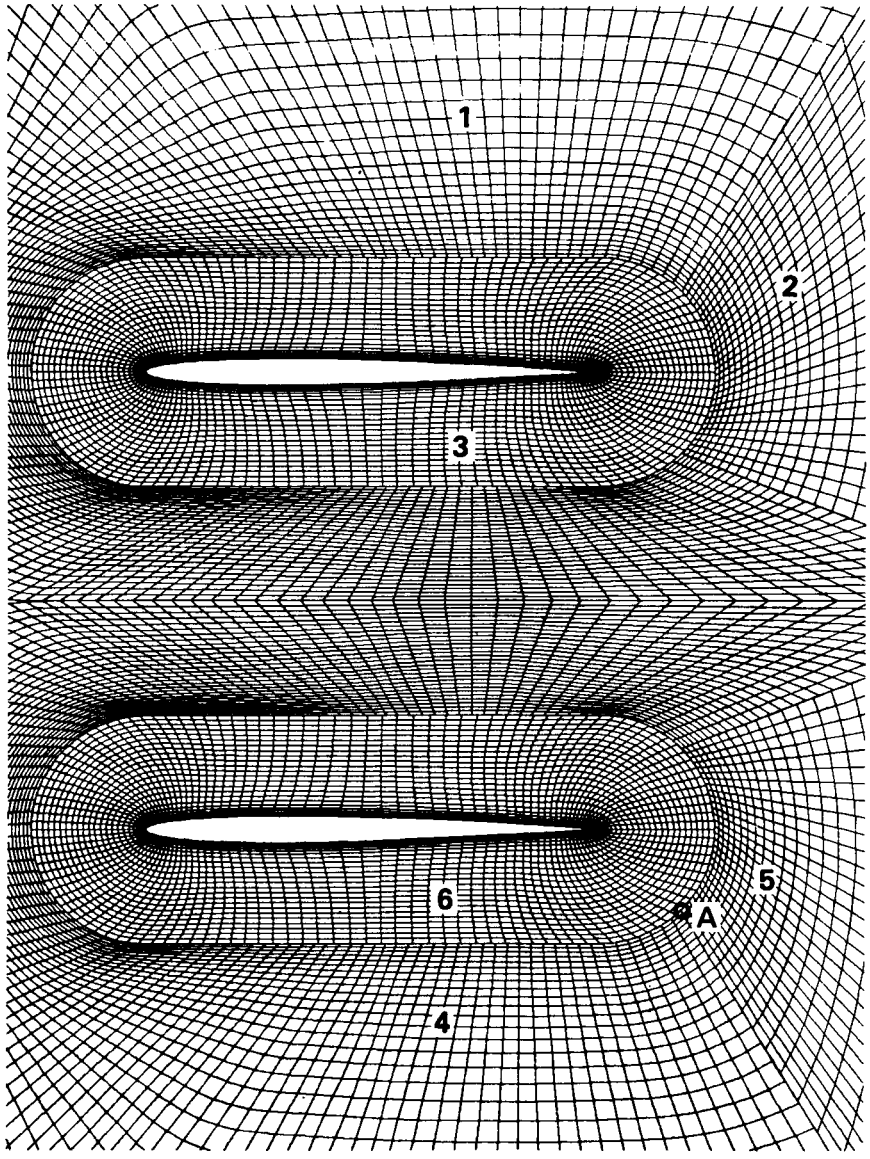

Fig. 11 Six-zone grid for the two-airfoil configuration
(b) enlarged view of zones 3 and 6

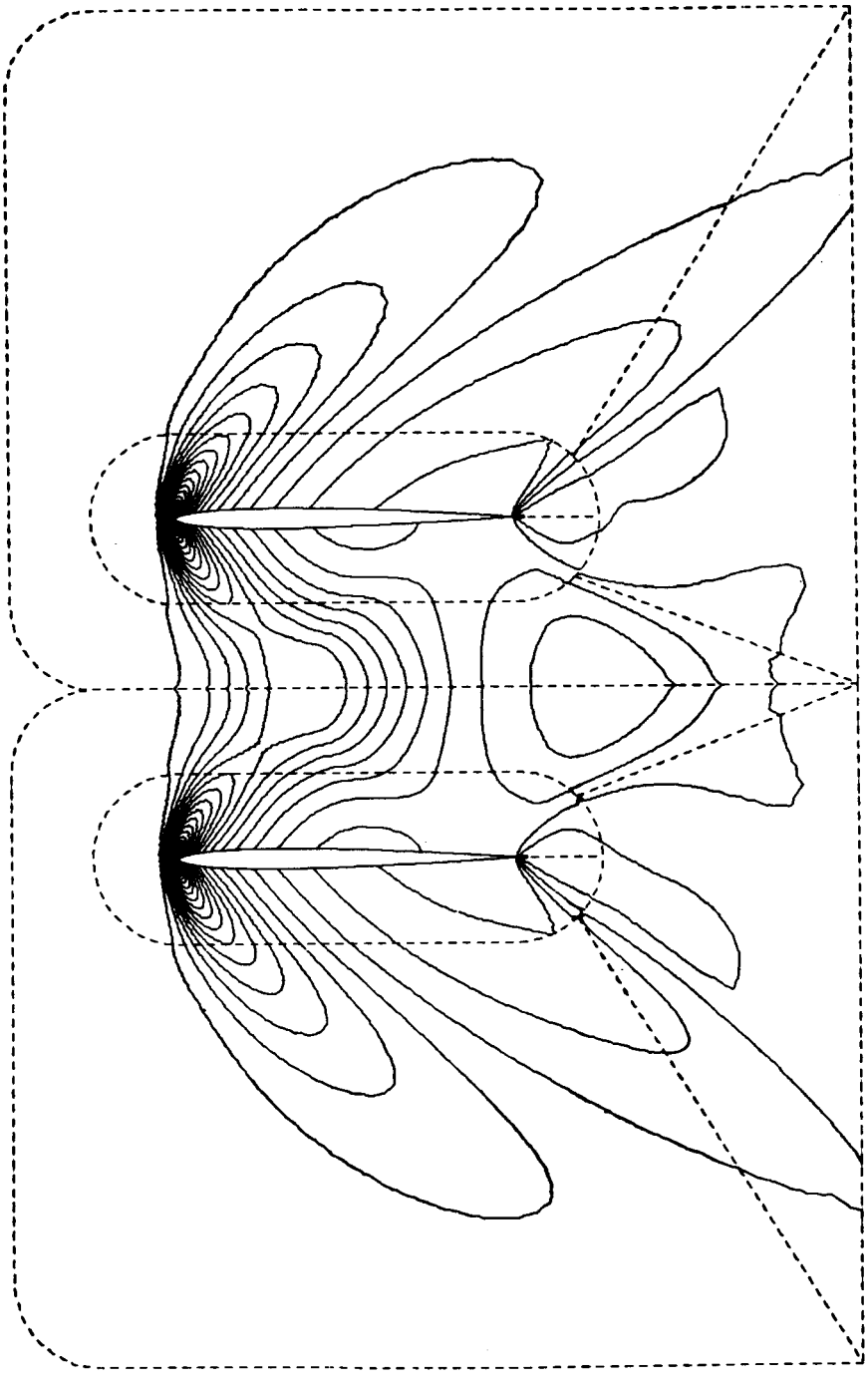

Fig. 12 Pressure contours for supersonic flow about the double-airfoil configuration, computed on the six-zone grid $M_\infty = 1.5$, $\alpha = 0°$

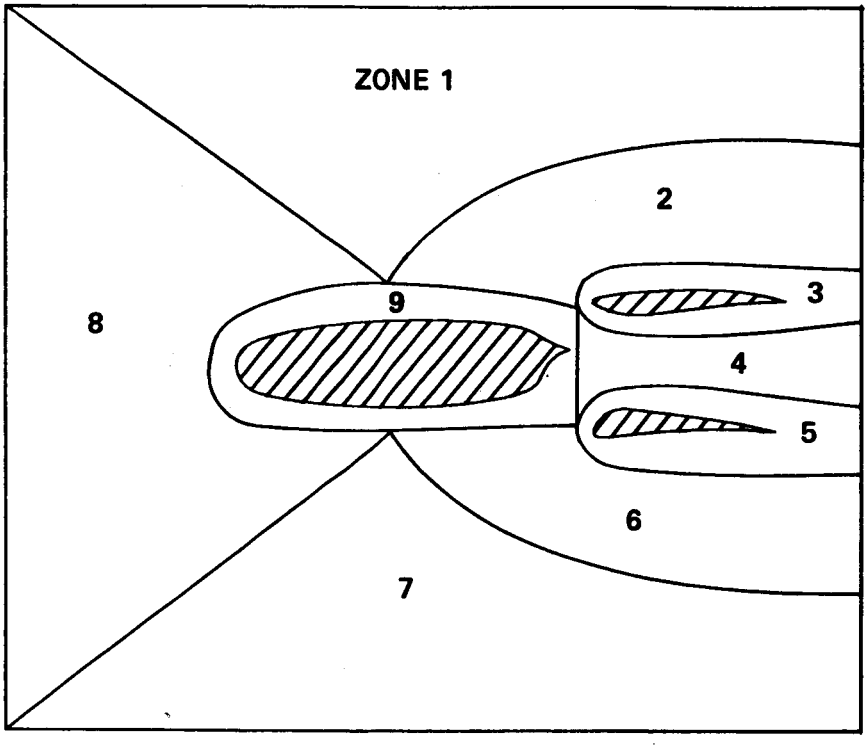

Fig. 13 Zoning suggestion for the "augmentor wing" airfoil configuration

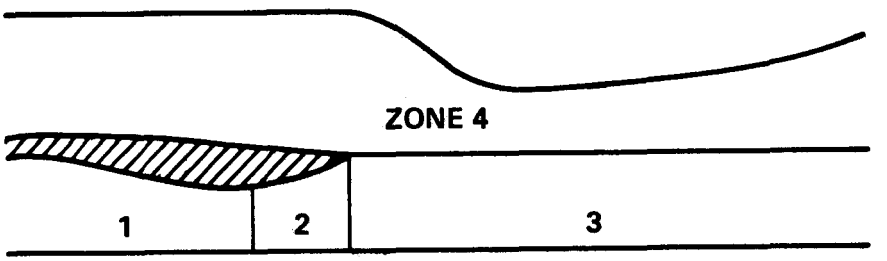

Fig. 14 Zoning suggestion for the dual-throat nozzle problem

CHAPTER 4

DEVELOPMENT OF A THREE-DIMENSIONAL PATCHED GRID SCHEME

As researchers in the field of computational fluid dynamics (CFD) attack problems of increasing geometric complexity, especially in three dimensions, the need arises for a more versatile approach to grid generation than the traditional, single-module type of mesh definition. Consider, for example, the discretization of the flow field about the Space-Shuttle orbiter with external tank and rocket boosters (fig. 15a). Multiple-body problems, such as this one, are challenges using even the most advanced grid-generation techniques given the necessary constraints on grid quality (e.g., smoothness, desired clustering in gradient regions).

The zonal concept simplifies mesh generation by partitioning the flow field into several regions within which grids are independently generated. Consider again the problem depicted in figure 15a and imagine a partitioning of the flow field at cross-section A as in figure 15b. A division of the field into well-shaped, four-sided zones (actually, six-sided blocks for this three-dimensional problem) permits the use of existing grid generation techniques within each zone. The subregional grids could be simply patched together along the specified interfaces. A proposed zoning for cross-section B is shown in figure 15c (this zoning is completely independent of the one shown in fig. 15b, however).

Chapter 2 is a review of a conservative, zonal scheme for patched grids in two dimensions, that is, grids that interface along a curve. (The grid lines may be point-discontinuous at the zonal interface, as shown previously in fig. 1c.) The procedure has been tested in a variety of settings, including the computation of blast-wave diffraction, flow about a double-airfoil configuration, and flow about rotor-stator combinations at both subsonic and supersonic free-stream Mach numbers. Calculations have demonstrated the ability of shocks as well as vortices to pass through zonal interfaces with minimal distortion (Rai,

1986; Hessenius and Rai, 1986; Rai, 1985a; Rai, 1985b; Rai, 1985c).

This two-dimensional patching technique may be readily applied to three-dimensional, parabolic problems where grid generation is performed in two dimensional planes (normal to the body axis), and the solution is obtained by marching downstream in the streamwise coordinate. But a fully three-dimensional, zonal computation using patched grids requires a a division of the flow field into well-proportioned, six-sided blocks. There are three levels of difficulty associated with the implementation of a conservative, three-dimensional scheme for patched grids.

1) The simplest form of patching in three dimensions occurs when a coarse grid is refined in certain regions by the subdivision of coarse grid cells into several fine grid cells. The flux-balancing procedure to ensure conservation at the zonal interface is greatly simplified when integer mesh-cell ratios (zone to zone at the interface) are present.
2) A more general form of patching occurs when arbitrary point distributions are permitted at the interface in each zone. At this level, however, the interface is restricted to be planar in physical space.
3) The most general form of patching is interfacing along an arbitrary (nonplanar) surface with arbitrary point distributions at the zonal interface in each zone.

The focus of this work is on the development of a three-dimensional, globally conservative, boundary scheme for patched grids, applicable in generalized coordinates for arbitrary point distributions on a planar zonal surface (level 2 above). As was done in the original two-dimensional work by Rai (1986), the three-dimensional scheme is derived within the framework of an explicit, first-order method for the solution of the Euler equations. It can then be generalized for second-order accurate, implicit computations as it was in two dimensions (Rai, 1985).

4.1 Three-Dimensional Governing Equations

The unsteady Euler equations in three dimensions may be written as

$$Q_t + E_x + F_y + G_z = 0 \tag{4.1}$$

where

$$Q = \begin{pmatrix} \rho \\ \rho u \\ \rho v \\ \rho w \\ e \end{pmatrix} \quad E = \begin{pmatrix} \rho u \\ p + \rho u^2 \\ \rho uv \\ \rho uw \\ (e+p)u \end{pmatrix} \quad F = \begin{pmatrix} \rho v \\ \rho uv \\ p + \rho v^2 \\ \rho vw \\ (e+p)v \end{pmatrix} \quad G = \begin{pmatrix} \rho w \\ \rho uw \\ \rho vw \\ p + \rho w^2 \\ (e+p)w \end{pmatrix}$$

and

$$p = (\gamma - 1)[e - \frac{1}{2}\rho(u^2 + v^2 + w^2)]$$

Again, ρ is the density; p is the pressure; u, v and w are the velocity components in the x, y, and z directions, respectively; and e is the total energy per unit volume. Applying the independent-variable transformation

$$\tau = t$$

$$\xi = \xi(x, y, z, t)$$

$$\eta = \eta(x, y, z, t)$$

$$\varsigma = \varsigma(x, y, z, t)$$

to equation (4.1), one obtains the Euler equations in generalized coordinates

$$\tilde{Q}_\tau + \tilde{E}_\xi + \tilde{F}_\eta + \tilde{G}_\varsigma = 0 \tag{4.2}$$

where

$$\tilde{Q} = Q/J$$

$$\tilde{E}(Q, \xi) = (\xi_t Q + \xi_x E + \xi_y F + \xi_z G)/J$$

$$\tilde{F}(Q, \eta) = (\eta_t Q + \eta_x E + \eta_y F + \eta_z G)/J$$

$$\tilde{G}(Q, \varsigma) = (\varsigma_t Q + \varsigma_x E + \varsigma_y F + \varsigma_z G)/J$$

with the following metric identities

$$J^{-1} = x_\xi y_\eta z_\varsigma + x_\varsigma y_\xi z_\eta + x_\eta y_\varsigma z_\xi - x_\xi y_\varsigma z_\eta - x_\eta y_\xi z_\varsigma - x_\varsigma y_\eta z_\xi$$

$$\xi_x = J(y_\eta z_\varsigma - z_\eta y_\varsigma) \qquad \eta_x = J(y_\varsigma z_\xi - z_\varsigma y_\xi)$$

$$\xi_y = J(z_\eta x_\varsigma - x_\eta z_\varsigma) \qquad \eta_y = J(z_\varsigma x_\xi - x_\varsigma z_\xi)$$

$$\xi_z = J(x_\eta y_\varsigma - y_\eta x_\varsigma) \qquad \eta_z = J(x_\varsigma y_\xi - y_\varsigma x_\xi)$$

$$\varsigma_x = J(y_\xi z_\eta - z_\xi y_\eta) \qquad \xi_t = -x_\tau \xi_x - y_\tau \xi_y - z_\tau \xi_z$$

$$\varsigma_y = J(z_\xi x_\eta - x_\xi z_\eta) \qquad \eta_t = -x_\tau \eta_x - y_\tau \eta_y - z_\tau \eta_z$$

$$\varsigma_z = J(x_\xi y_\eta - y_\xi x_\eta) \qquad \varsigma_t = -x_\tau \varsigma_x - y_\tau \varsigma_y - z_\tau \varsigma_z$$

An explicit, conservative, finite-difference scheme for integrating equation (4.2) is given by

$$\frac{\tilde{Q}^{n+1} - \tilde{Q}^n}{\Delta\tau} + \frac{\hat{E}^n_{(i+1/2,j,k)} - \hat{E}^n_{(i-1/2,j,k)}}{\Delta\xi} + \frac{\hat{F}^n_{(i,j+1/2,k)} - \hat{F}^n_{(i,j-1/2,k)}}{\Delta\eta} + \frac{\hat{G}^n_{(i,j,k+1/2)} - \hat{G}^n_{(i,j,k-1/2)}}{\Delta\varsigma} = 0 \tag{4.3}$$

where $\hat{E}^n_{i+1/2,j,k}$, $\hat{F}^n_{i,j+1/2,k}$ and $\hat{G}^n_{i,j,k+1/2}$ are numerical fluxes consistent with the transformed fluxes $\tilde{E}$, $\tilde{F}$, and $\tilde{G}$, respectively. The expressions for the numerical fluxes depend on the chosen numerical integration method (discussed in section 4.5).

4.2 Metric Computations for Free-Stream Preservation

The computation of numerical flux requires an evaluation of the following metric quantities: ξ_x/J, ξ_y/J, ξ_z/J for $\hat{E}$ (see eq. (4.2) definition). A proper determination of the metrics is necessary for the maintenance of free-stream conditions in undisturbed areas of the flow. In free-stream regions, the governing equations degenerate to derivatives of metric quantities alone. For example, the continuity, x-momentum, and energy equation become, at free stream, the single expression

$$\partial_\xi(\frac{\xi_x}{J}) + \partial_\eta(\frac{\eta_x}{J}) + \partial_\varsigma(\frac{\varsigma_x}{J}) = 0$$

(Similar equations containing metric derivatives only can be written for the y- and z-momentum equations at free stream.) In three dimensions, simple three-point central

differences in the calculation of the inverse metrics (i.e., y_η, z_ζ, etc.) to construct the needed metrics will not guarantee free-stream preservation on an arbitrary grid; that is, such a metric construction will not satisfy the above equation within acceptable numerical error bounds. The problem arises from the fact that analytical derivative operators are commutative, whereas numerical difference operators are not. In two dimensions, it is fortuitous that central differencing of the inverse metrics will yield perfect preservation of free-stream conditions.

Pulliam and Steger (1978) suggest two possible approaches to metric computation in three dimensions to gain free-stream preservation:

1) employ special weighted averages in the differencing of the inverse metrics such that perfect error cancellation occurs when metrics are differenced in the governing equations at free-stream conditions
2) reformulate the governing equations by subtracting the free-stream fluxes from the original equations.

Kordulla and Vinokur (1983), however, recommend an approach to the problem of metric definition that is consistent with our "control volume" method of solution at zonal-boundary points. In fact, their technique for defining the transformation metrics is standard in finite-volume computations. Their procedure is described in the following paragraph and is adopted in this work.

Consider the computational cell about the point (i,j,k) in figure 16 (cell sides are located halfway between neighboring grid points). The $\hat{E}_{(i+1/2,j,k)}$ flux is the flux through the nonplanar cell face, ABCD. The computation of $\hat{E}$ requires the metrics ξ_x/J, ξ_y/J, and ξ_z/J which can be interpreted as the $\hat{i}$, $\hat{j}$, and $\hat{k}$ components, respectively, of the surface vector $\vec{S}_{ABCD}$. (The unit vectors $\hat{i}$, $\hat{j}$, and $\hat{k}$ are along the x, y, and z axes, respectively.) The surface vector, $\vec{S}$, is a vector unique to a surface described by four vertices. The magnitude of $\vec{S}$ is an approximation of the area of the surface, and the direction of this vector is normal to both diagonals of the surface. The derivation of various forms of

the expression for $\vec{S}$ is given by Kordulla and Vinokur (1983), but the simplest form is presented here.

$$\vec{S}_{ABCD} = \frac{1}{2}(\vec{r}_D - \vec{r}_B) \times (\vec{r}_C - \vec{r}_A) \tag{4.4}$$

In the above expression, $\vec{r}_K$ is the position vector to point K from an arbitrarily placed origin. The components of $\vec{S}_{ABCD}$ are the metrics ξ_x/J, ξ_y/J, and ξ_z/J needed to define $\hat{E}$ through cell-face ABCD. The use of equation (4.4) to define the metrics at all cell faces will ensure the preservation of free-stream quantities when integrating the governing equations without boundary conditions given free-stream initial conditions. This claim has been verified numerically in the computations presented in this work.

An exact evaluation of the cell volume, J^{-1}, needed to advance the solution in time, is not necessary in steady-state applications since it, in fact, functions only as a scaling of the time step. For the steady-state results of Chapter 5, J^{-1} is simply evaluated at the cell center (grid point) using central differencings in the expression of equation (4.2). A more accurate computation of the cell volume is necessary for time-dependent calculations; interested readers are referred to the work of Kordulla and Vinokur (1983) for one possible approach.

4.3 Solution at Interior Points

Consider a two-zone, three-dimensional computation such as that depicted in figure 17a (problem is shown as a quadrilateral in computational (ξ, η, ς) space, with maximum grid dimensions $IM^{(m)}$, $JM^{(m)}$, and $KM^{(m)}$ where m corresponds to zone number). The zonal interface is shown as a shaded plane at $\eta = JM^{(1)}$ in zone 1 and $\eta = 1$ in zone 2. The interior points (away from boundaries, including zonal boundaries) in each zone are explicitly updated by solving equation (4.3) using the procedure in section 4.2 to define the metrics.

4.4 Solution at the Zonal-Boundary Plane

4.4.1 Development of Conservative Flux-Interpolation Scheme

In this section, the development of a conservative flux-interpolation scheme for three-dimensional patching at a planar zonal boundary is outlined. The specific details of its implementation and coding are discussed in a subsequent section (4.4.2).

The solution procedure at the zonal boundary is a two-step process.

1) The zonal-boundary points in one of the two zones are updated using a scheme that guarantees global conservation across the boundary. This scheme requires integrating the governing equations using equation (4.3) while interpolating for fluxes needed from the adjacent zone.
2) The solution at points on the zonal boundary in the neighboring zone is found by interpolating the solution found in step 1 along the zonal interface thus ensuring continuity of the dependent variables.

Consider again the problem shown in figure 17a. A view of the zonal boundary plane with ξ, ς = constant lines is shown in figure 17b where (x) points belong to zone 2 and (•) points belong to zone 1. If one chose to integrate the boundary points in zone 2 while interpolating for the solution in zone 1, then the flux cell associated with the point (i2,1,k2) on the zonal boundary in zone 2 is like that of figure 18. Notice that the cell is formed by extrapolation of grid lines into zone 1 to the flux-balance plane ($\eta = 1/2$ in zone 2 or $\eta = JM^{(1)} - 1/2$ in zone 1). Five of the six fluxes necessary to update point (i2,1,k2) using equation (4.3), namely, $\hat{E}^{(2)}_{(i2+1/2,1,k2)}$, $\hat{E}^{(2)}_{(i2-1/2,1,k2)}$, $\hat{F}^{(2)}_{(i2,3/2,k2)}$, $\hat{G}^{(2)}_{(i2,1,k2+1/2)}$, and $\hat{G}^{(2)}_{(i2,1,k2-1/2)}$, are readily formed from values of the dependent variables in zone 2. The flux through the flux-balance plane, $\hat{F}^{(2)}_{(i2,1/2,k2)}$, is obtained by interpolation of zone-1 fluxes, as explained in the following paragraphs.

A planform view of the flux-balance plane is presented in figure 19 showing the projections of both zone 1 and zone 2 grid points on this plane. The locations of zone 1 points (•) on the plane are found by simply averaging the coordinate values at $\eta = JM^{(1)}$ and

$\eta = JM^{(1)} - 1$. The locations of zone 2 points (x) require extrapolation of zone 2 grid lines to this imaginary j2=1/2 surface (a detailed description of the extrapolation is given in the next section). The cell face associated with the point (i2,1,k2) and the flux $\hat{F}^{(2)}_{(i2,1/2,k2)}$ is labeled as RSTU. Cell faces of zone 1 points are also shown by segmented lines.

The zonal-boundary scheme developed for two-dimensional problems in Rai's work (1986) and for three-dimensional applications as described in this section guarantees global conservation of mass, momentum, and energy in a discrete sense at the zonal interface. To affect this global conservation, the surface integral of the zone 1 numerical flux, $\hat{F}$, on the flux-balance plane must be equal to the surface integral of the zone 2 numerical flux on this same plane. The discretized form of this requirement may be written

$$\begin{aligned}
&\frac{1}{4}\left[\hat{F}^{(1)}_{(1,j1,1)} + \hat{F}^{(1)}_{(IM^{(1)},j1,1)} + \hat{F}^{(1)}_{(1,j1,KM^{(1)})} + \hat{F}^{(1)}_{(IM^{(1)},j1,KM^{(1)})}\right] \\
&+\frac{1}{2}\sum_{i1=2}^{IM^{(1)}-1}\left[\hat{F}^{(1)}_{(i1,j1,1)} + \hat{F}^{(1)}_{(i1,j1,KM^{(1)})}\right] + \frac{1}{2}\sum_{k1=2}^{KM^{(1)}-1}\left[\hat{F}^{(1)}_{(1,jJ1,k1)} + \hat{F}^{(1)}_{(IM^{(1)},j1,k1)}\right] \\
&+\sum_{i1=2}^{IM^{(1)}-1}\sum_{k1=2}^{KM^{(1)}-1}\hat{F}^{(1)}_{(i1,j1,k1)} \\
&= \frac{1}{4}\left[\hat{F}^{(2)}_{(1,j2,1)} + \hat{F}^{(2)}_{(IM^{(2)},j2,1)} + \hat{F}^{(2)}_{(1,j2,KM^{(2)})} + \hat{F}^{(2)}_{(IM^{(2)},j2,KM^{(2)})}\right] \\
&+\frac{1}{2}\sum_{i2=2}^{IM^{(2)}-1}\left[\hat{F}^{(2)}_{(i2,j2,1)} + \hat{F}^{(2)}_{(i2,j2,KM^{(2)})}\right] + \frac{1}{2}\sum_{k2=2}^{KM^{(2)}-1}\left[\hat{F}^{(2)}_{(1,j2,k2)} + \hat{F}^{(2)}_{(IM^{(2)},j2,k2)}\right] \\
&+\sum_{i2=2}^{IM^{(2)}-1}\sum_{k2=2}^{KM^{(2)}-1}\hat{F}^{(2)}_{(i2,j2,k2)} \qquad (4.5)
\end{aligned}$$

where j1 = $JM^{(1)} - 1/2$ and j2 = 1/2. The left and right sides of this equation are the discrete forms of the surface integral of the numerical flux, $\hat{F}$, on the flux-balance plane in zone 1 and zone 2, respectively. Like its two-dimensional counterpart (eq. (2.6)), equation (4.5) is a necessary, but not a sufficient condition to uniquely define the unknown $\hat{F}^{(2)}_{(i2,j2,k2)}$ fluxes. However, a generalization of equation (2.5) for three-dimensional application does

satisfy the above equation of global conservation. Again referring to figure 19 and the flux cell face RSTU on this planar surface,

$$\hat{F}^{(2)}_{(i2,j2,k2)} = \int_U^R \int_U^T \frac{\hat{F}^{(1)}_{(i1,j1,k1)}}{|\vec{S}^{(1)}_{(i1,j1,k1)}|} \quad dx \quad dz \tag{4.6}$$

In essence, the integrand of equation (4.6) is a representation of the zone-1 flux per unit area at the flux-balance surface. (A piecewise-constant distribution of numerical flux over a cell face is assumed in this work.) Zone-1 flux per unit area is then integrated over the area of the zone-2 cell face to yield the total flux through face RSTU. In discrete form, equation (4.6) becomes

$$\hat{F}^{(2)}_{(i2,j2,k2)} = |\vec{S}^{(2)}_{(i2,j2,k2)}| \sum_{k1=1}^{KM^{(1)}} \sum_{i1=1}^{IM^{(1)}} N^{(i2,j2,k2)}_{(i1,j1,k1)} \frac{\hat{F}^{(1)}_{(i1,j1,k1)}}{|\vec{S}^{(1)}_{(i1,j1,k1)}|} \tag{4.7}$$

The $N^{(i2,j2,k2)}_{(i1,j1,k1)}$ are interpolation coefficients that represent the dependence of $\hat{F}^{(2)}_{(i2,j2,k2)}$ on the $\hat{F}^{(1)}_{(i1,j1,k1)}$ fluxes. Physically, these terms are nothing more than ratios of the areas of overlap of RSTU with zone-1 cell faces to the total area of RSTU, that is

$$N^{(i2,j2,k2)}_{(i1,j1,k1)} = \frac{A^{(i2,j2,k2)}_{(i1,j1,k1)}}{|\vec{S}^{(2)}_{(i2,j2,k2)}|} \tag{4.8}$$

where $A^{(i2,j2,k2)}_{(i1,j1,k1)}$ denotes the area of overlap of the cell face associated with (i1,j1,k1) with that of (i2,j2,k2) on the flux-balance plane. One final condition is necessary to ensure that equation (4.7) satisfies the statement of global conservation (eq. (4.5)), that is

$$\sum_{k1=1}^{KM^{(1)}} \sum_{i1=1}^{IM^{(1)}} N^{(i2,j2,k2)}_{(i1,j1,k1)} = 1 \tag{4.9}$$

Equation (4.9) states that the area of a cell face in zone 2 on the flux-balance plane is identically equal to a sum of the areas of zone-1 cell faces, ensuring that the flux from the zone-1 side of the flux-balance plane is completely transferred to the zone-2 side of this plane.

Given the definition of flux from a neighboring zone (eq. (4.7)), it is now possible to update all points on the zonal-boundary plane in zone 2 by solution of equation (4.3). The solution at points on this plane in zone 1 is then found by interpolating the zone-2 dependent variables on the interface using a procedure described in Appendix A.

4.4.2 Implementation of Zonal-Boundary Scheme

Equation (4.7) defines the flux through a flux-balance plane and therefore the flux from a neighboring zone at the zonal boundary. Use of equation (4.7) will, by definition, ensure global conservation in the discrete sense. The $\hat{F}^{(1)}_{(i1,j1,k1)}$ terms in this expression are formed in a conventional manner using the definition of numerical flux for a given numerical integration scheme. The metric terms (components of $\vec{S}$) are computed using equation (4.4). The interpolation coefficients, $A^{(i2,j2,k2)}_{(i1,j1,k1)}$ of equation (4.8), are the remaining quantities to be determined. A schematic of the procedure for computing these terms is shown in figure 20 and is discussed in the following paragraphs.

Assuming the integration of zone-2 points on the zonal-boundary plane (followed by an interpolation for values at zone-1 points on this boundary), the flux-balance plane is located in zone 1 halfway between the last two constant η-coordinate planes (see again fig. 17a). It is necessary to find the projections of both zone-1 and zone-2 points on this ficticious plane. The locations of zone-1 points are found by simply averaging the coordinate values at $\eta = JM^{(1)}$ and $\eta = JM^{(1)} - 1$. The locations of zone 2 points require an extrapolation of zone-2 grid lines to this imaginary j2=1/2 surface. The extrapolation is performed in such a way as to emulate the point relationships on the zonal-boundary surface using linear interpolation over triangles as described by Chung (1978) (see also Appendix A).

Since only three points define a plane, it is necessary to work with triangular portions of each cell face to determine areas of overlap. The cell area on the flux-balance plane associated with each zone-2 point is now considered in turn and is divided into a number of triangles. On a rectangular, planar zonal boundary, each cell is adequately described

using only two triangles. Similarly, the cell areas associated with zone-1 points on the flux-balance plane must also be "triangulated." Given the triangles associated with a zone-2 point, one must now compute the areas of overlap with all zone-1 point triangles. The total area of overlap of all triangles of zone-2 point (i2,j2,k2) with all triangles of zone-1 point (i1,j1,k1) is stored in the coefficient $A_{(i1,j1,k1)}^{(i2,j2,k2)}$.

The problem in computing the flux-interpolation coefficients $A_{(i1,j1,k1)}^{(i2,j2,k2)}$ is now reduced to finding the common area of two overlapping triangles. An unsuccessful attempt was made to develop an analytical expression for determining the polygon of overlap and hence the area. If such an expression is indeed derivable, computation of the $A_{(i1,j1,k1)}^{(i2,j2,k2)}$s would be inexpensive enough for unsteady (moving grid) applications where a new evaluation is necessary at each time step. In this work, however, an algorithmic approach was employed that, although computationally intensive, resulted in an insignificant amount of computing overhead because only one evaluation of the $A_{(i1,j1,k1)}^{(i2,j2,k2)}$s is needed for these applications. A modified Sutherland-Hodgman clipping algorithm (as outlined by Newman and Sproull, 1979, see Appendix B), borrowed from the field of computer graphics, is used to find the vertices of the polygon of overlap (fig. 21). The area of any convex polygon with n ordered vertices may be found by the following expression

$$area = \frac{1}{2}\left|\sum_{i=1}^{n}(x_{i+1}y_i - x_i y_{i+1})\right| \tag{4.10}$$

where $x_{n+1} = x_1$ and $y_{n+1} = y_1$. (The polygon resulting from the overlap of two triangles will, conveniently, always be convex.) The accuracy with which the overlapping areas are computed determines the degree of free-stream preservation at a planar zonal boundary. In this case, triangular overlaps can be computed to machine accuracy enabling perfect free-stream preservation.

The procedure depicted in figure 20 (and described above) is by no means optimal. There are "smart" ways to avoid unnecessary computation by eliminating the triangulation of zone-1 points far from the zone-2 point under consideration.

4.5 Numerical Integration Scheme: Osher Algorithm

In the development of the three-dimensional patched grid method in the previous section, it is assumed that a conservative finite-difference scheme is used to define the numerical fluxes $\hat{E}$, $\hat{F}$, and $\hat{G}$. The results which follow in Chapter 5 were obtained with the first-order accurate Osher algorithm. This scheme has been used extensively in two dimensions and is outlined for three-dimensional calculations in Osher and Chakravarthy's work (1983). The algorithm as presented in the reference is unsuitable for general computations, however, since it requires that ξ_x, η_x, and ζ_x are nowhere zero. A necessary modification of the scheme for an arbitrary grid is described in this section.

The Osher scheme is an upwind, shock-capturing algorithm based on a Riemann solver. Unlike an exact Riemann solver, it uses compression waves to approximate shocks, thereby simplifying the algorithm. The numerical flux functions may be written as

$$\begin{aligned}
\hat{E}_{i+1/2,j,k} &= \tilde{E}_{i+1,j,k} - \int_{Q_{i,j,k}}^{Q_{i+1,j,k}} \left(\frac{\partial \tilde{E}}{\partial Q}\right)^{+} dQ \\
\hat{F}_{i,j+1/2,k} &= \tilde{F}_{i,j+1,k} - \int_{Q_{i,j,k}}^{Q_{i,j+1,k}} \left(\frac{\partial \tilde{F}}{\partial Q}\right)^{+} dQ \qquad (4.11) \\
\hat{G}_{i,j,k+1/2} &= \tilde{G}_{i,j,k+1} - \int_{Q_{i,j,k}}^{Q_{i,j,k+1}} \left(\frac{\partial \tilde{G}}{\partial Q}\right)^{+} dQ
\end{aligned}$$

where $\tilde{E}$, $\tilde{F}$, and $\tilde{G}$ are given in equation (4.2). The integrals are evaluated along subpaths in state space chosen to coincide with the right eigenvectors of the Jacobian matrices $\partial\tilde{E}/\partial\tilde{Q}$, $\partial\tilde{F}/\partial\tilde{Q}$, and $\partial\tilde{G}/\partial\tilde{Q}$ for the ξ, η, and ζ directions, respectively. Figure 22 depicts the three subpaths between any two adjacent grid points (m-1 and m or m and m+1) where σ denotes the eigenvalue associated with each subpath. (Subpath end points or states are labeled at 1/3 intervals.) The "+"in equation (4.11) indicates contributions resulting from positive eigenvalues along the subpaths, i.e., the subintegrals will be zero if the corresponding eigenvalue is negative all along the subpath. If not zero, the subintegrals are simply flux differences between the end points of the subpath, assuming there are no

sonic points along the path. The treatment of sonic points is outlined fully by Osher and Chakravarthy (1983).

Key to the development of the Osher algorithm is the identification of invariant quantities, called Riemann invariants, along each subpath. By definition, Riemann invariants, Ψ, associated with the nth eigenvalue must satisfy

$$\nabla_Q \Psi \cdot \vec{r}_n(Q) = 0 \tag{4.12}$$

where $\vec{r}_n$ denotes the right eigenvector associated with the nth eigenvalue. It may be shown that, given the above definition, the Ψ quantities are invariant along their distinctive subpath (Chakravarthy and Osher, 1982). (Equation (4.12) is the only condition necessary to qualify a Riemann invariant.) Consequently they will be used to determine values of the dependent variables, Q, at the intermediate states and, ultimately, the flux at these points.

Figure 22 presents Riemann invariants suggested by Osher and Chakravarthy (1983) for three-dimensional computations. Equating these invariants along their respective subpaths with known values at grid points (for example, m-1 and m) produces ten equations for the ten unknown quantities at intermediate states (m-2/3 and m-1/3). Note that should ξ_x, η_x, or ζ_x be anywhere zero, $\hat{v}$ and $\hat{w}$ are no longer linearly independent, and the equation set degenerates to nine linearly independent equations for ten unknowns. Hence, it is necessary to identify a new $\hat{v}$ and $\hat{w}$ that are always independent along the 1, 4, 3, and 6 subpaths.

Assume the following form for $\hat{v}$ and $\hat{w}$, where c_i are constants yet to be determined

$$\begin{aligned} \hat{v} &= c_1 u + c_2 v + c_3 w \\ \hat{w} &= c_4 u + c_5 v + c_6 w \end{aligned} \tag{4.13}$$

Taking the gradient of both $\hat{v}$ and $\hat{w}$ with respect to the dependent variables Q produces

the row vectors

$$\nabla_Q \hat{v} = \left[-(\frac{c_1}{\rho}u + \frac{c_2}{\rho}v + \frac{c_3}{\rho}w), \quad \frac{c_1}{\rho}, \quad \frac{c_2}{\rho}, \quad \frac{c_3}{\rho}, \quad 0 \right]$$
$$\nabla_Q \hat{w} = \left[-(\frac{c_4}{\rho}u + \frac{c_5}{\rho}v + \frac{c_6}{\rho}w), \quad \frac{c_4}{\rho}, \quad \frac{c_5}{\rho}, \quad \frac{c_6}{\rho}, \quad 0 \right] \tag{4.14}$$

The eigenvector associated with the $\sigma = D(\hat{u} - c)$ subpath (fig. 22) provides the most stringent test for the qualification of a Riemann invariant by equation (4.12) and may be written as

$$\vec{r} = \left[-\frac{\rho}{c}, \quad k_x\rho - \frac{\rho}{c}u, \quad k_y\rho - \frac{\rho}{c}v, \quad k_z\rho - \frac{\rho}{c}w, \quad \varepsilon \right] \tag{4.15}$$

where

$$\varepsilon = \frac{\rho(u^2 + v^2 + w^2)}{2c} - k_x\rho u - k_y\rho v - k_z\rho w + \frac{\rho c}{(\gamma - 1)}$$

From equation (4.12) (using eqs. (4.14) and (4.15)), the following constraints on the constants, c_i, are derived

$$c_1k_x + c_2k_y + c_3k_z = 0$$
$$c_4k_x + c_5k_y + c_6k_z = 0 \tag{4.16}$$

Note that the above constraints are satisfied if the c_i are chosen such that the vectors $[c_1, c_2, c_3]$ and $[c_4, c_5, c_6]$ are orthogonal to the particular metric $[k_x, k_y, k_z]$. Furthermore, the vectors $[c_1, c_2, c_3]$ and $[c_4, c_5, c_6]$ must be linearly independent to ensure the same for $\hat{v}$ and $\hat{w}$. One way to meet all requirements is to rotate the $[k_x, k_y, k_z]$ vector to a coordinate axis in xyz-space and choose the other two coordinate axes as the transformed "c"vectors. For instance, if R is a rotation matrix and

$$R \begin{pmatrix} k_x \\ k_y \\ k_z \end{pmatrix} = \begin{pmatrix} 1 \\ 0 \\ 0 \end{pmatrix}$$

then

$$\begin{pmatrix} c_1 \\ c_2 \\ c_3 \end{pmatrix} = R^{-1} \begin{pmatrix} 0 \\ 1 \\ 0 \end{pmatrix}$$
$$\begin{pmatrix} c_4 \\ c_5 \\ c_6 \end{pmatrix} = R^{-1} \begin{pmatrix} 0 \\ 0 \\ 1 \end{pmatrix}$$

Details of this procedure are given in Appendix C.

Excluding a redefinition of the invariants $\hat{v}$ and $\hat{w}$, there are no other required changes to the algorithm for use in general computations. The reader is referred to the work of Osher and Chakravarthy (1983) for a more detailed description of the scheme, including the treatment of sonic points as they occur along subpaths.

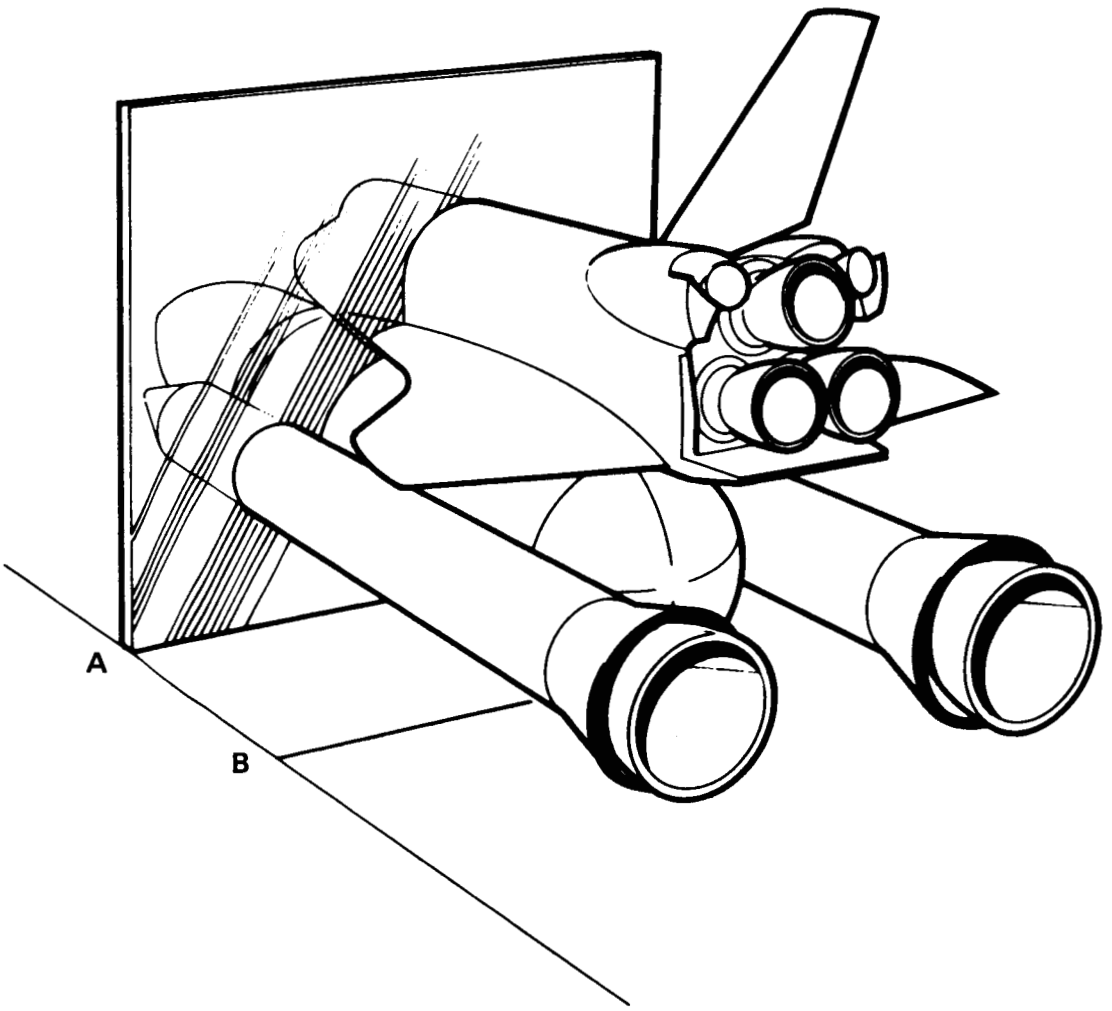

Fig. 15 (a) View of the Space Shuttle orbiter with external tank and rocket boosters

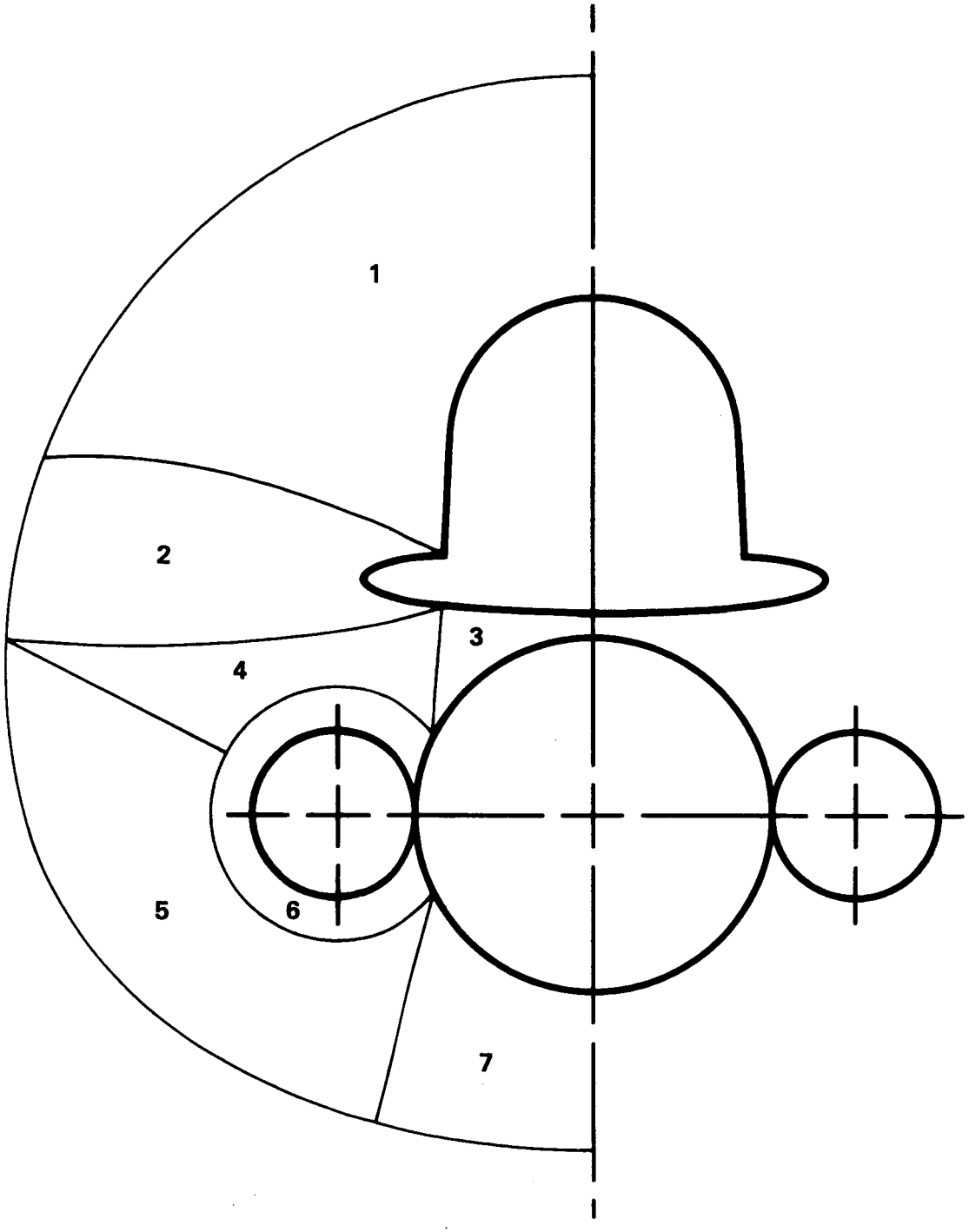

Fig. 15 (b) Zoning suggestion at cross-section A

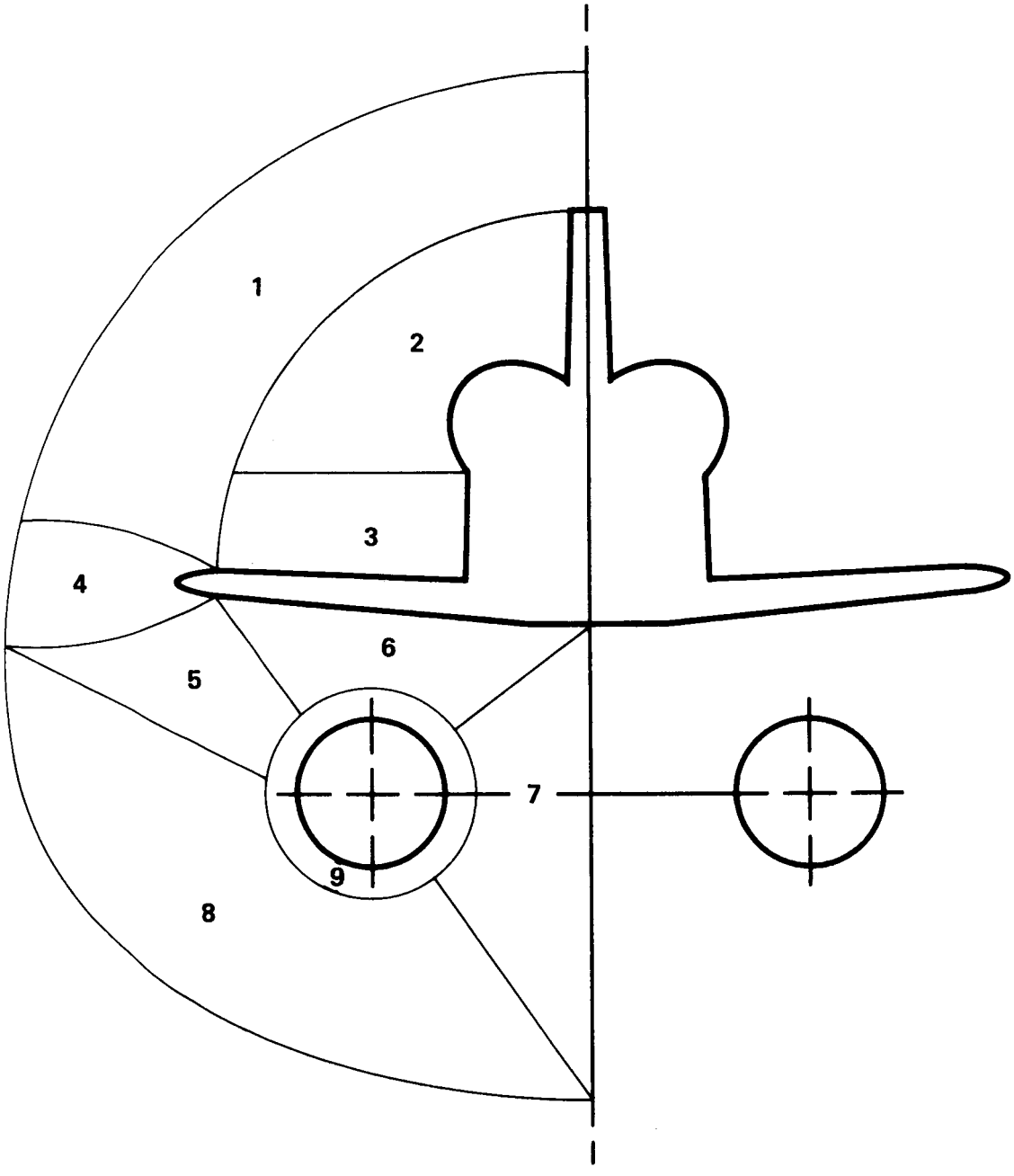

Fig. 15 (c) Zoning suggestion at cross-section B

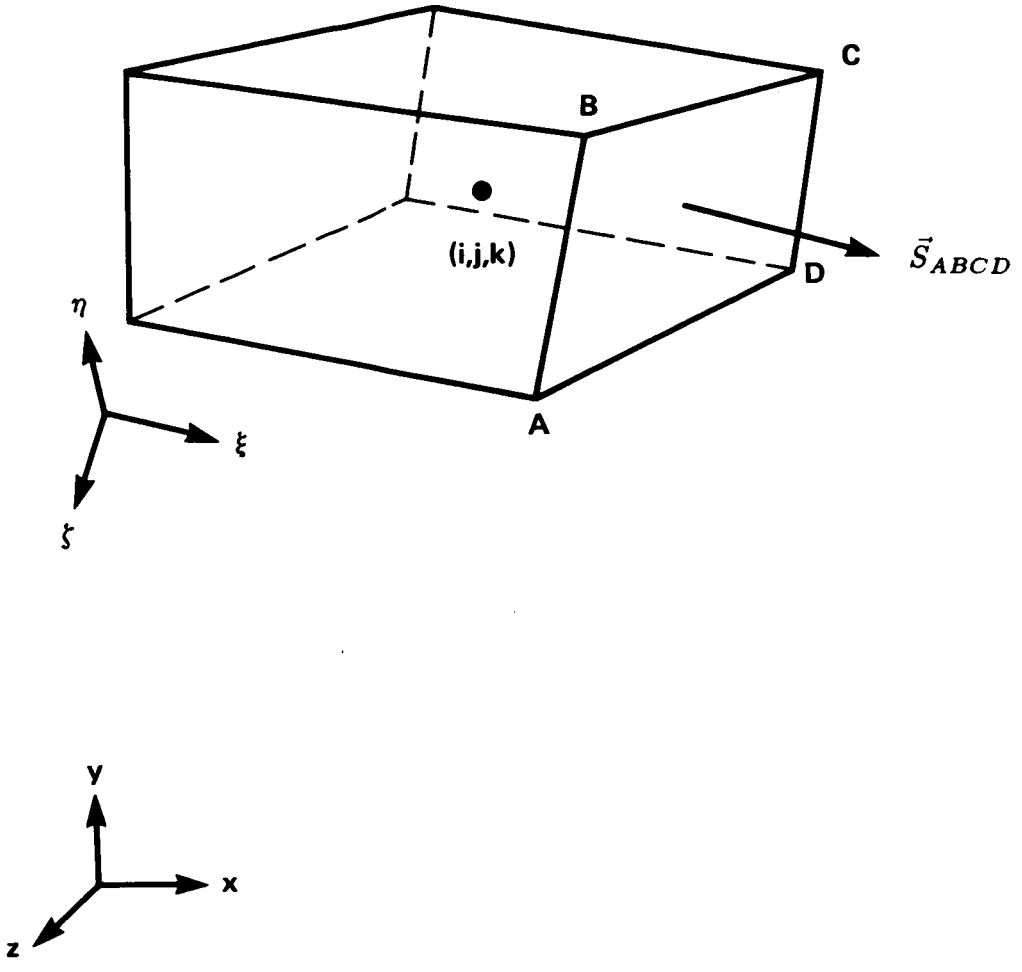

Fig. 16 Computational cell associated with the point (i,j,k)

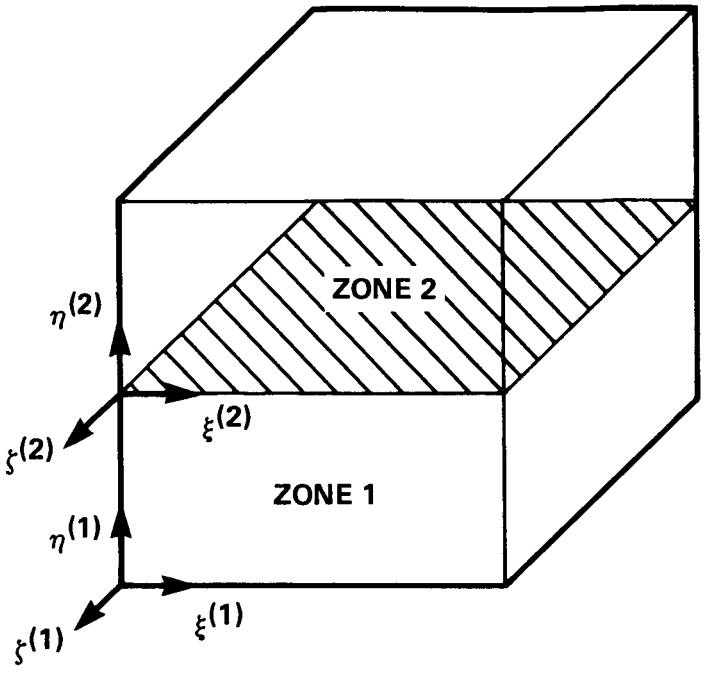

(a)

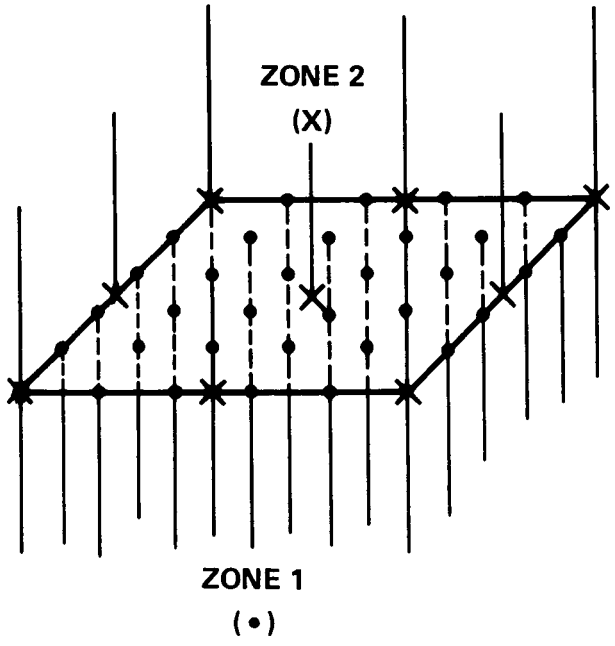

(b)

Fig. 17 Sketch of a two-zone, three-dimensional problem.
(a) computational domain (b) enlarged view of zonal-boundary plane.

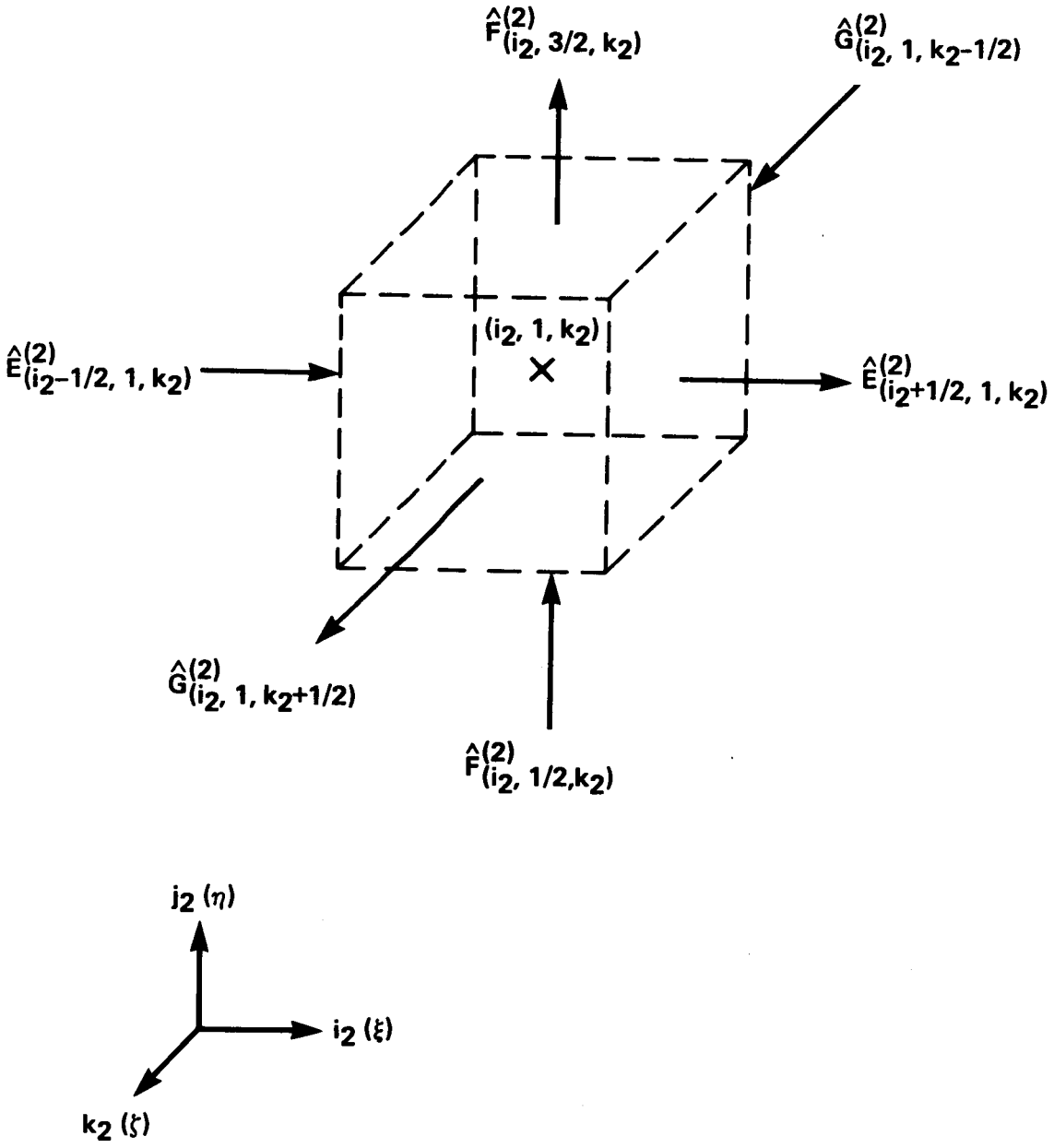

Fig. 18 Computational cell associated with the point (i2,1,k2)

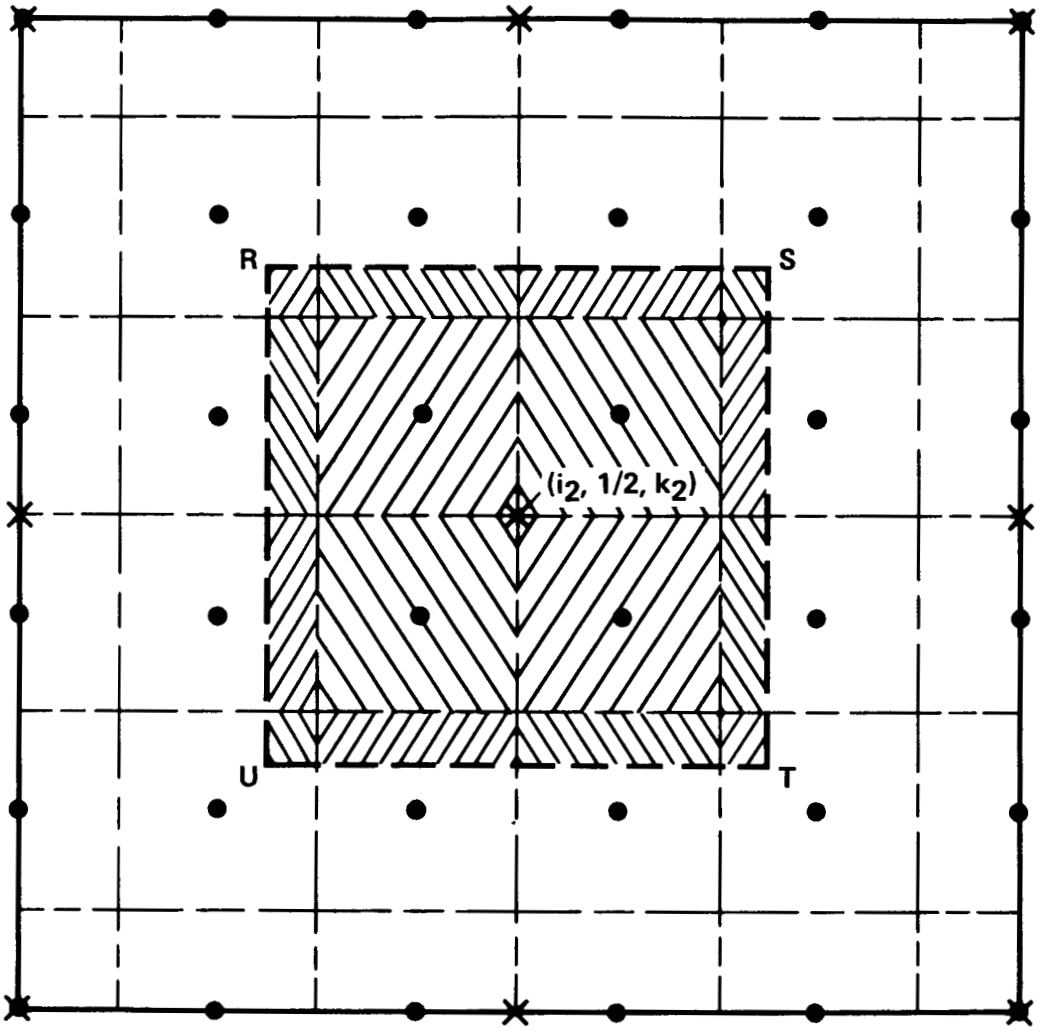

Fig. 19 Planform view of the flux-balance plane

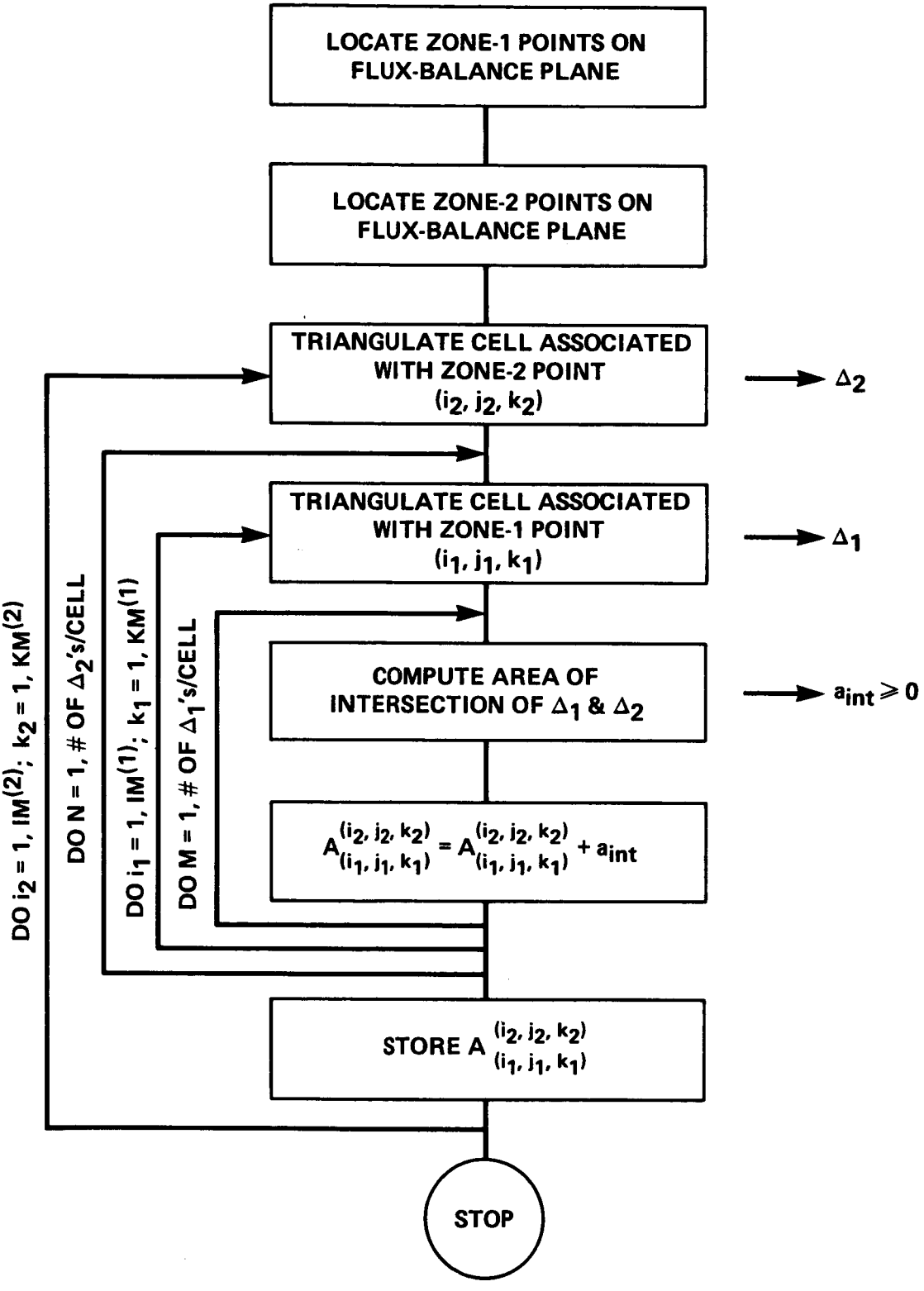

Fig. 20 Schematic of logic necessary for the computation of flux-interpolation coefficients, $A^{(i2,j2,k2)}_{(i1,j1,k1)}$

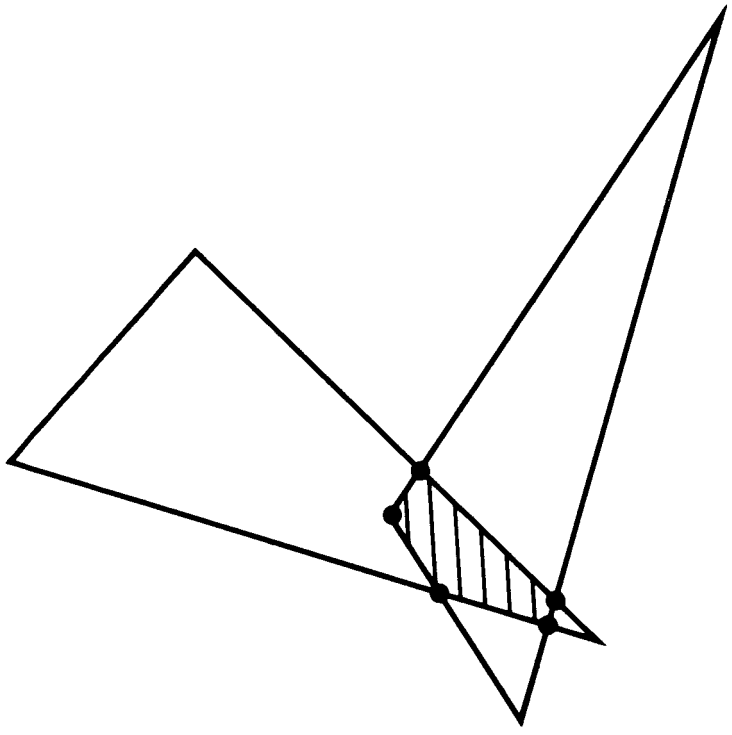

Fig. 21 Sketch depicting the overlap of two triangles.

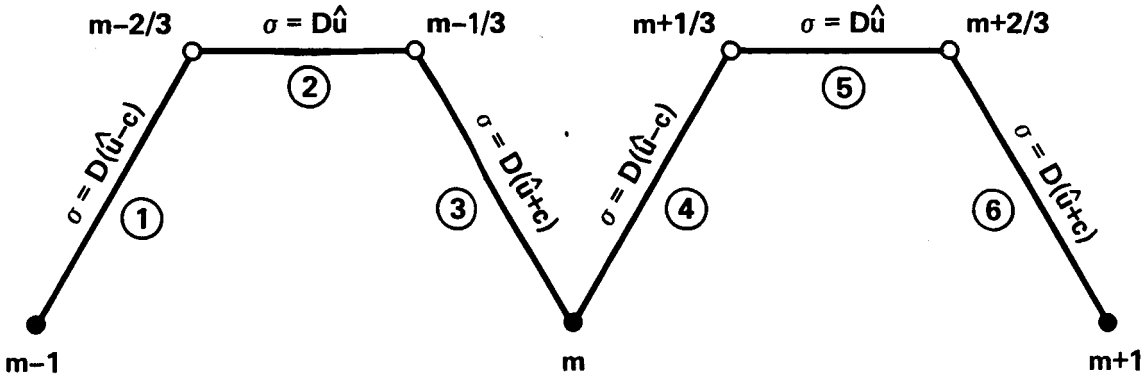

RIEMANN INVARIANTS ALONG SUBPATHS

① AND ④ : $\hat{u} + \frac{2}{\gamma-1}\, c,\ p/\rho^{\gamma},\ \hat{v},\ \hat{w}$

② AND ⑤ : $\hat{u},\ p$

③ AND ⑥ : $\hat{u} - \frac{2}{\gamma-1}\, c,\ p/\rho^{\gamma},\ \hat{v},\ \hat{w}$

WHERE

$$c = \left(\frac{\gamma p}{\rho}\right)^{1/2}$$

$$\hat{u} = \frac{k_t + k_x u + k_y v + k_z w}{D}$$

$$\hat{v} = \frac{-k_y u + k_x v}{D}$$

$$\hat{w} = \frac{-k_z u + k_x w}{D}$$

$$D = (k_x^2 + k_y^2 + k_z^2)^{1/2}$$

AND k = ξ, η, OR ζ AS APPROPRIATE

Fig. 22 Schematic representation of Osher algorithm and the identification of Riemann invariants along subpaths.

CHAPTER 5

APPLICATION OF A THREE-DIMENSIONAL PATCHED GRID SCHEME

The three-dimensional interfacing technique developed in Chapter 4 for patched grids is used in the computation of supersonic flow about a canard/wing combination mounted on a wall. This problem was chosen to demonstrate the use of grid patching in the solution of flow about a multiple-body configuration that is typically difficult to grid. The results of this computation indicate that a stable solution can be obtained with the conservative interfacing technique and that smooth solutions are generated despite discontinuities in grid lines.

5.1 Problem Description

A planform sketch of the problem is shown in figure 23a. The canard section is a 3% biconvex airfoil, the wing section a NACA 0006. Both canard and wing are of constant chord with aspect ratios of 1.5 and 2.0, respectively, and are swept at an angle of 25°. Single-module type grid generation for this configuration would be difficult because of the y-coordinate offset of the wing from the canard (see fig. 23b, offset is 10% of canard chord). Hence this problem is a good candidate for a patched grid treatment.

The sharp leading and trailing edges of the canard suggest an H-grid treatment of the flow region, while the blunt leading edge of the wing requires a C-grid. In a two-zone, patched grid approach to the configuration, a 49 x 50 x 26 point H-grid about the canard (grid dimensions are in the streamwise, nearly normal and spanwise directions, respectively) interfaces with a 111 x 30 x 34 point C-grid about the wing along a planar-zonal boundary (also swept at 25°). The wall-plane cross section of the grid (an x-y plane) is shown in figure 24. Note that the grid lines are point discontinuous at the zonal interface in the y-direction. (The wing grid has been clustered in the streamwise direction near the zonal interface to match the streamwise spacing in the canard grid, thus avoiding metric

discontinuities arising from abrupt changes in spacing.) Grid-line discontinuities also exist in the spanwise or z-direction on the zonal-boundary plane. In fact, there are only three spanwise planes that are coincident in the canard and wing zones: the wall plane (minimum z), the domain boundary plane (maximum z), and a plane through the canard tip. The constant-section, canard and wing grids transition at the tip of each body to grids about flat plates with zero thickness. A view of the grid along the span of the canard (a y-z plane) is shown in figure 25. (The wing grid in this region is identical in nature.) Figure 26 presents a three-dimensional perspective of the wall-plane grid with the canard and wing.

The canard and wing zones are shown as quadrilaterals in computational space in figure 27. The boundary conditions are indicated on the faces of each computational domain. Tangency is enforced on body surfaces. However, there is flow through the flat-plate extensions of the wing and canard, as well as through the wake of the wing. A symmetry condition is imposed at the wall plane, and conservative flux interpolations are performed on the zonal-boundary plane. The inflow is fixed at supersonic free-stream conditions. All other boundaries in the flow domain are sufficiently distant to maintain free-stream flow with the exception of the downstream boundary. This boundary (supersonic outflow in the wing domain) is updated by extrapolating from the interior.

Although geometrically a two-zone problem, the flow field was actually divided into seven blocks (four blocks in the spanwise direction of the wing and three in the spanwise direction of the canard, as shown in fig. 28). This blocking was performed to circumvent in-core memory limitations of the Cray X-MP. Therefore, only one block of data resides in core at a given time while the remaining data resides in easily accessible extended storage (solid-state device). The blocks, which are processed sequentially, overlap by one plane in the spanwise (ς) direction to readily permit the transfer of data between blocks. (Since the grid lines are continuous from spanwise block to spanwise block, it is not necessary to use the patched grid scheme at these block interfaces.)

For this application, the entire flow field is initialized with free-stream conditions at a Mach number of 2.0. Equation (4.3), with the first-order Osher scheme flux definitions of equation (4.11), is integrated to convergence. The solution is considered converged if the maximum change in the density (from step to step) divided by the time step does not exceed 10^{-5}. This convergence criterion is met after approximately 8000 time steps on the grids previously described. The canard-wing calculations presented here required approximately 24 hours of Cray X-MP computer time using a fully vectorized version of the flow solver. The advantage of extending this zonal-boundary procedure for use with implicit schemes (with their characteristic accelerated convergence rates) is evident.

5.2 Computed Results

Figures 29 and 30 present the results of a computation of the flow at $\alpha = 0°$. (In all figures the flow is generally from left to right). Figures 29a and 29b depict pressure contours in both zones on a plane through the canard tip (one of the three coincident z-planes). Note the expected symmetry of the canard contours (from top to bottom), as well as that of the attached leading- and trailing-edge shocks (weakened near the tip). The trailing-edge shock waves pass through the zonal-boundary plane to intercept the detached wing-bow shock. A very slight asymmetry in the wing solution results from the offset of the canard chord from the wing in the y-direction. Despite the grid-line discontinuities in the y-direction and the z-direction on either side of this spanwise plane, the solution near the zonal boundary between canard and wing is smooth and continuous. As in the two-dimensional applications, an occasional mismatch of contour lines may be observed at the zonal plane. The interpolation technique in the contour-plotting routine is different from the interpolation procedure used at the zonal boundary; hence, small errors may arise in plotting.

Pressure contours on the upper surfaces of both canard and wing are displayed in figure 30. Again there is evidence of leading- and trailing-edge canard shocks, strong gradients near the leading edge of the wing, and a wing trailing-edge shock. The flow over

the canard is primarily two dimensional except near the tip within the Mach cones (see again fig. 23a, μ is the Mach angle). Likewise, the wing experiences little departure from two-dimensional flow except at the wall and at the tip.

Figures 31 and 32 present results for the flow over canard and wing at $\alpha = 2°$. Again, pressure contours are shown in the spanwise plane through the canard tip (fig. 31). At $\alpha = 2°$, there is a leading-edge expansion on the upper surface of the canard with a lower-surface shock and a decided asymmetry in the wing solution with greater expansion on the wing upper surface as compared to figure 29. The contour lines indicate that the solution is smooth and continuous in the vicinity of the zonal boundary. In figure 32, note that the wing upper-surface pressures are significantly altered in the spanwise region near the canard tip because of canard downwash. Although in theory one would expect to observe a relatively weak tip vortex formation at $\alpha = 2°$, no vortical motion is detected in these results. The tracking of such a vortex requires at least a second-order accurate numerical integration scheme in conjunction with a very fine grid. The dissipative nature of a first-order accurate numerical method precludes the capture and propagation of vortical motion.

As a form of code validation, the computed canard pressures at $\alpha = 0°$ and $\alpha = 2°$ flow conditions are compared with linear theory (a numerical solution of the Prandtl-Glauert equation from the code PAN AIR as described by Carmichael and Erickson, 1981) in figures 33 and 34. (Since the flow is supersonic at the zonal-boundary plane and therefore there is no upstream influence of the wing on the canard, it is appropriate to compare the present results with theory for a canard alone.) The two results are in good agreement throughout the span. The slight discrepancies in pressure noted at the leading edge are the result of the smearing of the leading-edge shock by the first-order numerical method of the present computation.

5.3 Discussion

The canard/wing application was chosen to demonstrate the usefulness of a grid-patching technique in the solution of geometrically complex problems. The intention of this work is to provide a three-dimensional extension of Rai's (1986) two-dimensional zonal-grid scheme that is globally conservative and stable. The preceding computations indicate that this goal has been reached. The calculations are conservative by the very nature of the flux interpolation scheme developed in Chapter 4. By definition, the fluxes at the zonal boundary satisfy a statement of discrete conservation. Other researchers (Benek et al., 1983; Rai, 1985c) working with overlapping grid systems suggest that the nonconservative nature of their interface schemes gives rise to high-frequency oscillations at the zonal boundary. The solutions presented here (as well as the second-order accurate results of Rai (1985) in two dimensions) are free from oscillations in the zonal-boundary region.

The ability to obtain a stable solution using grid patching, however, requires some care in grid construction. In performing stability analyses for various two-dimensional interface schemes, Eriksson and Rai (to be published) find that if using a central-difference integration method, it is necessary to integrate the points on the zonal boundary of the coarser grid and interpolate for the points on the boundary of the finer grid. An instability will result if coarse grid fluxes are divided to form fluxes for the finer grid using Rai's (1986) approach to grid patching in two dimensions. Although Eriksson and Rai did not observe such behavior with upwind integration methods (given modest grid-density ratios across the boundary), their work suggests that the choice of zonal-boundary points to integrate versus interpolate is not as arbitrary as once thought.

The present work supports this conclusion. The first grid systems generated for this problem were characterized by up to 10 to 1 grid-density ratios from zone to zone in the spanwise direction. Points were clustered in the region of the canard tip for body definition, but there was no corresponding resolution in the wing zone interfacing with

this region. Although the coarser (wing) grid was not expected to support the regional gradients as accurately as the finer (canard) grid, no stability or convergence problems were anticipated. However, when the coarse grid fluxes were divided to form fluxes for the finer grid (as would be the case if the wing zonal-boundary points were integrated), the computation would not converge while errors (build-up of pressure contours) accumulated at the zonal interface. The stable results presented here were obtained by both reducing the grid-density ratio to at most 3 to 1 and also by changing the zone of integration such that the flux for a coarse grid cell was specified by the summation of appropriate fine grid fluxes. The unreasonable matching of a fine grid with a coarse one in a gradient region has an expected effect on solution accuracy but also introduces a stability problem. For this reason, patched grid systems should be characterized by modest grid-density ratios at the zonal boundary (less than 3 to 1 in gradient regions). Furthermore, the coarser side of the interface should be chosen as the zone of integration versus interpolation.

The numerical integration scheme used in this study, the Osher upwind method, is first-order accurate. Likewise, the assumptions made in the construction of the zonal-boundary fluxes (piecewise-constant variation of fluxes) and the use of linear interpolation to enforce continuity at the patch boundary produce first-order accurate results at the interface.

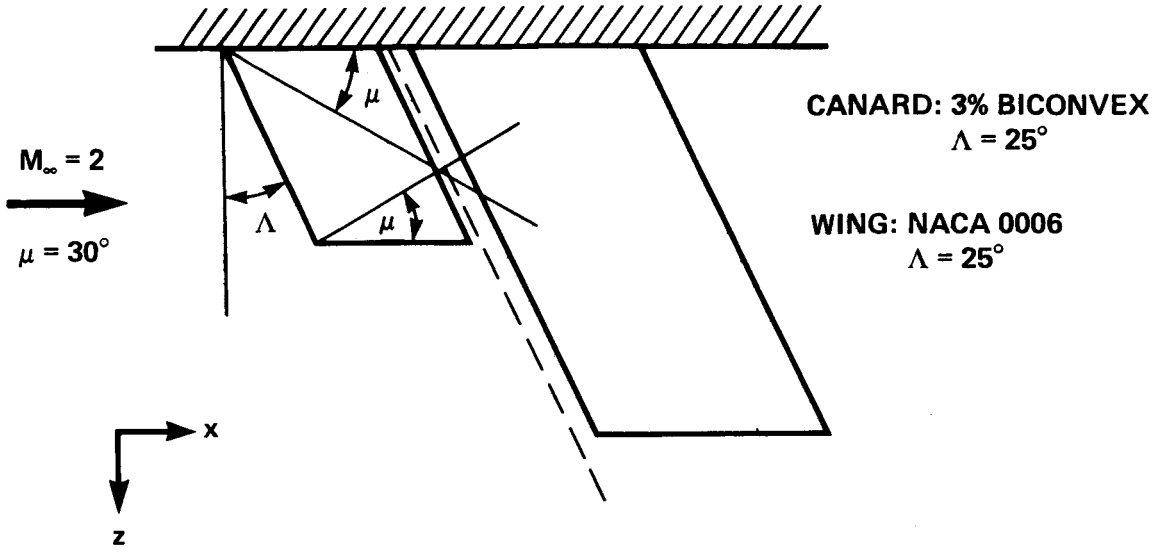

(a)

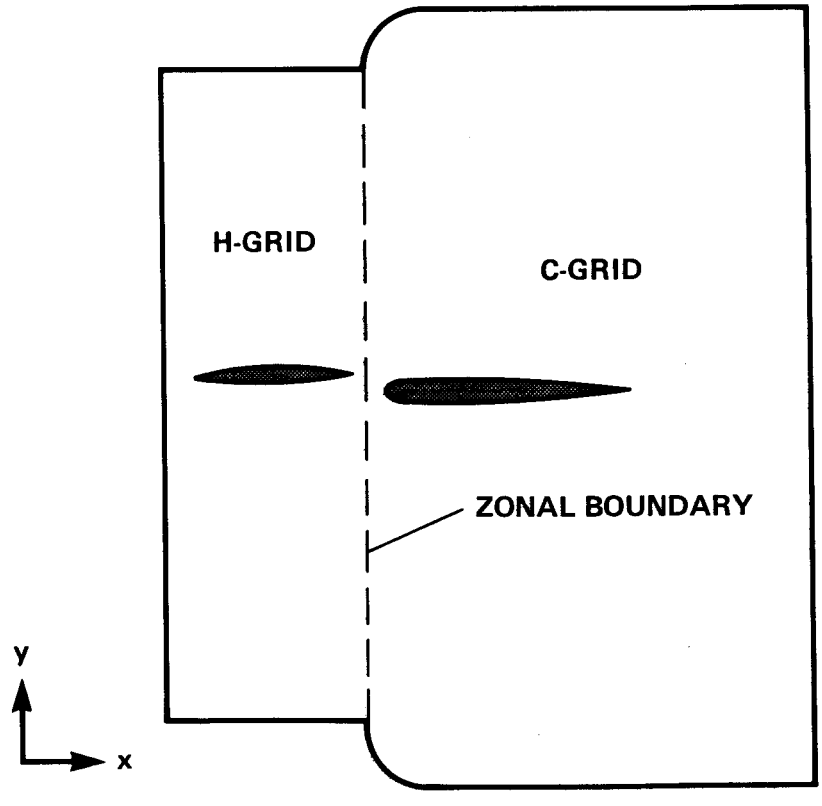

(b)

Fig. 23 Sketch of wing-canard problem setup
(a) planform view (b) wall-plane view

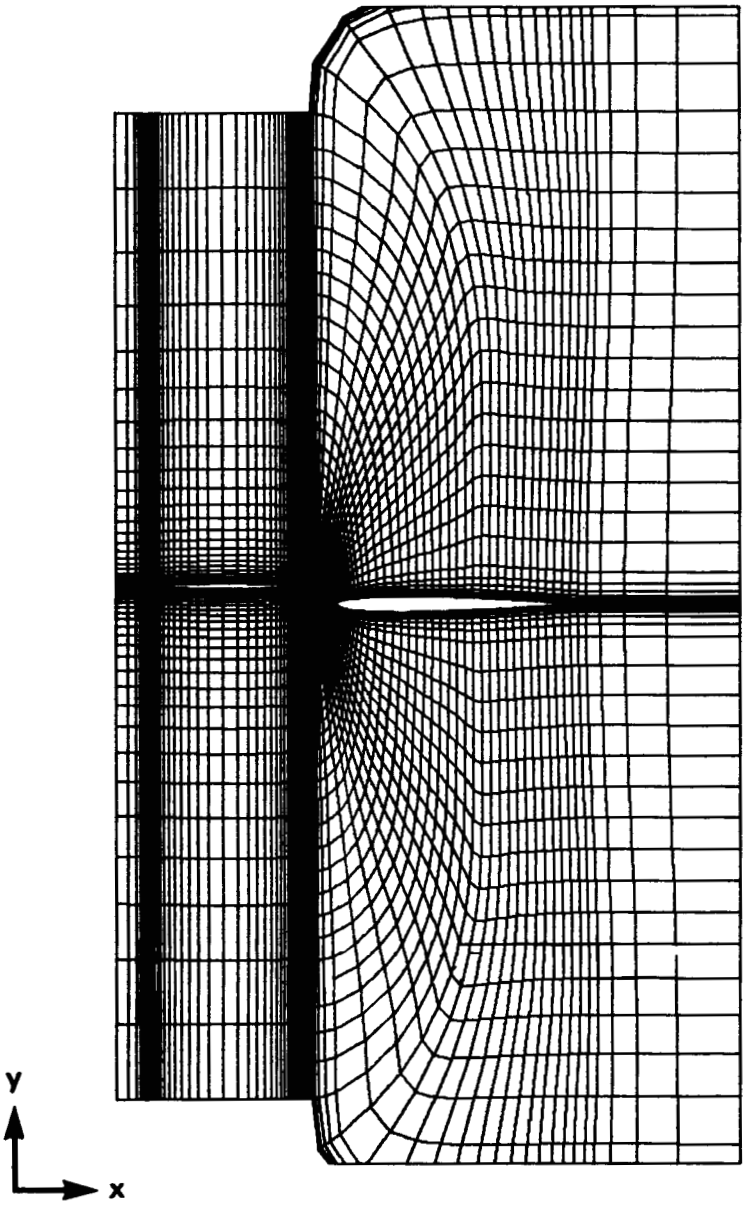

Fig. 24 Two-zone grid at wall-plane cross-section (minimum z).

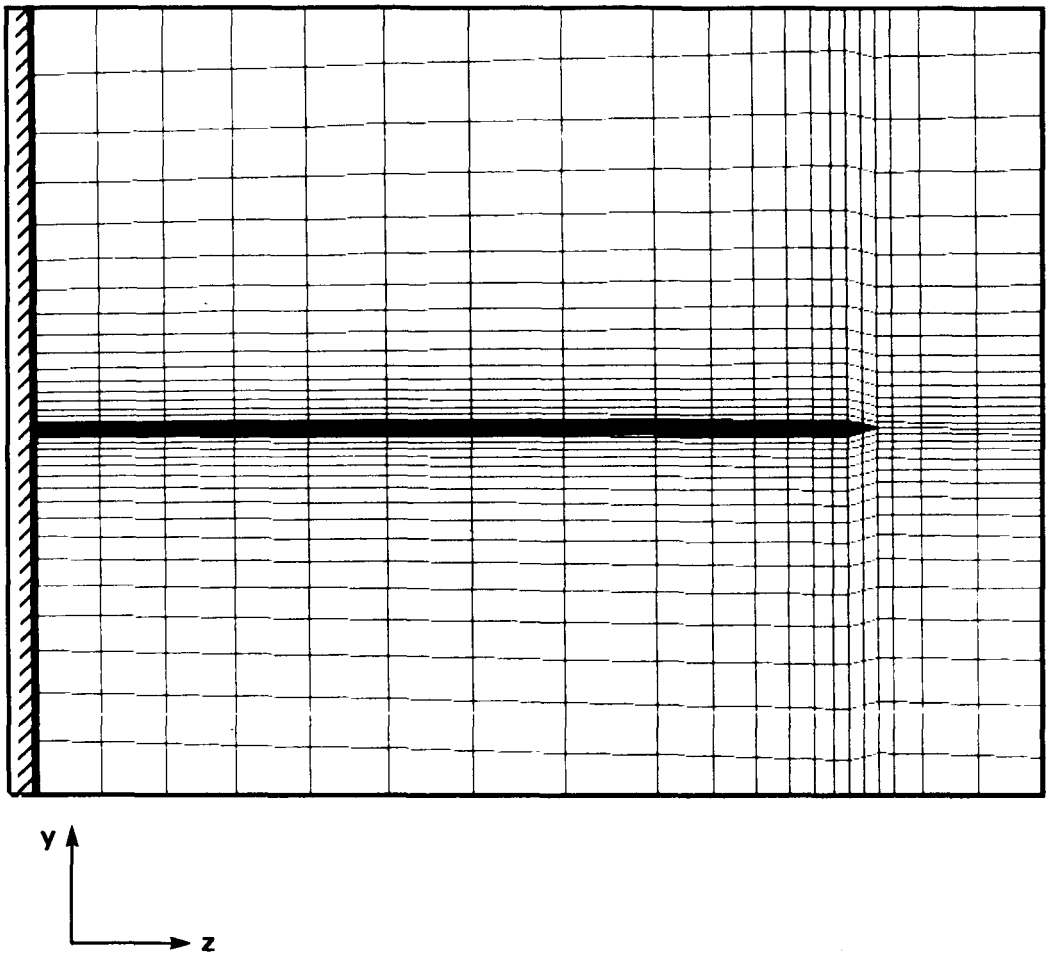

Fig. 25 Spanwise view of grid at canard tip

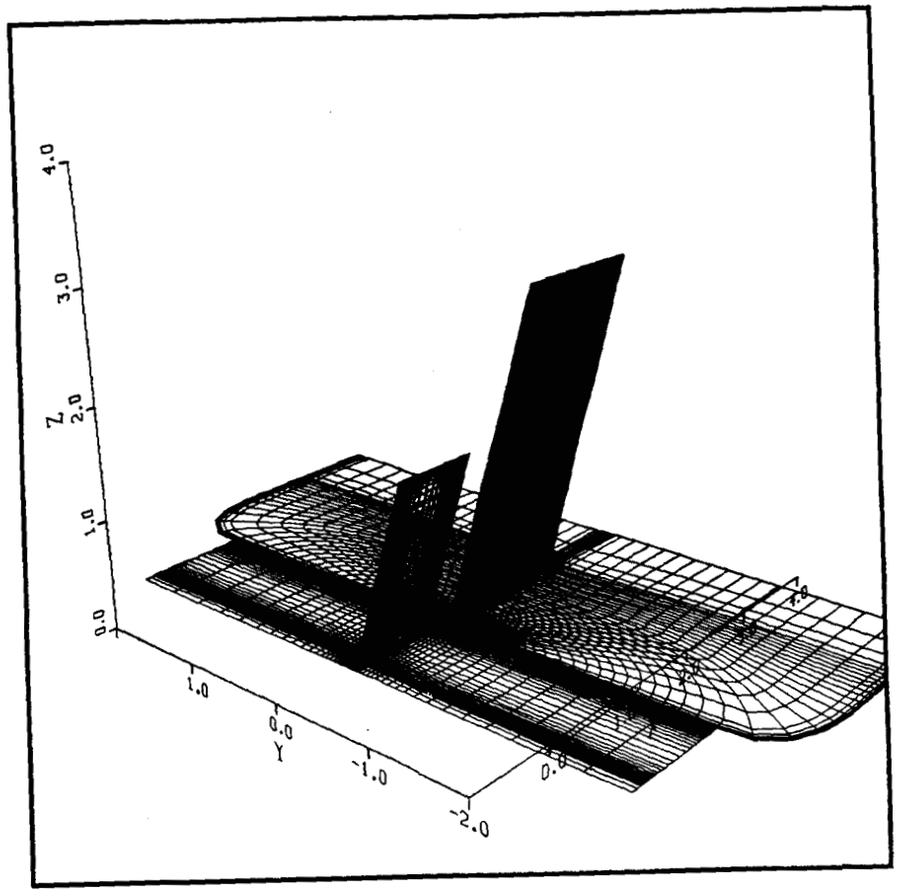

Fig. 26 Three-dimensional view of wing-canard and wall-plane grid

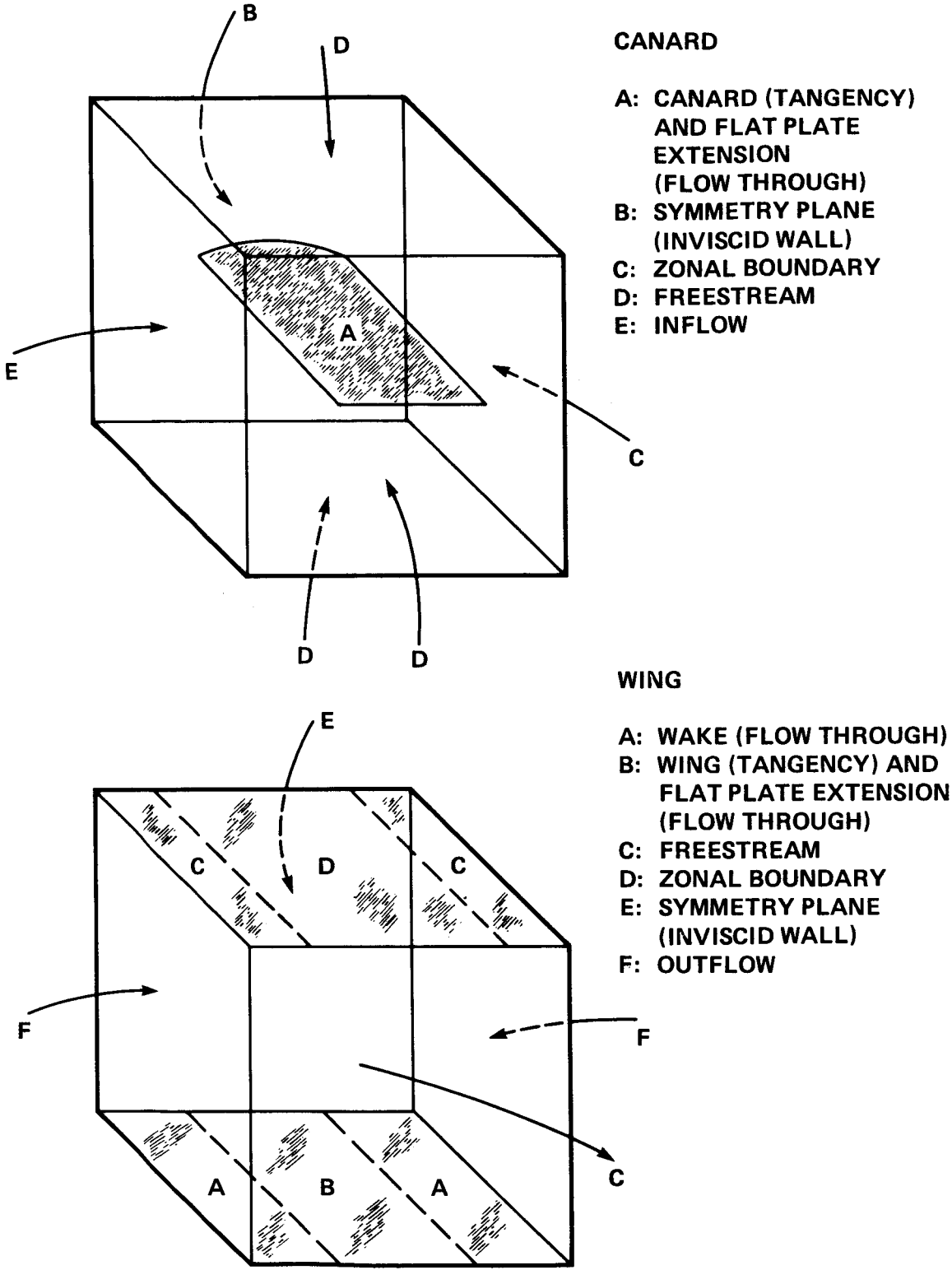

Fig. 27 Boundary conditions in the computational domain

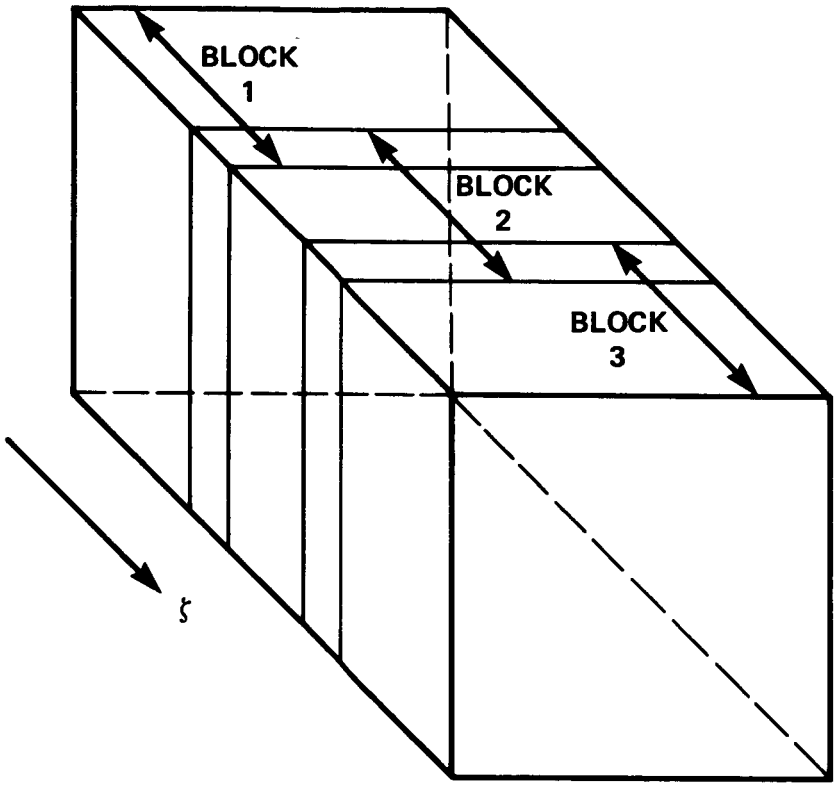

Fig. 28 Sketch depicting the blocking of a computational domain

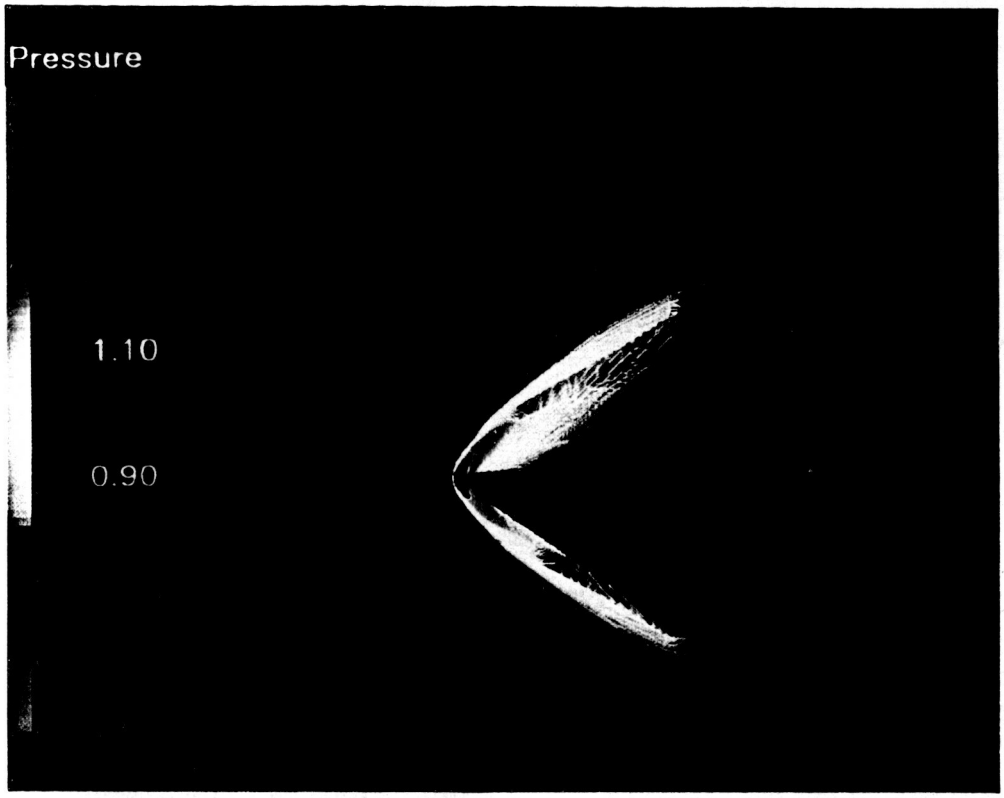

(a) view of entire flow field.

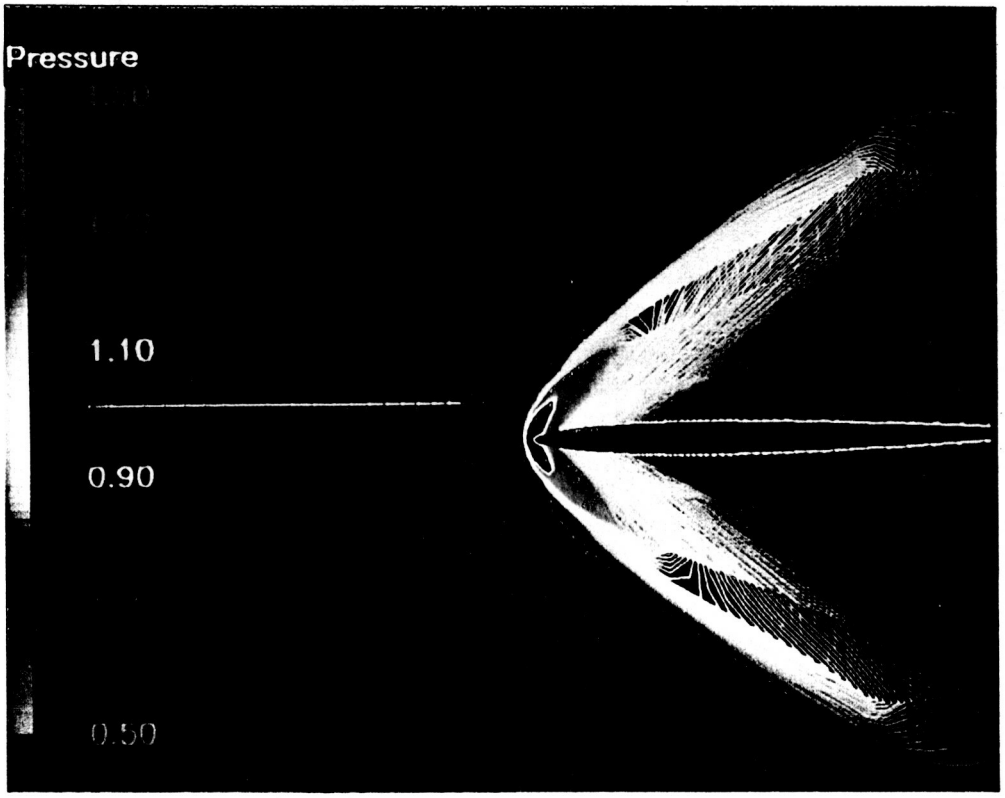

(b) close-up of zonal boundary.

Fig. 29 Pressure contours in the plane of the canard tip, $M_\infty = 2$, $\alpha = 0°$

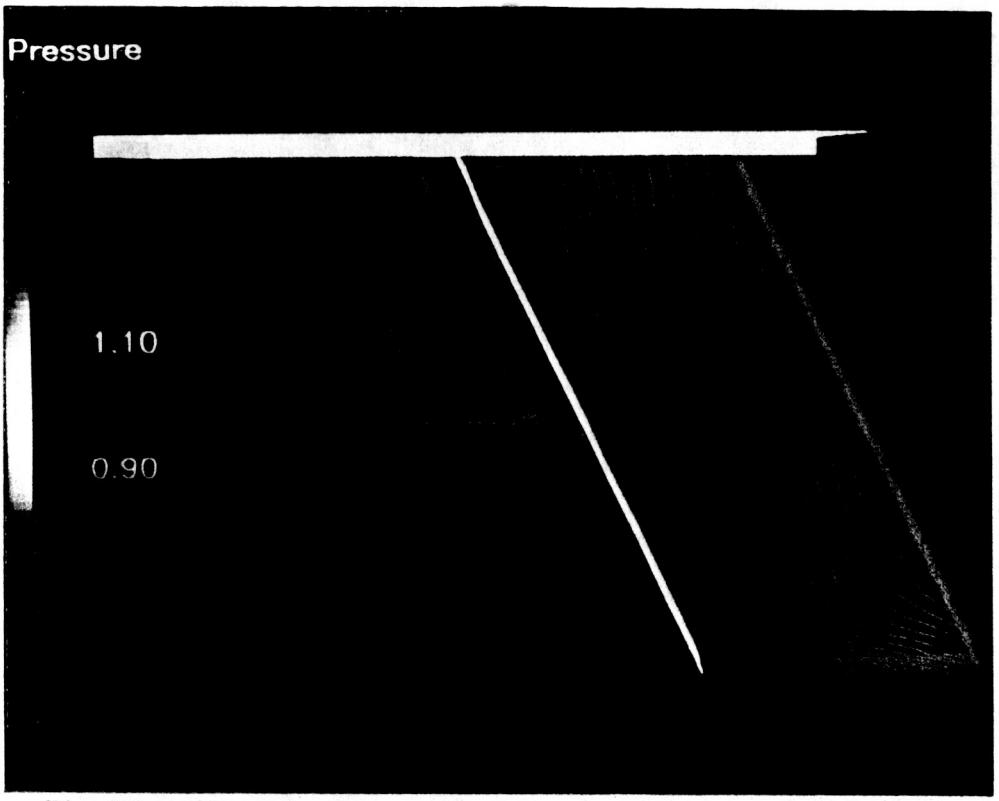

Fig. 30 Upper-surface pressure contours on canard and wing, $M_\infty = 2$, $\alpha = 0°$

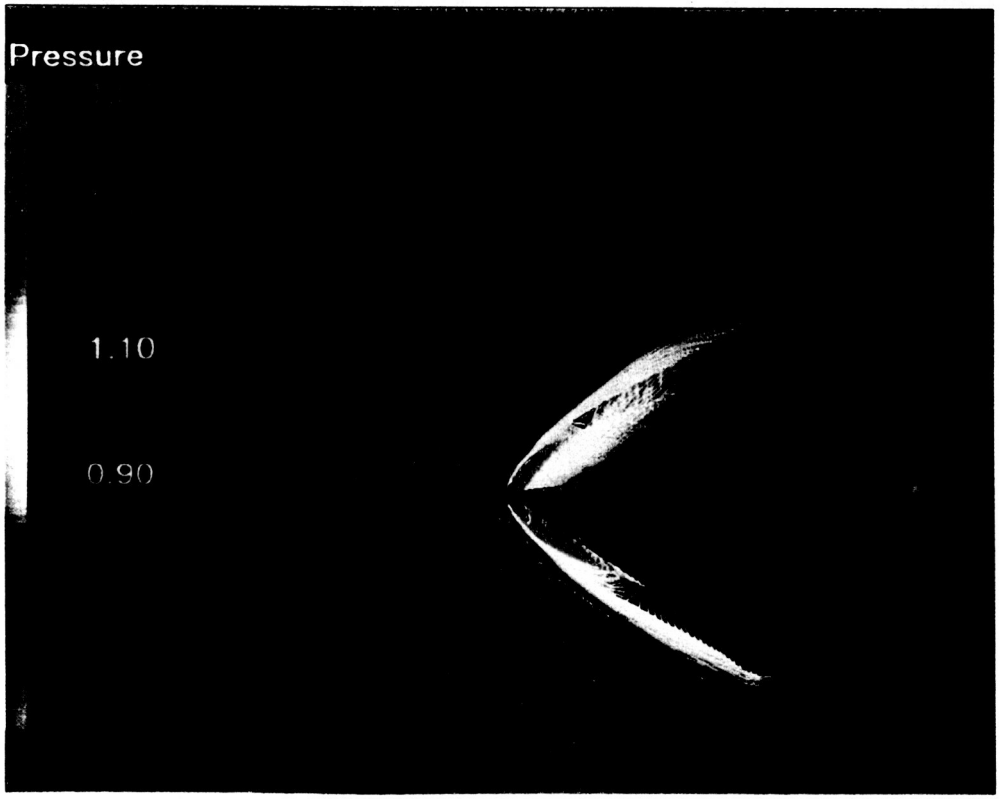

(a) view of entire flow field.

Fig. 31 Pressure contours in the plane of the canard tip, $M_\infty = 2$, $\alpha = 2°$

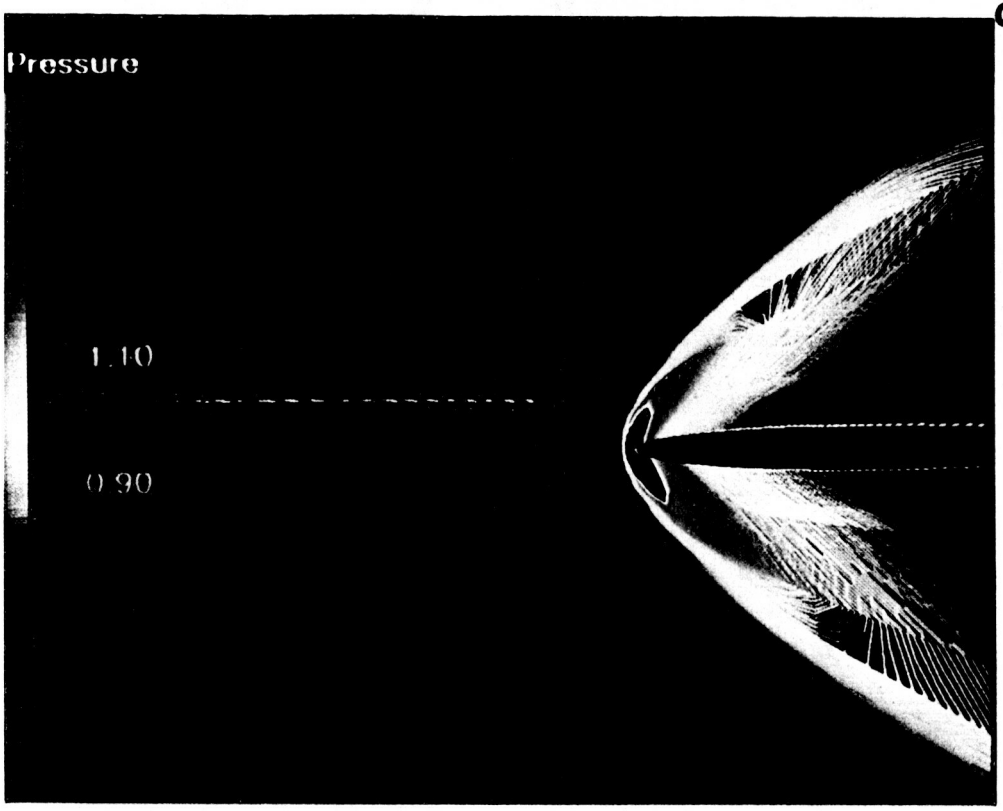

(b) close-up of zonal boundary.

Fig. 31 Pressure contours in the plane of the canard tip, $M_\infty = 2$, $\alpha = 2°$

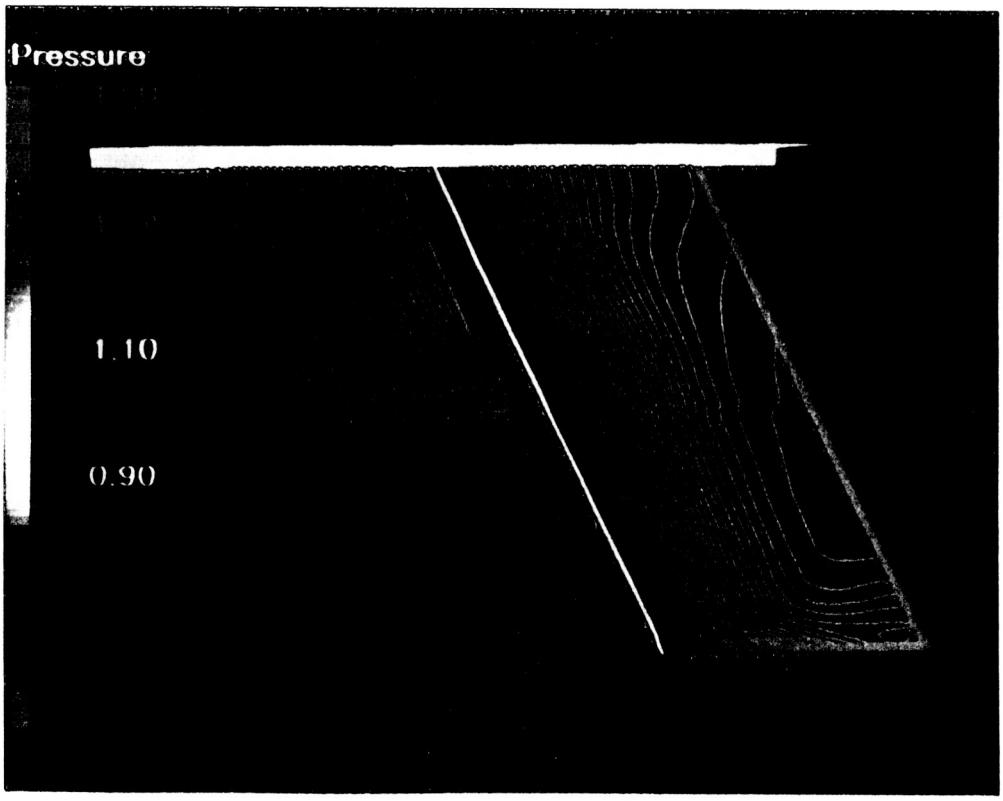

Fig. 32 Upper-surface pressure contours on canard and wing, $M_\infty = 2$, $\alpha = 2°$

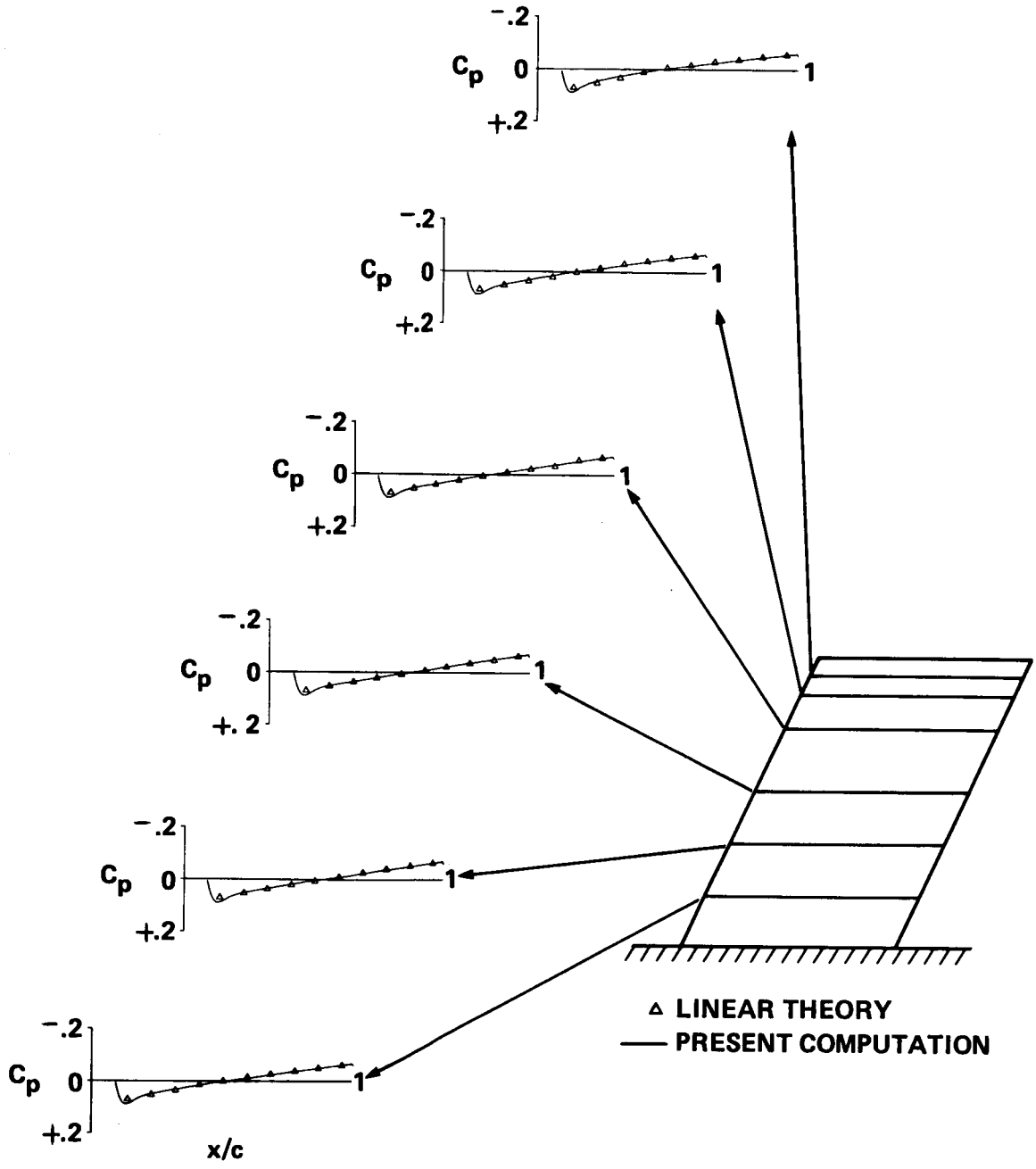

Fig. 33 Canard pressure coefficient comparisons with theory at various span stations, $M_\infty = 2$, $\alpha = 0°$

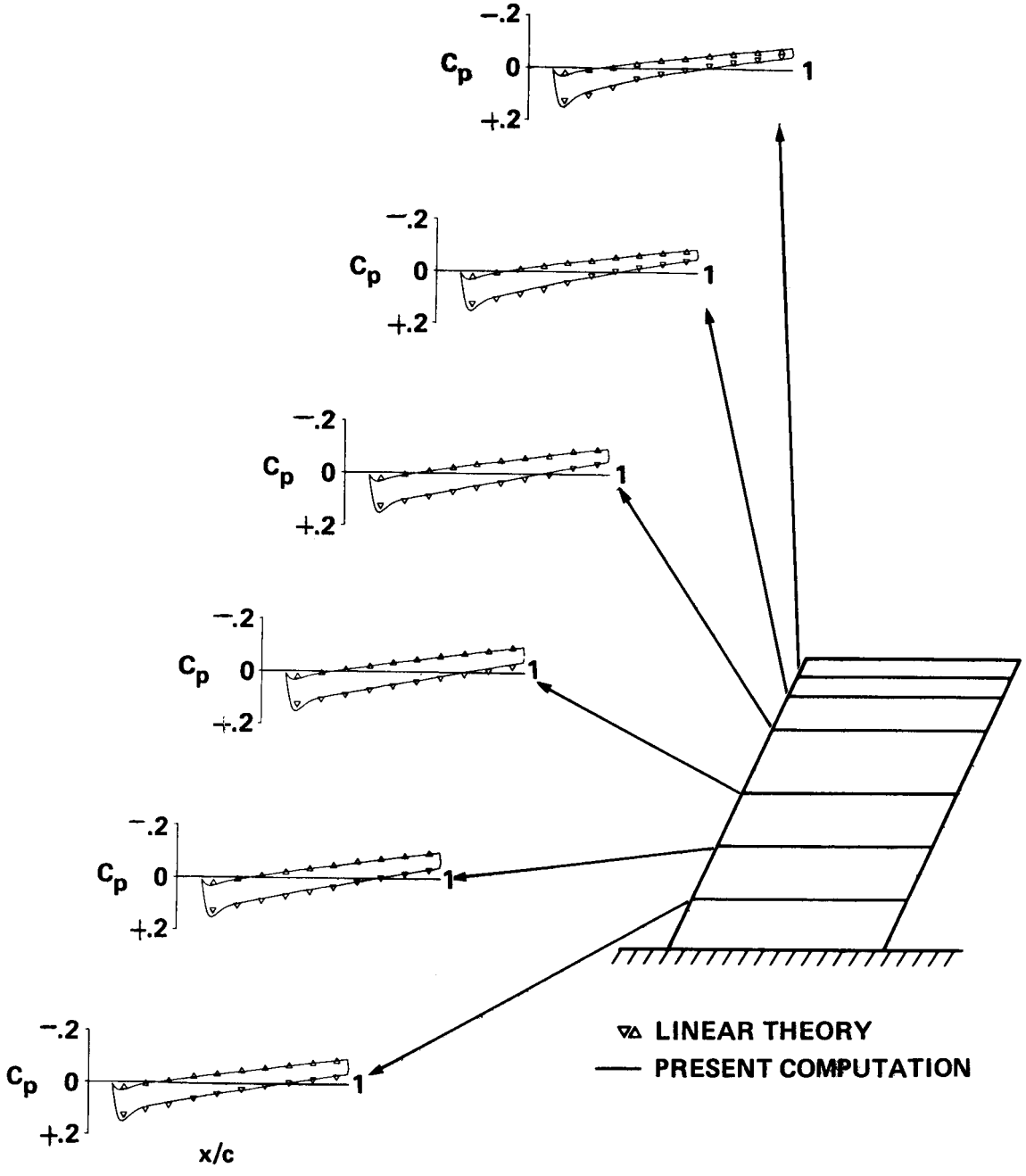

Fig. 34 Canard pressure coefficient comparisons with theory at various span stations, $M_\infty = 2$, $\alpha = 2°$

CHAPTER 6

CONCLUSIONS

6.1 Summary

Through advances in computer hardware and numerical procedures, researchers in the field of CFD are now able to attempt the calculation of flow about geometrically complex bodies. With this capability comes the need for alternatives to the single-grid approach to mesh generation. The creation of a single grid about a complete configuration or a multiple-body geometry is a time-consuming and perhaps even impossible task given the necessary constraints on grid quality. Researchers are exploring the use of composite grids for these complex applications whereby subregional grids are patched or overlaid to form a global mesh. The grid in each region or zone can then be generated somewhat independently of grids in other regions using existing grid-generation methods.

The focus of this work is on the development of a grid-patching technique for three-dimensional problems that maintains global conservation. The technique is derived within the framework of an explicit, first-order, upwind method and is applicable in generalized coordinates for arbitrary point distributions on a planar zonal surface. The zonal interface scheme guarantees the conservation of mass, momentum, and energy across the patch boundary in a discrete sense.

Calculations of the flow about a double-airfoil configuration (two- dimensional) and a wing-canard combination (three-dimensional) demonstrate the usefulness of the method in simplifying grid generation for multiple-body problems. The computations presented here are the first conservative zonal-grid calculations in three dimensions for patching grids with arbitrary point distributions at the interface. Stable, conservative calculations are possible, despite discontinuities in grid lines across the zonal plane, given some attention to the construction of the subregional grids. In the design of a patched grid system, it is important to ensure modest grid-density ratios across the boundary (especially in regions

of high solution gradient) and to choose the zone of integration such that a coarse grid flux results from the summation of fine grid fluxes.

6.2 Recommendations for Further Study

The complexity of the zonal-boundary scheme proposed in this work arises from the constraint that the scheme preserve global conservation at the patch boundaries. Any number of simpler (but nonconservative) interpolation techniques could be used at patched grid interfaces. However, for applications in which discontinuities propagate from zone to zone or pass through a zonal boundary, a conservative treatment of these interfaces is necessary to guarantee a correct (if not smooth) solution (Benek et al., 1983; Hessenius and Pulliam, 1982; Rai et al., 1984). Even in regions of smooth flow, the use of a nonconservative boundary technique is the suspected cause of "glitches"at a zonal interface (Rai, 1985c). There is clearly a need for the development of methods for the conservative treatment of zonal interfaces for use with composite-grid systems (both patched and overlapping).

In theory, it is quite simple to extend the present work to the conservative patching of grids at an arbitrary, nonplanar surface. However, as was demonstrated in this study, the conservation principle is theoretically simple, but complicated to implement. There should be modifications of the procedure described by figure 20 to account for the case when zone-1 triangles and zone-2 triangles are not coplanar. This modification would entail projecting the zone-1 triangle vertices onto the plane defined by a zone-2 triangle before performing the clipping procedure to find the area of overlap. The finer the zonal surface is "triangulated", the greater the degree of accuracy and computational expense.

Another unresolved problem in three-dimensional, conservative grid patching is the reconcilation of a zone-1 versus a zone-2 view of a curved boundary. Consider the sketch of a flux-balance plane in which one edge is curved (fig. 35). This situation would occur when a zonal boundary intersects a body boundary. A coarse, zone-1 grid is shown in figure 35b (denoted by x grid points) as well as a fine, zone-2 representation of the same curved edge (denoted by (•) points). If the flux from the fine grid is summed to define the flux into

a coarse grid cell on this surface, as is recommended, then discrepancies occur near this curved edge. The coarse grid is not completely contained within the fine grid, and therefore it is difficult to make the computation conservative on the coarse grid in this region. The best approach to this problem is not apparent, but strict conservation in this region may be an unnecessary requirement. Perhaps it is not so important to be conservative near these edges of the zonal surface since most, if not all, boundary conditions on these edges are nonconservative anyway.

The majority of the computational expense in calculating the flux interpolation coefficients is in the determination of the overlapping area between two triangles. This task is now done by a clipping routine borrowed from the field of computer graphics. It seems entirely feasible that an analytical formula could be developed to find the polygon of overlap given the vertices of two triangles. An unsuccessful attempt was made to derive such a formula in the course of this study. The discovery of such an expression is necessary to permit the efficient computation of unsteady, moving grid applications (three-dimensional) using a patched grid system. (Moving grid calculations would require the evaluation of the flux interpolation coefficients at each time step.)

The problems cited above in extending the patched grid scheme for general usage are all geometry related. However, for practical applications, the interfacing scheme must be used with second-order accurate, implicit numerical methods. The necessary modifications in three dimensions would directly follow the work of Rai (1985) with his two-dimensional, patched grid scheme. Figures 36a and 36b present first-order and second-order accurate (Osher method) results of Rai for the zonal blunt-body problem previously described in Chapter 3. Pressure contours are shown for the Mach 2 flow over a portion of a cylinder, and the zonal interface in denoted by the curve AB. As with the first-order results of this effort and of figure 36a, the second-order accurate solution is smooth and continuous across the zonal boundary (fig. 36b). Furthermore, the second-order accurate shock location agrees well with the highly accurate result of Lyubimov and Rusanov (1973) (shown

as square symbols in this figure). Because of the success of this two-dimensional work, no fundamental problems are anticipated in the use of the three-dimensional interfacing scheme with a second-order accurate numerical method.

As stated previously, the zonal-boundary condition developed in this study as well as its two-dimensional counterpart (Rai, 1986) produce a locally first-order accurate result at the interface. Various analyses, including the recent work of Allmaras and Baron (1986), show that a given integration scheme which is nth-order accurate and used with a boundary scheme of $n-1$-order accuracy, global accuracy still remains of order n. For this reason, the results of Rai in figure 36b are globally second-order accurate. At this time, however, it is unclear if it is possible to develop a zonal-boundary scheme that is better than first-order accurate at the interface. Allmaras and Baron (1986) report on a two-dimensional analysis of patched grid schemes in a finite volume framework using Runge-Kutta methods. The authors conclude that it is impossible to develop a conservative interface formulation that results in local second-order accuracy (first-order accuracy is possible at best). Although it is difficult to make a direct analogy between the schemes tested in by Allmaras and Baron (1986) and the one presented here, further study is warranted to determine if there indeed is a fundamental limitation on the accuracy of a conservative, interfacing method for the patching of grids.

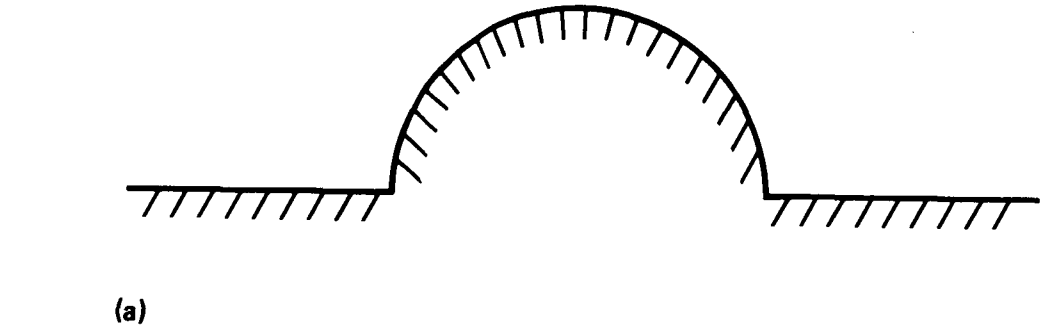

(a)

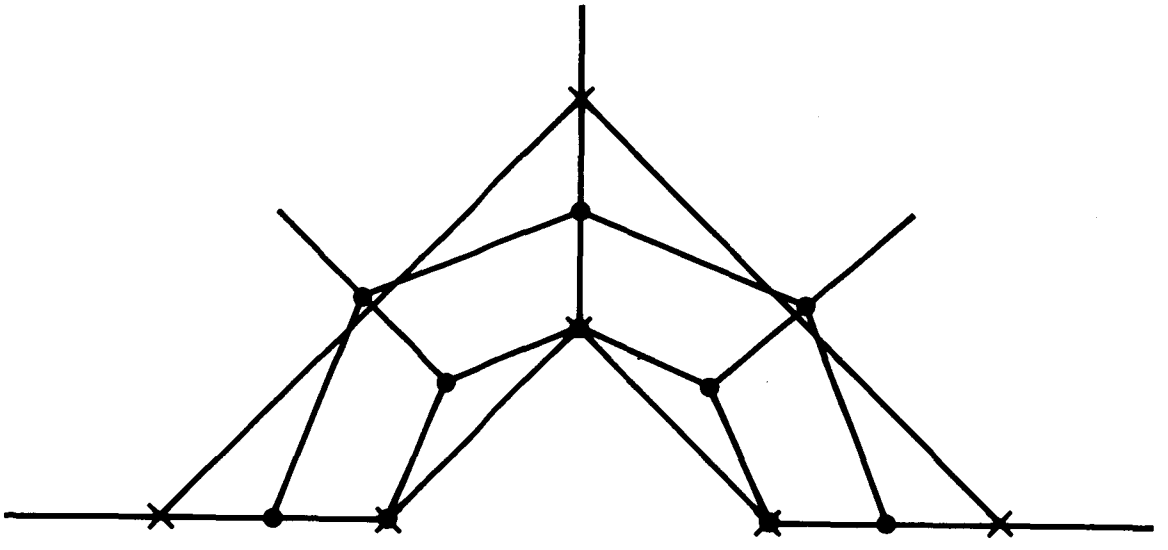

(b)

Fig. 35 View of a flux-balance plane with a curved edge
(a) actual surface geometry (b) superimposed fine and coarse grid discretization

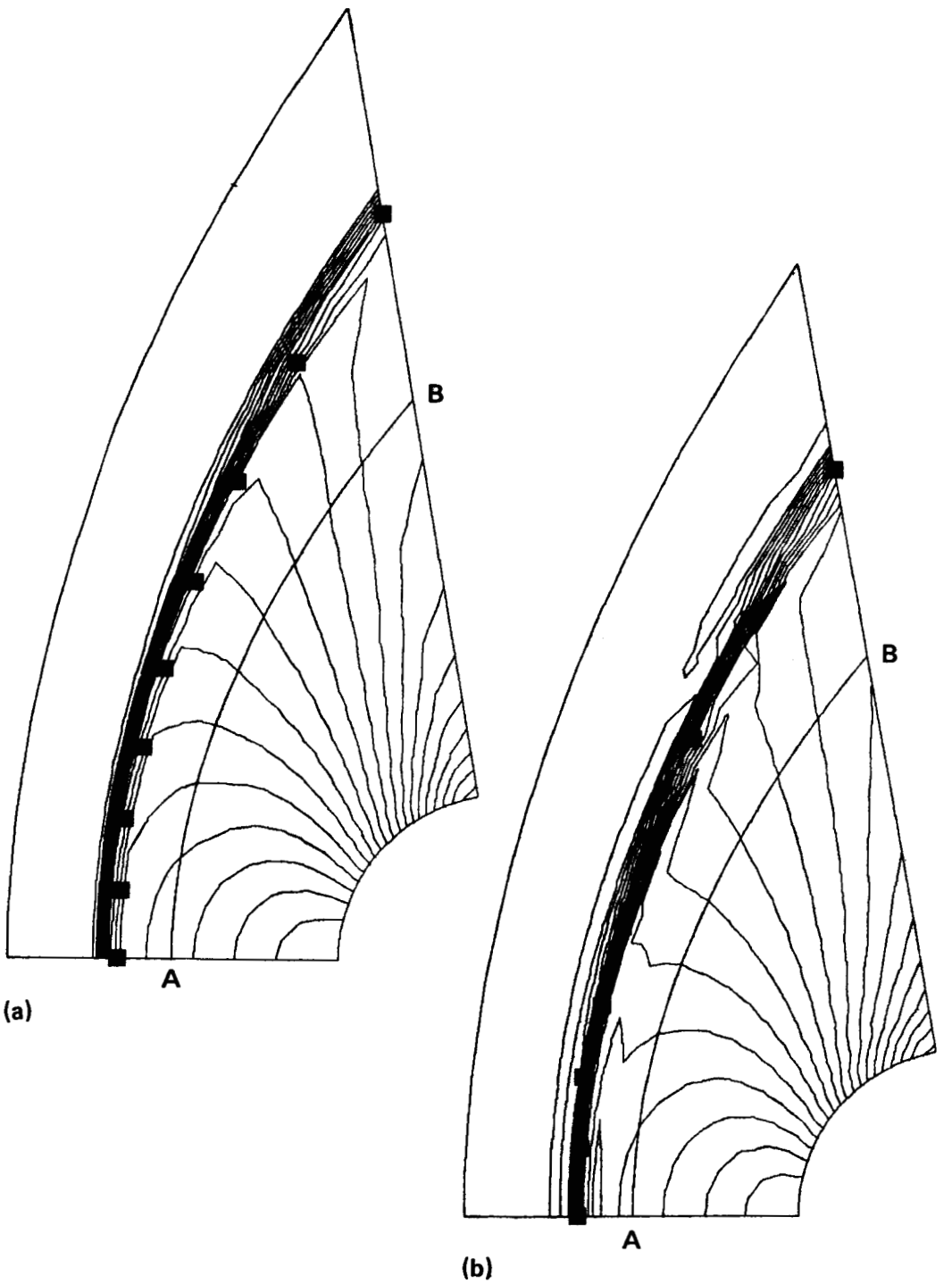

Fig. 36 Comparison of Rai's (a) first-order and (b) second-order accurate results for a two-zone blunt body computation (Ref. 32)

APPENDIX A

INTERPOLATION OVER TRIANGLES

The following interpolation procedure is commonly used in finite-element calculations and is used here in the three-dimensional zonal-boundary scheme:

1) for extrapolating grid lines into a neighboring zone to the flux-balance plane, and
2) for interpolating the dependent variables for points on the zonal boundary in the neighboring zone.

This appendix outlines the interpolation method of Chung (1978).

We wish to interpolate for the variable u at the point (x,y) given knowledge of this function at the vertices of a triangle that contains (x,y) (see fig. 37). Assuming a linear variation of u in both x and y within the triangle,

$$u = s_0 + s_1\bar{x} + s_2\bar{y} \tag{A.1}$$

where

$$\bar{x} = x - \frac{1}{3}\sum_{i=1}^{3} x_i$$

$$\bar{y} = y - \frac{1}{3}\sum_{i=1}^{3} y_i$$

We may determine the constants s_0, s_1, and s_2 in equation (A.1) by constructing and solving the following system of equations using known values of u at the triangle vertices.

$$\begin{aligned} u_1 &= s_0 + s_1\bar{x}_1 + s_2\bar{y}_1 \\ u_2 &= s_0 + s_1\bar{x}_2 + s_2\bar{y}_2 \\ u_3 &= s_0 + s_1\bar{x}_3 + s_2\bar{y}_3 \end{aligned} \tag{A.2}$$

Solving Eq. (A.2) for s_0, s_1, and s_2 and substituting into Eq. (A.1), we obtain

$$u = \Phi_1 u_1 + \Phi_2 u_2 + \Phi_3 u_3 \tag{A.3}$$

where

$$\Phi_i = a_i + b_i\bar{x} + c_i\bar{y}$$

$$a_1 = \frac{1}{|D|}(x_2y_3 - x_3y_2) \qquad a_2 = \frac{1}{|D|}(x_3y_1 - x_1y_3) \qquad a_3 = \frac{1}{|D|}(x_1y_2 - x_2y_1)$$

$$b_1 = \frac{1}{|D|}(y_2 - y_3) \qquad b_2 = \frac{1}{|D|}(y_3 - y_1) \qquad b_3 = \frac{1}{|D|}(y_1 - y_2)$$

$$c_1 = \frac{1}{|D|}(x_3 - x_2) \qquad c_2 = \frac{1}{|D|}(x_1 - x_3) \qquad c_3 = \frac{1}{|D|}(x_2 - x_1)$$

and

$$|D| = det \begin{pmatrix} 1 & x_1 & y_1 \\ 1 & x_2 & y_2 \\ 1 & x_3 & y_3 \end{pmatrix}$$

It may be shown that $a_1 = a_2 = a_3 = \frac{1}{3}$.

To interpolate values of the dependent variables on the zonal-boundary plane, the variable u above is replaced by the vector Q (eq. (4.1)).

To locate points on the flux-balance plane using this interpolation procedure, we must first compute the Φ coefficients using the known point relationships on the zonal-boundary plane. Coordinate locations on the flux-balance plane are then found by the linear combination of these Φ coefficients with coordinate values of the same triangle formed on the flux-balance plane.

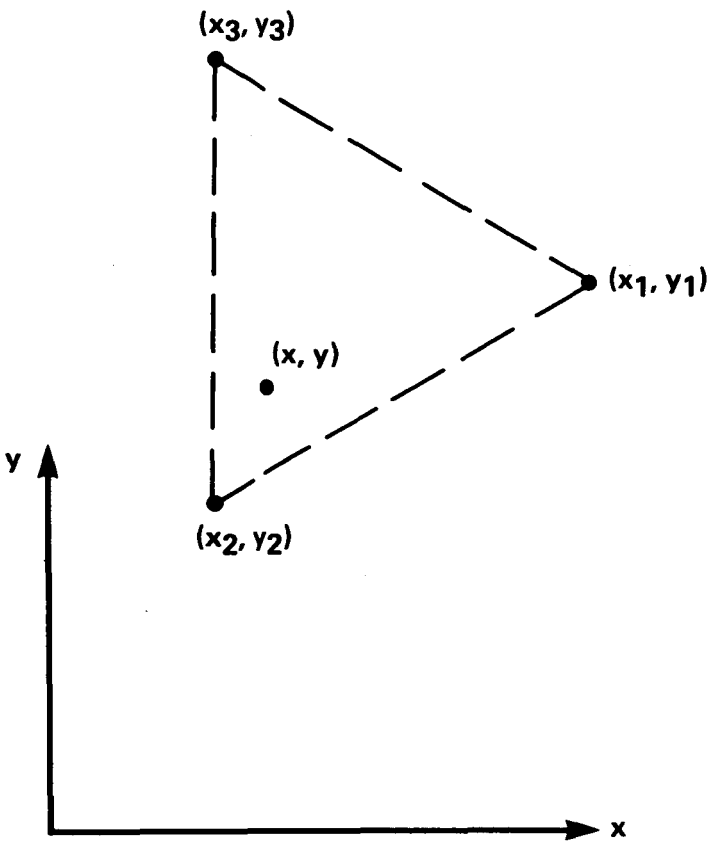

Fig. 37 Coordinate system and arrangement for interpolation over triangles

APPENDIX B

A MODIFIED SUTHERLAND-HODGMAN CLIPPING ALGORITHM

A modification of the Sutherland-Hodgman clipping algorithm (Newman and Sproull, 1979) is used to find the vertices of the polygon formed by the overlap of two coplanar triangles. A flow chart of the modified procedure is presented in figure 38, and the necessary changes are discussed herein. A detailed description of the original algorithm is given by Newman and Sproull (1979).

We wish to find the area of overlap of the zone-1 triangle (vertices A_1, A_2, and A_3) with the zone-2 triangle (vertices B_1, B_2, and B_3). (For convenience, a fourth vertex is added that is equivalent to the first vertex.) The area of overlap may be easily determined given the vertices of the polygon of overlap. The procedure for finding these vertices (Fig. 38) involves clipping the zone-2 triangle against the edges of the zone-1 triangle. In general, however, it is necessary to repeat the procedure to identify all vertices, reversing the roles of the zone-1 and zone-2 triangles for each pair of triangles. The results of each pass are combined and the vertices ordered to properly describe the polygon of overlap. The area may then be computed using equation (4.10).

The procedure outlined is straightforward and easily coded. The unknown vertices are either the intersection points of triangle line segments or are triangle vertices internal to the "frame" triangle (points on the visible side of a frame triangle edge).

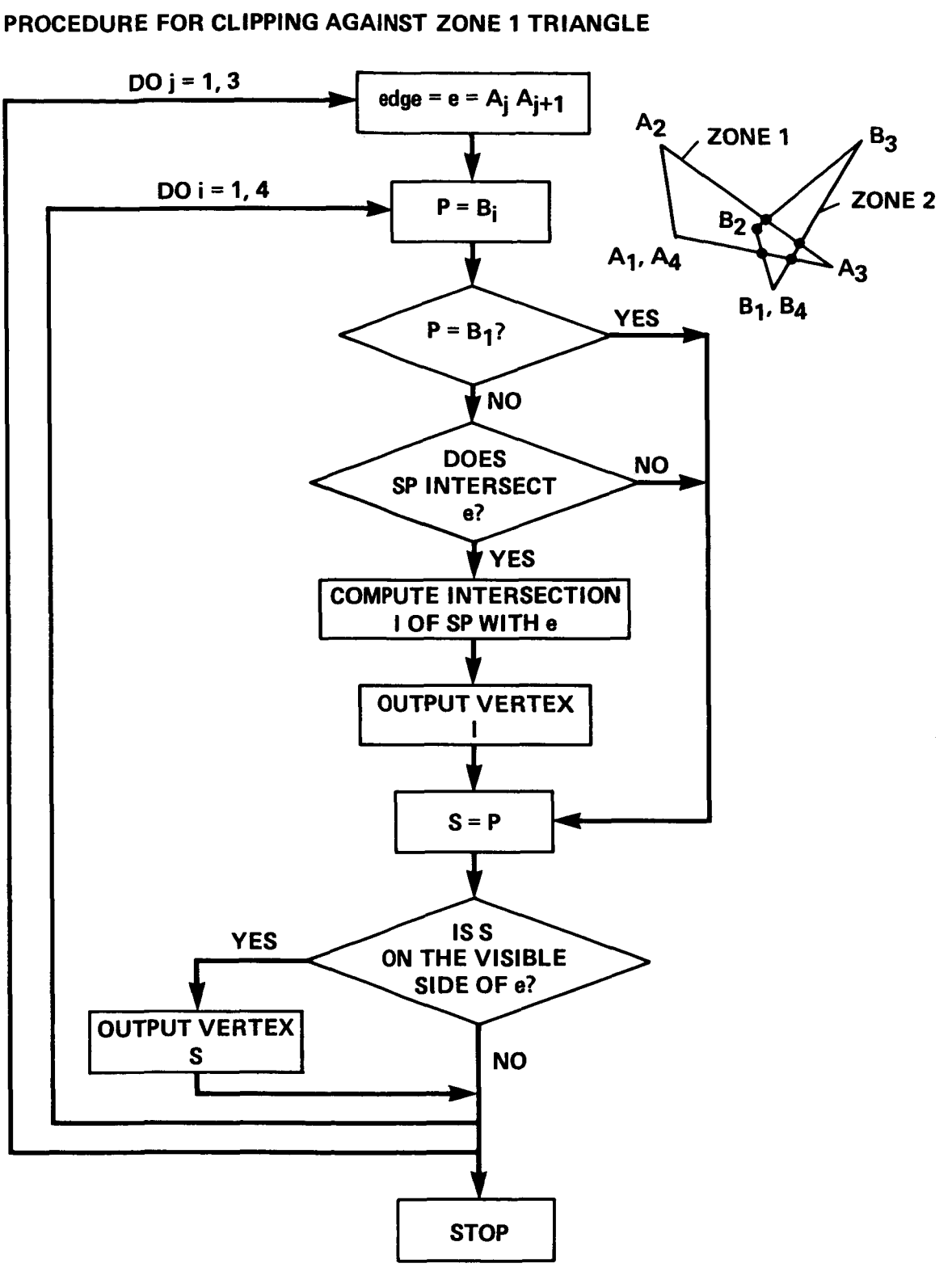

Fig. 38 Schematic of procedure: modified Sutherland-Hodgman clipping algorithm

APPENDIX C

DETERMINATION OF RIEMANN INVARIANTS FOR THE 3-D OSHER ALGORITHM

As shown in Chapter 4, it is necessary to redefine the Riemann invariants, $\hat{v}$ and $\hat{w}$, for Osher-algorithm computations on an arbitrary grid. The constraint equations (4.16) suggest that we choose the coefficients, c_i, such that the vectors $[c_1, c_2, c_3]$ and $[c_4, c_5, c_6]$ are orthogonal to the vector $[k_x, k_y, k_z]$ and to each other where

$$\begin{aligned} \hat{v} &= c_1 u + c_2 v + c_3 w \\ \hat{w} &= c_4 u + c_5 v + c_6 w \end{aligned} \tag{C.1}$$

This may be accomplished in the following manner.

Find a transformation matrix, T, that rotates a unit vector on the x-coordinate axis to the vector $[k_x/D, k_y/D, k_z/D]$ where $D = (k_x + k_y + k_z)^{1/2}$

$$T \begin{pmatrix} 1 \\ 0 \\ 0 \end{pmatrix} = \begin{pmatrix} k_x/D \\ k_y/D \\ k_z/D \end{pmatrix}$$

where

$$T = \begin{pmatrix} C_\alpha C_\beta & -C_\beta S_\alpha & -S_\beta \\ S_\alpha & C_\alpha & 0 \\ C_\alpha S_\beta & -S_\alpha S_\beta & C_\beta \end{pmatrix} \tag{C.2}$$

$$S_\alpha = sin(\alpha) = k_y/D$$

$$C_\alpha = cos(\alpha) = (k_x^2 + k_z^2)^{1/2}/D$$

$$S_\beta = sin(\beta) = k_z/(k_x^2 + k_z^2)^{1/2}$$

$$C_\beta = cos(\beta) = k_x/(k_x^2 + k_z^2)^{1/2}$$

and α and β are angles described in figure 39. Then, by definition (refer again to fig. 22)

$$\hat{u} - k_t/D = T \begin{pmatrix} 1 \\ 0 \\ 0 \end{pmatrix} \cdot \begin{pmatrix} u \\ v \\ w \end{pmatrix}$$

and we choose

$$\hat{v} = T \begin{pmatrix} 0 \\ 1 \\ 0 \end{pmatrix} \cdot \begin{pmatrix} u \\ v \\ w \end{pmatrix}$$

$$\hat{w} = T \begin{pmatrix} 0 \\ 0 \\ 1 \end{pmatrix} \cdot \begin{pmatrix} u \\ v \\ w \end{pmatrix}$$

Therefore,

$$\begin{pmatrix} \hat{u} - k_t/D \\ \hat{v} \\ \hat{w} \end{pmatrix} = T^T \begin{pmatrix} u \\ v \\ w \end{pmatrix}$$

and the coefficients c_i are the following components of the T matrix :

$$\begin{aligned} c_1 &= -C_\beta S_\alpha \\ c_2 &= C_\alpha \\ c_3 &= -S_\alpha S_\beta \\ c_4 &= -S_\beta \\ c_5 &= 0 \\ c_6 &= C_\beta \end{aligned} \qquad (C.3)$$

Note that if both k_x and k_z are zero, certain entries of the T matrix are then undefined. This condition is easily remedied by initially choosing to rotate the unit axis vector (x, y, or z) "closest" to the given $[k_x/D, k_y/D, k_z/D]$ vector. This practice will ensure a non-zero denominator in the expressions for S_β and C_β.

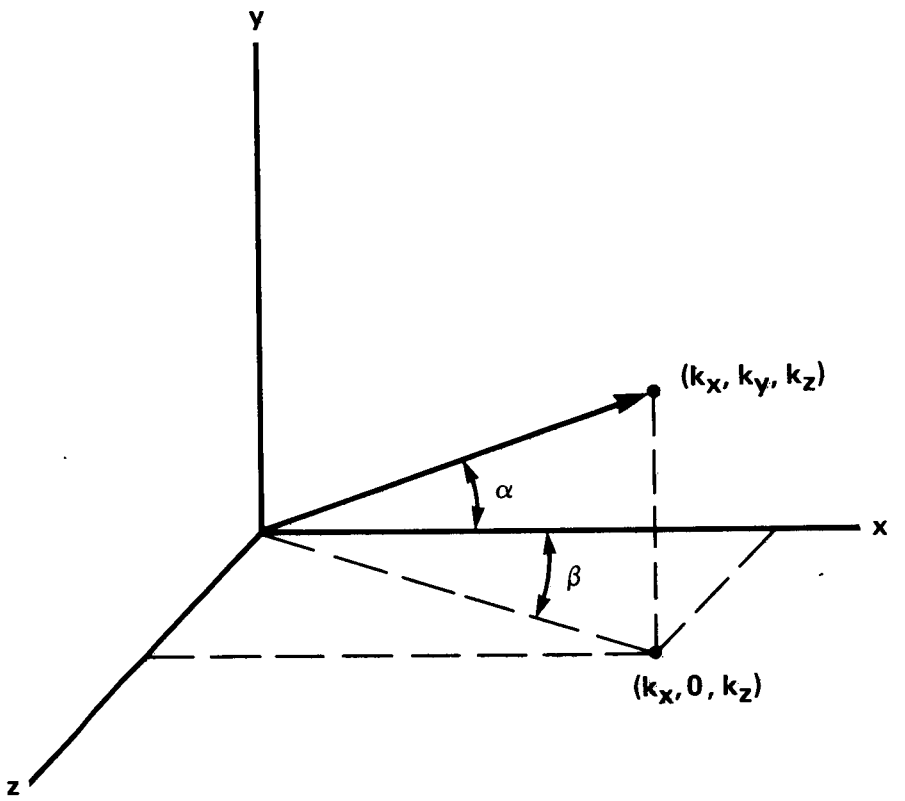

Fig. 39 Coordinate system and angle definitions for the determination of Riemann invariants.

REFERENCES

Allmaras, S. R.; and Baron, J. R.: Embedded Mesh Solutions of the 2-D Euler Equations: Evaluation of Interface Formulations. AIAA Paper 86-0509, January, 1986.

Atta, E. H.: Component-Adaptive Grid Interfacing. AIAA Paper 81-0382, June, 1981.

Atta, E. H.; and Vadyak, J.: A Grid Interfacing Zonal Algorithm for Three Dimensional Transonic Flows About Aircraft Configurations. AIAA Paper 82-1017, June, 1982.

Baker, T. J.; Jameson, A.; and Vermeland, R. E.: Three-Dimensional Euler Solutions with Grid Embedding. AIAA Paper 85-0121, January, 1985.

Benek, J. A.; Steger, J. L.; Dougherty, F. C.: A Flexible Grid Embedding Technique with Application to the Euler Equations. AIAA Paper 83-1944, Proceedings of the AIAA Computational Fluid Dynamics Conference, AIAA CP834, 1983, pp. 373-382.

Benek, J. A.; Buning, P. G.; and Steger, J. L.: A 3-D Chimera Grid Embedding Technique. AIAA Paper 85-1523-CP, July, 1985.

Berger, M. J.: Adaptive Mesh Refinement for Hyperbolic Partial Differential Equations. Ph.D. Dissertation, Computer Science Dept., Stanford Univ., 1982.

Berger, M. J.: On Conservation at Grid Interfaces. ICASE Report 84-43, 1984.

Berger, M. J.; and Jameson A.: Automatic Adaptive Grid Refinement for the Euler Equations. Proceedings of the 9th International Conference on Numerical Methods in Fluid Dynamics, 1984, pp. 14-16.

Bush, R. H.: External Compression Inlet Predictions Using an Implicit, Upwind, Multiple Zone Approach. AIAA Paper 85-1521, July, 1985.

Cambier, L.; Ghazzi, W.; Veuillot, J. P.; and Viviand, H.: A Multi-Domain Approach for the Computation of Viscous Transonic Flows by Unsteady Type Methods. Recent Advances in Numerical Methods in Fluids. W. G. Habashi ed., vol. 3, Pineridge Press (Swansea), 1984.

Carmichael, R. L.; and Erickson, L. L.: PAN AIR - A Higher Order Panel Method for Predicting Subsonic or Supersonic Linear Potential Flows About Arbitrary Configurations. AIAA Paper 81-1255, June, 1981.

Caruso, S.: Adaptive Grid Techniques for Elliptic Fluid Flow Problems. Ph.D. Dissertation, Mechanical Engineering Dept., Stanford Univ., 1985.

Chakravarthy, S. R.: Inviscid Analysis of Dual-Throat Nozzle Flows. AIAA Paper 81-1201, June, 1981.

Chakravarthy, S. R.; and Osher, S.: Numerical Experiments with the Osher Upwind Scheme for the Euler Equations. AIAA Paper 82-0975, June, 1982.

Chang, J. L. C.; Kwak, D.; Dao, S. C.; and Rosen, R.: A Three-Dimensional Incompressible Flow Simulation Method and its Application to the Space Shuttle Main Engine, Part I - Laminar Flow. AIAA Paper 85-0175, January, 1985.

Chapman, D. R.: Trends and Pacing Items in Computational Aerodynamics. Lecture Notes in Physics. vol. 141, W. C. Reynolds and R. W. MacCormack ed., Springer-Verlag (New York), 1980, pp. 1-12.

Chung, T. J.: Finite Element Analysis in Fluid Dynamics. McGraw-Hill (New York), 1978, pp. 68-71.

Dougherty, F. C.: Development of a Chimera Grid Scheme with Applications to Unsteady Problems. Ph.D. Dissertation, Aeronautics and Astronautics Dept., Stanford Univ., 1985.

Eriksson, L. E.: Euler Solutions on O-O Grids Around Wings Using Local Refinement. Proceedings of the 6th Gamm Conference on Numerical Methods in Fluid Mechanics, 1985.

Eriksson, L. E.; and Rai, M. M.: A Stability Analysis of Various Patched Grid Interface Conditions for Hyperbolic Equations. to be published.

Flores, J.; Holst, T. L.; and Sorenson, R. L.: Transonic Solutions for a Multielement Airfoil Using the Full-Potential Equation. AIAA Paper 84-0300, January, 1984.

Hessenius, K. A.; and Pulliam, T. H.: A Zonal Approach to Solution of the Euler Equations. AIAA Paper 82-0969, June, 1982.

Hessenius, K. A.; and Rai, M. M.: Applications of a Conservative Zonal Scheme to Transient and Geometrically Complex Problems. Computers and Fluids, vol. 14, no. 1, 1986, pp. 43-58.

Holst, T. L.; Kaynak, U.; Gundy, K. L.; Thomas, S. D.; Flores, J.; and Chaderjian, N. M.: Numerical Solution of Transonic Wing Flows Using an Euler, Navier-Stokes Zonal Approach. AIAA Paper 85-1640, July, 1985.

Kordulla, W.; and Vinokur, M.: Efficient Computation of Volume in Flow Predictions. AIAA J., vol. 21, no. 6, 1983, pp. 917-918.

Kutler, P.: A Perspective of Theoretical and Applied Computational Fluid Dynamics. AIAA J., vol. 23, no. 3, 1985, pp. 328-341.

Lasinski, T. A.; Andrews, A. E.; Sorenson, R. L.; Chaussee, D. S.; Pulliam, T. H.; and Kutler, P.: Computation of the Steady Viscous Flow over a Tri-Element Augmentor Wing Airfoil. AIAA Paper 82-0021, January, 1982.

Lombard, C. K.; and Venkatapathy, E.: Implicit Boundary Treatment for Joined and Disjoint Patched Mesh Systems . AIAA Paper 85-1503, July, 1985.

Lyubimov, A. N.; and Rusanov, V. V.: Gas Flows Past Blunt Bodies. NASA TT-F 715, 1973.

Newman, W. M.; and Sproull, R. F.: Principles of Interactive Computer Graphics. McGraw Hill (New York), 1979, pp. 69-72.

Nietubicz, C. J.; Pulliam, T. H.; and Steger, J. L.: Numerical Solution of the Azimuthal-Invariant Thin-Layer Navier-Stokes Equations. AIAA Paper 79-0010, June, 1979.

Norton, R. J. G.; Thompkins, W. T. Jr.; and Haimes, R.: Implicit Finite Difference Schemes with Non-Simply Connected Grids – A Novel Approach. AIAA Paper 84-0003, January, 1983.

Osher, S.; and Chakravarthy, S.: Upwind Schemes and Boundary Conditions with Applications to Euler Equations in General Geometries. J. Computational Phys., vol. 50, 1983, pp. 447-481.

Pulliam, T. H.; and Steger, J. L.: On Implicit Finite-Difference Simulations of Three Dimensional Flow. AIAA Paper 78-10, June, 1978.

Rai, M. M.; Hessenius, K. A.; and Chakravarthy, S. R.: Metric-Discontinuous Zonal Grid Calculations using the Osher Scheme. Computers and Fluids, vol. 12, no. 3, 1984, pp. 161-175.

Rai, M. M.: An Implicit, Conservative, Zonal-Boundary Scheme for Euler Equation Calculations. NASA CR-3865, 1985.

Rai, M. M.: A Relaxation Approach to Patched-Grid Calculations with the Euler Equations. AIAA Paper 85-0295, January, 1985.

Rai, M. M.: Navier-Stokes Simulations of Rotor-Stator Interaction using Patched and Overlaid Grids. AIAA Paper 85-1519-CP, July, 1985.

Rai, M. M.: A Conservative Treatment of Zonal Boundaries for Euler Equation Calculations. J. Computational Phys., vol. 62, no. 2, 1986, pp. 472-503.

Rubbert, P. E.; and Lee, K. D.: Patched Coordinate Systems. Numerical Grid Generation. J. F. Thompson ed., North-Holland (New York), 1982, pp. 235-252.

Sorenson, R. L.: A Computer Program to Generate Two-Dimensional Grids about Airfoils and Other Shapes by the Use of Poisson's Equation. NASA TM-81198, 1980.

Steger, J. L.; and Warming, R. F.: Flux Vector Splitting of the Inviscid Gas Dynamics Equations with Application to Finite Difference Methods. J. Computational Phys., vol. 40, no. 2, 1981, pp. 263-293.

Steger, J. L.: On Application of Body Conforming Curvilinear Grids for Finite Difference Solution of External Flow. Numerical Grid Generation. J. F. Thompson ed., North-Holland (New York), 1982, pp. 295-316.

Steger, J. L.; Dougherty, F. C.; and Benek, J. A.: A Chimera Grid Scheme. Proceedings of the ASME Mini-Symposium on Advances in Grid Generation, 1983, pp.59-69.

Thompson, D. S.: A Mesh Embedding Approach for Prediction of Transonic Wing-Body-Store Flow Fields. Proceedings of the Symposium on Numerical Boundary Condition Procedures, NASA CP 2201, 1981, pp. 403-427.

Thompson, J. F.; Warsi, Z. U. A.; and Mastin, C. W.: Boundary-Fitted Coordinate Systems for Numerical Solution of Partial Differential Equations – A Review. J. Computational Phys., vol. 47, no. 1, 1982, pp. 1-108.

Veuillot, J. P.; and Cambier, L.: A Sub-Domain Approach for the Computation of Compressible Inviscid Flows. ONERA Publication 1984-61, 1984.

Weatherill, N. P.; and Forsey, C. R.: Grid Generation and Flow Calculations for Complex Aircraft Geometries using a Multi-Block Scheme. AIAA Paper 84-1665, July, 1984.

NASA
National Aeronautics and Space Administration

Report Documentation Page

1. Report No.	2. Government Accession No.	3. Recipient's Catalog No.
NASA TM-88326		

4. Title and Subtitle	5. Report Date
Conservative Zonal Schemes for Patched Grids in Two and Three Dimensions	April 1987
	6. Performing Organization Code

7. Author(s)	8. Performing Organization Report No.
Kristin A. Hessenius	A-86317
	10. Work Unit No. 505-60-01

9. Performing Organization Name and Address	11. Contract or Grant No.
Ames Research Center Moffett Field, CA 94035	
	13. Type of Report and Period Covered
12. Sponsoring Agency Name and Address	Technical Memorandum
National Aeronautics and Space Administration Washington, DC 20546	14. Sponsoring Agency Code

15. Supplementary Notes

Point of Contact: Kristin A. Hessenius, Ames Research Center, MS 258-1, Moffett Field, CA 94035 (415) 694-6447 or FTS 464-6447

16. Abstract

The computation of flow over complex geometries, such as realistic aircraft configurations, poses difficult grid generation problems for computational aerodynamicists. The creation of a traditional, single-module grid of acceptable quality about an entire configuration may be impossible even with the most sophisticated of grid generation techniques. A "zonal approach," wherein the flow field is partitioned into several regions within which grids are independently generated, is a practical alternative for treating complicated geometries. This technique not only alleviates the problems of discretizing a complex region, but also facilitates a block-processing approach to computation thereby circumventing computer memory limitations. The use of such a zonal scheme, however, requires the development of an interfacing procedure that ensures a stable, accurate, and conservative calculation for the transfer of information across the zonal boundaries.

The primary purpose of this work is to derive sufficient conditions for the conservative patching of grids along a plane in three dimensions. The ability of this scheme to simplify grid generation and to produce a stable, conservative computation is demonstrated in the solution of the flow about a multiple-body problem. A study of the use of a two-dimensional conservative zonal scheme and its application to geometrically complex problems is also included.

17. Key Words (Suggested by Author(s))	18. Distribution Statement
Computational fluid dynamics Grid generation Zonal methods Patched grids	Unclassified-Unlimited Subject Category - 34

19. Security Classif. (of this report)	20. Security Classif. (of this page)	21. No. of pages	22. Price
Unclassified	Unclassified	101	A05

NASA FORM 1626 OCT 86

For sale by the National Technical Information Service, Springfield, Virginia 22161